Vascular self-healing optimization and evaluation by means of four-point bending.

Gerlinde Lefever & Jannes Van Cauwenberghe

Master thesis submitted under the supervision of
Prof. Dr. ir. Danny Van Hemelrijck

The co-supervision of
ir. Pieter Minnebo

Academic year
2015-2016

In order to be awarded the Master's Degree in
Civil Engineering

Acknowledgements

This master thesis is the achievement of hard work and perseverance, but most of all it is the result of teamwork. Besides the two of us, a lot of other people contributed to the process and should be thanked for their advice, benevolence to help and the support in setbacks.

As being our supervisor, we first want to thank Pieter Minnebo, who was always ready to help, render advice and answer our questions with a smile. It is said that good supervision is the art of getting average people to do great work, which made his contribution essential in reaching our goals. Further on, we would like to thank our promotor, professor Danny Van Hemelrijck, for his honest opinions and effort to motivate us till the end. A special thanks goes to the technicians Daniel Debondt and Gabriel van den Nest. Their experience and knowledge provided great assistance and their joviality made our days in the lab more enjoyable. Moreover, we are very grateful to Frans Boulpaep for lending a hand with the Instron equipment and the application of strain gauges. There was no problem that he could not solve. Next on, we want to show appreciation to professor Aggelis, Eleni, Evin, Georgis and Sokratis for their tips and tricks using acoustic emission and the analysis of the data. Also, many thanks go to Silke for her assistance in applying our first speckle pattern to the beam.

Last, but certainly not least, we would like to thank our parents for their support during this stressful period, our fellow students who wrote their thesis at the MeMC department for lightening up our days with jokes and kind words of support and our good friend David for proofreading our thesis.

Finally, it should be said that, although some periods were rough, the collaboration kept us going and made us very proud of what we achieved during this year.

Abstract

Vascular self-healing optimization and evaluation by means of four-point bending.

Gerlinde Lefever
Master of Science in Civil Engineering
Construction and Geomaterials

Jannes Van Cauwenberghe
Master of Science in Civil Engineering
Water Resources

2015-2016

Concrete is one of the most used construction materials. Despite great performance and relatively low cost, steel reinforcement is indispensable to compensate for the low tensile strength. However, cracks are easily induced, which can provoke ingression of aggressive substances, causing corrosion of the reinforcement. Inspection and maintenance are expensive and difficult to perform. Self-healing concrete aims to eliminate these drawbacks.
Vascular self-healing of concrete is a bio-inspired technique in which a network of hollow tubes, filled with a healing agent, is embedded in the concrete. Among the different techniques, this technique is chosen, because of its potential for multiple healing.
The main objectives are firstly to seal the cracks to avoid penetration of ingressive liquids, and secondly to regain mechanical properties. The focus is set on upscaling of the currently existing technique by enhancing the survivability during the concrete casting process and by reducing the production cost. The vascular tubes are made of Inorganic Phosphate Cement and clay. They will be fabricated by moulding and extrusion respectively. A reservoir, accessible from outside the concrete, is provided, which can be embedded in the concrete element to store healing agent. The reservoir is 3D-printed in polyamide and connected to the tubes. For improving the casting resistance, different shapes of tubes are investigated. Finally, concrete beams containing vascular healing systems are tested under four-point bending, which gave result to successful self-healing.

Keywords: *vascular self-healing, concrete, four-point bending, Inorganic Phosphate Cement (IPC), clay, tube shape*

Abstract

Optimalisatie van vasculaire zelfhelende systemen en evaluatie door middel van vierpuntsbuiging.

Gerlinde Lefever
Master of Science in Civil Engineering
Construction and Geomaterials

Jannes Van Cauwenberghe
Master of Science in Civil Engineering
Water Resources

2015-2016

Beton behoort tot een van de meest gebruikte bouwmaterialen. Ondanks de goede prestaties en relatief lage kost, is stalen wapening onmisbaar om de lage treksterkte te compenseren. Scheuren zullen echter toch ontstaan, met als gevaar het insijpelen van reactieve substanties en corrosie als gevolg. Inspectie en onderhoud zijn duur en moeilijk uit te voeren. Zelfhelend beton kan deze nadelen elimineren.
Zelfheling met behulp van een vasculair netwerk is een biologisch geïnspireerde techniek waarbij holle buisjes, gevuld met zelfhelende vloeistof, in beton worden geplaatst. Voor onderzoek werd deze techniek verkozen omwille van haar potentieel tot meervoudige heling.
De doelstelling bestaat uit twee delen: enerzijds de scheuren waterdicht maken en anderzijds het herstellen van de mechanische eigenschappen. De focus wordt gelegd op het verbeteren van de huidige techniek door de overlevingskans tijdens het storten te vergroten, alsook de kosten te verminderen. De vasculaire buisjes worden vervaardigd uit klei en anorganisch fosfaatcement (IPC) door extrusie en gietwerk in mallen respectievelijk. Een reservoir ter opslag van helend agens, bereikbaar van buitenaf, wordt in het betonnen element gegoten. Dit reservoir is 3D-geprint in polyamide en verbonden met de buisjes. Om de weerstand tegen storten te vergroten, worden verschillende vormen onderzocht. Uiteindelijk worden betonnen balken met dergelijke vasculaire systemen getest onder vierpuntsbuiging met een succesvol resultaat als gevolg.

Sleutelwoorden: *vasculair netwerk, zelfhelend beton, vierpuntsbuiging, Inorganic Phosphate Cement (IPC), klei, vorm buisjes*

Résumé

Optimisation des systèmes d'auto-guérison vasculaires et l'évaluation par flexion à quatre points.

Gerlinde Lefever

Master of Science in Civil Engineering
Construction and Geomaterials

Jannes Van Cauwenberghe

Master of Science in Civil Engineering
Water Resources

2015-2016

Le béton est l'un des matériaux de construction les plus utilisés. Malgré sa bonne performance et un coût relativement faible, des renforcements en acier sont indispensables afin de compenser sa faible résistance à la traction. Néanmoins, des fissures sont facilement induites, qui peuvent provoquer l'ingression de substances agressives, ce qui cause la corrosion de l'armature. L'inspection et la maintenance sont chères et difficiles à réaliser. L'auto-guérison vise à éliminer ces inconvénients. L'auto-guérison vasculaire du béton est une technique bio-inspirée, où un réseau de tubes creux, remplis d'un liquide de guérison, est intégré dans le béton. Parmi les différentes techniques, celle-ci est choisie, en raison de son potentiel de guérison répété.

Les objectifs principaux sont d'un part à sceller les fissures, pour éviter la pénétration des liquides agressifs, et d'autre part de récupérer les propriétés mécaniques. L'accent est mis sur la mise à l'échelle de la technique existante en améliorant l'applicabilité pendant le coulage du béton et en réduisant le coût de production. Les tubes du système vasculaire sont faits en ciment inorganique (IPC) et en argile. Ils sont fabriqués en utilisant respectivement un moule et de l'extrusion. Un réservoir, accessible de l'extérieur, est prévu dans le béton et conserve l'agent de guérison. Le réservoir est imprimé en polyamide et relié aux tubes. Afin d'améliorer la résistance à l'écoulement, différentes formes de tubes sont examinés. Enfin, des poutres en béton contenant des systèmes vasculaires sont testées par flexion à quatre points, ce qui a donné la réussite de l'auto-guérison.

Mots clés: *auto-guérison vasculaire, béton, flexion à quatre points, Inorganic Phosphate Cement (IPC), argile, forme de tubes*

List of Figures

List of Tables

Introduction

Concrete possesses a high compressive strength, resistance against high temperatures and is a relatively low cost material. On the other hand, the tensile strength of concrete is low, what makes this material sensitive to crack formation in its tensile zones [1]. In order to take up these tensile forces, steel reinforcement is used. It contributes in limiting the crack width, but will never totally prevent crack formation. Cracks limit the service life of a structure as they allow for aggressive substances to penetrate into the material and cause damage inside. When these substances reach the reinforcement bars, corrosion is likely to occur and will eventually lead to fatal collapse.

The maintenance and repair is thus crucial to extend the service life of a construction. To have an idea: in the U.S. the annual economic impact for maintaining, repairing or replacing damaged structures is estimated at $18-21 billion [2] for 2020. In addition, it is estimated that half of the repairs are short-lived, which means they will need re-repairing. Each time a construction needs to be repaired, it has to be inactivated. This leads to social and environmental costs; for example, when a bridge has to be repaired, it is not possible to use it during the reparation. Each day that this bridge is inactive, the cost for society gets higher.

A second aspect concerns the production of concrete itself. The raw materials that are used in the production process have a relatively high energy consumption and greenhouse gas emissions [3]. The CO_2 production of cement is estimated at 5-7% of the total CO_2 production in the world.

A solution to these problems can be found in using the self-healing ability of concrete. It provides the advantage that structures can be healed while performing their task. As a result, costs of maintenance and repair are diminished and lifetime is increased, however, with an increase in initial cost [2]. The concept of self-healing is a topic of many interests. Within the last few decades self-healing has proven its reliability on small-scale specimens. The aim now is to upscale the concept of vascular system for industrial use.

Literature review

2.1 Self-healing processes

Self-healing processes can be divided into two main categories: intrinsic or autogenous healing and autonomous healing. Within these two main categories, distinction is made between the different techniques that give rise to the self-healing process in the cracked concrete matrix. The scope of the master thesis is on autonomous self-healing. It is however only complete to give an introduction about the process and results of autogenous healing as well.

2.1.1 Intrinsic healing

Intrinsic healing concerns all techniques that make use of the self-healing capabilities of concrete itself. Thanks to the composition of the cement matrix, self-healing can be seen as being inherent to the material. A partition can be made between the mechanisms that are fully autogenous and the ones that are helped by additives.

Autogenous healing

Autogenous healing results mainly from two mechanisms, being: hydration of unhydrated cement particles, shown in figure 2.1, or the dissolution and carbonation of $Ca(OH)_2$ [1], according to following chemical reaction: $Ca^{2+} + 3\,H_2O + CO_2 \rightleftharpoons CaCO_3 + 2\,H_3O^+ + 2\,OH^-$. In both cases, water is essential to be present.

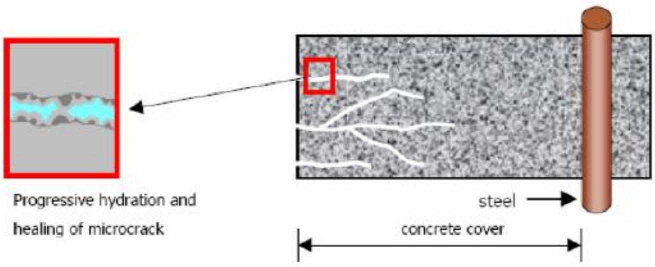

Figure 2.1: Schematic reproduction of the hydration process [3]

Whichever of these two mechanims will occur depends on the age of the concrete. At early age, concrete holds a high amount of unhydrated cement particles, making hydration of unhydrated cement particles most likely to occur. As cracking occurs, these unreacted particles may get in touch with moisture that intrudes the crack. Upon this contact, hydration can occur, which will (partially) fill the crack. In aged concrete, the most important healing mechanism will be the precipitation of $CaCO_3$ [4].
Although autogenous healing seems to be an easy and effective solution for healing cracks, a drawback is that it is only effective when crack widths are between 200 and 300 μm [4].

Improved autogenous healing

In order to make autogenous healing more effective, the healing mechanism may be helped by additives or a restriction of the crack width as been summarized by K. Van Tittelboom et al. [1]. Three different methods are described underneath:

1. **Use of expansive additives**
   Upon contact with water, these additives expand and close cracks. An example are sulfoaluminate based agents [3] but more commonly used are SAPs, which is short for superabsorbent polymers (also called hydrogels). They are capable of absorbing huge amounts of water, up to 100 times their volume. The swelling of the particles is due to osmotic pressure, but depends strongly on the alkalinity of the solution [5, 6]. When the SAPs are mixed in fresh concrete, swelling starts. Water is returned afterwards for hydration of the cement particles. The SAPs now shrink and leave small pores. As further cracking occurs, the cracks will propagate through these pores and make it possible for liquids to enter. The SAPs will then swell again, blocking the crack entrance. The power of these SAPs is thus more related to self-sealing than self-healing, since regain in strength is not considered.
   A drawback of working with SAPs lies in the pores that are formed after hydration. These pores provide a reduction in strength of the concrete. A solution could be the modification of the polymers as tried by Lopez-tendero et al. [7] to prevent the SAPs from swelling at high pH level, since the pH inside concrete is quite high during mixing.

2. **Hydration by using pozzolanic materials**
   Pozzolanic materials, such as fly ash, can be added to the concrete mixture. A large amount of these materials will remain unhydrated and therefore they can be used to promote autogenous healing of the cracks by hydration [1, 8].

3. **Restriction of the crack width**

   It was seen that autogenous healing could be only effective when crack widths are small (between 200 and 300 μm). A possibility for increasing the self-healing capacity is then to limit the crack width. This can be done by using fibres. A comparison has been made by Homma et al. [9] between different types of fibres. Three different specimens were prepared and tested, using polyethylene fibres, steel cord and a combination of both. Results showed that many crystallization products were found when using polyethylene. These products were found on the crack surface, as well as on the fibres themselves. In the specimens containing only steel cord, none of this crystallization has been seen. Even more, the steel cord started to corrode, causing an expansion inside the concrete material. However this corrosion effect was also observed in the so called hybrid specimens, a tension test pointed out that the combination of steel cord and polyethylene provided an increase in strength recovery. Some years later, Nishiwaki et al. [10] made a similar comparison, but using polypropylene, ethylene vinyl alcohol, poly vinyl alcohol and polyacetal. The conclusion remains the same, being: the use of synthetic fibres increases the self-healing capability of the concrete. The synthetic fibres act as a precipitation surface. Since more precipitation in the cracks means more healing product, the effectiveness is proven.

Autogenous healing using bacteria

This self-healing technique is based on the application of mineral producing bacteria. The process of self-healing consists in calcium carbonate formation by the ureolytic bacteria: carbonate ions precipitate with the calcium ions present in the concrete or added in the form of a mineral precursor and in this way, calcium carbonate minerals are formed that help closing the crack.

For a long time, only the external application of bacteria was studied [11]. This method is very labour intensive and cannot really be seen as a self-healing technique.

To overcome the costs of inspection and application, H.M. Jonkers et al. [11] made a study about incorporating bacteria in the concrete matrix. The bacteria should be able to resist mechanical stresses due to mixing, withstand high alkalinity (because of the formation of portlandite) and be oxygen tolerant. A match with these criteria was found within the genus Bacillus.

A possible problem concerns the viability of the bacteria within the concrete matrix: the bacteria have to remain viable for a long period of time to be able to act as a self-healing mechanism. Tests pointed out that the viability of unprotected spores was lower than 4 months, even though they should have a viability of more than 50 years when kept in dry state. The cause of this shortened viability is likely due to the ongoing hydration process, which affects the pore size diameter. When the pore diameter becomes smaller than the size of the encapsuled bacteria, viability is over. A solution for this was found in using porous expanded clay particles, where bacteria and precursor

compounds are placed in [12]. The outcome of placing the clay particles into fresh concrete showed that no loss in viability was to be seen after six months, which is more in accordance to the viability in dry state.
With regard to the strength, results showed that adding a large number of bacteria lowered the strength, except when adding calcium lactate, which even gave a small increase in strength development [11]. As calcium lactate can work as a precursor compound, this is an ideal solution to lift both the self-healing as the strength of the concrete to a higher level.
With the aim of investigating the self-healing effectiveness, both a control sample (holding clay particles without bacteria or precursor) and a bacteria sample were fabricated. It can be seen in figure 2.2 that in the control sample (without bacteria) mineral precipitation occurred near the crack, while in the sample using bacteria it occurs inside the crack.

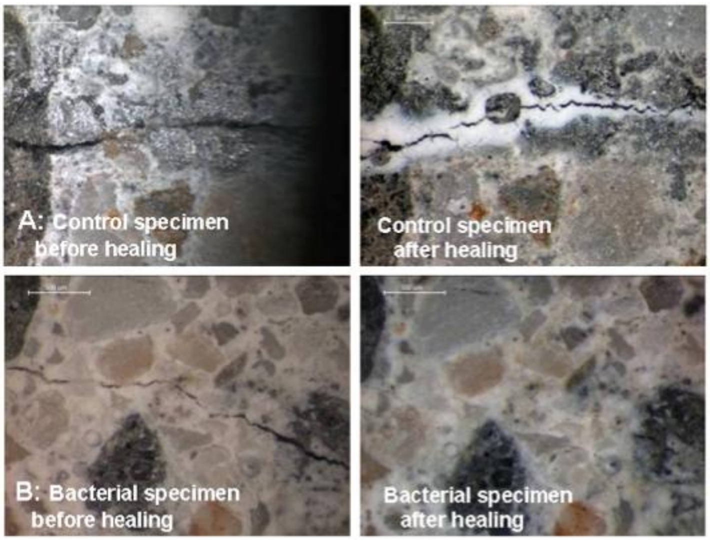

Figure 2.2: Light microscopic images (40x magnified) of pre-cracked control (A) and bacterial (B) concrete specimen before (left) and after (right) healing (2 weeks submersion in water) [12]

A simple permeability test revealed that the samples with bacteria are completely watertight. It can thus be concluded that bacteria have a significant effect on the self-sealing of concrete and are very promising for the future.
The question arises if this type of self-healing is economically feasible. A study conducted by Silva et al. [13] stated that the price of a cubic yard of concrete with self-healing bacteria in hydrogel capsules is around $\$4932$. To have a better idea of this cost value, a cubic yard of traditional concrete costs about $\$100$ [14]. An estimation to produce this self-healing system in an unsterile location was set on $\$611/yard^2$. Using epanded clay particles instead of hydrogel capsules would decrease the cost to $\$137/yard^2$, which is more acceptable from an economic point of view. Ofcourse, the large difference in price between hydrogel encapsulation and non-

self-healing concrete should be placed in its context: the cost of repair of concrete structures was estimated at $\$18-21$ billion per year in America [2].

2.1.2 Autonomous healing

In the previous chapter, the intrinsic healing properties of concrete and the different autogenous healing techniques were discussed. Besides the capability of concrete to heal itself, chemicals can be introduced with the ability to fill cracks if they occur. There are mainly three techniques to introduce these chemical liquids, being the healing agent: by encapsulation, by means of a vascular system or by applying the healing agent by hand. The latter is however very labour intensive and cannot be seen as 'self'-healing. Both the other techniques are discussed in the next paragraphs.

Capsule based self-healing

Chemical encapsulation is a technique where capsules, filled with a chemical fluid, are placed inside the concrete. The main idea is that, when cracks occur in the concrete piece, they will reach a capsule and the capsule will burst with the result that the encapsulated healing agent leaks out and fills the cracks. The fluid then reacts with material inside the concrete such that solid material is deposited in the crack to fill it. "*While some agents react upon contact with moisture or air or due to heating (Figure 2.3 A,B) or upon contact with the cementitious matrix itself (Figure 2.3 C,D), other agents react when making contact with a second component which is present in the matrix (Figure 2.3 E,F) or provided by additional capsules (Figure 2.3 G,H)*", Van Tittelboom and De Belie [1]. When a crack is filled - permeability properties are regained - but the mechanical properties are less than before, it is said that the concrete has a self-sealing ability. On the other hand, having a regain in strength compared to a non-self-healing sample is considered as self-healing.

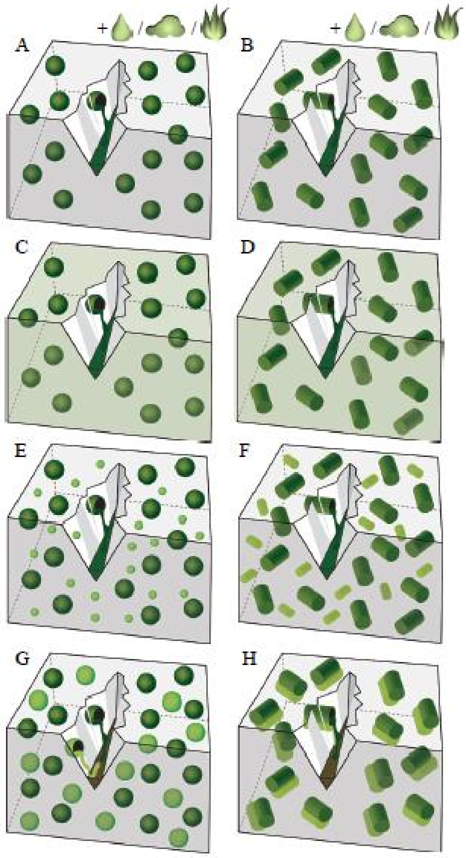

Figure 2.3: "*Capsule based self-healing approaches. Leakage of healing agent from the capsules into the crack due to gravitational and capillary forces. Reaction of spherical/cylindrical encapsulated agent (dark colored inclusions) upon contact with (A,B) moisture or air or due to heating; (C,D) the cementitious matrix; (E,F) a second component present in the matrix (small, light colored inclusions) or (G,H) a second component provided by additional capsules (big, light colored inclusions).*", Van Tittelboom and De Belie [1]

Healing agents

There is a wide range of healing agents available and many more still have to be investigated. The different reaction types and accompanying encapsulation methods are given in figure 2.3. A good agent should have a viscosity low enough to flow easily into the cracks due to capillary and gravity forces. On the other hand, the agent should stay in the crack for some time. If the viscosity is too low, the agent will leak out the cracks or disappear in the concrete matrix. A second property is the reaction time. It is preferable to have a fast reaction, such that the agent won't leave the crack and the crack can be filled in minimal time. However, a very fast reaction could be negative as well. The agent needs time to flow into the crack. If the agent for example hardens directly, before reaching the crack, the crack will not completely be healed. Furthermore, the healing agent should be efficient, stay active for a long period (as concrete structures have a typical life span of 50 to 100 years) and it is preferable to have the same or even better mechanical and permeability properties than before. At last, when the agent leaks out the capsule, and additional empty space is created. Part of this space could be filled if an expanding healing agent is used [1].

Some examples of healing agents upon which research has been done are listed below. Healing agents can be one-component (react upon contact with air, moisture or concrete) or two-component systems (react upon contact with each other). The advantage of a two-component system is that it has a longer lifetime.

- A saturated $Ca(OH)_2$ solution reacts with the unhydrated cement particles present in the cement matrix to form portlandite (solid $Ca(OH)_2$). This is the main healing process, together with the further hydration of unhydrated cement. If the solution is not saturated anymore, CO_2 will react with the healing agent to form $CaCO_3$ crystals. The latter reaction just takes place if the agent is in contact with CO_2. The forming of portlandite only happens if the agent reaches the cement. The advantage here is that premature hardening is avoided. [1, 15]
- Cailleux and Pollet [16] studied a mechanism where bisphenol-F epoxy resin is encapsulated inside spherical microcapsules, embedded inside a concrete repair mortar. Inside the mortar matrix, a hardener was dispersed that would cause a polymerization reaction with the epoxy resin. [1]
- "*Yang et al. [17, 18] used silica gel shell microcapsules filled with MMA monomer and triethylborane (TEB) serving as initiator. They showed that it was possible to mix the microcapsules into a mortar matrix and that contact of both components, after capsule breakage, resulted in bonding of the crack faces*", Van Tittelboom and De Belie [1]
- A two-component polyurethane based healing agent was used together with tubular glass capsules by Van Tittelboom et al. [19]

Capsules

Capsules should be designed that they survive mixing and pouring of concrete. It is essential to have a good bound between concrete and capsule, such that the capsule will crack and not slip. Preference is given to brittle capsules with low tensile strength; ductile capsules are more likely to deform instead of cracking. The problem however, is that the brittleness of the capsules increases drastically the chance of breakage during the mixing process and makes automation of the concrete fabrication on large scale difficult. One solution could be the use of a material that is initially ductile and flexible - this is the state where the capsules are mixed in the concrete - but becomes more brittle over time. Another option is to produce capsules of different materials. An example is gelatine-IPC, where the gelatine is used to encapsulate the healing agent and the IPC is used to have a good bonding with the concrete matrix. The combination of both makes it possible for the capsules to survive the mixing process [20]. Untill now, mostly glass capsules were used. The problem with glass capsules is the alkali-silica reaction that occurs upon contact with concrete, which forms an expansive calcium silicate gel and causes pressure inside the material. Hilloulin et al. [21] proposed to make use of polymeric capsules with a low glass transition temperature. Examples of these materials are: polylactic acid, polystyrene and polymethyl methacrylate/n-butyl methacrylate. To be sure these capsules would survive the mixing process, the capsules are heated so they become rubbery, which is a significant improvement compared to glass capsules. Polymer materials show a brittle behaviour and have elongation at rupture lower than 10%. This property is ideal for application in self-healing systems, since the capsules should break when the cracks in concrete pull them apart. Added to this, these polymer materials provide a higher tensile strength than concrete and a bond strength more or less equal to the one of glass and concrete; so they will not negatively affect the strength of the concrete specimen. The main drawback of using polymer capsules is the heating before mixing, certainly for industrialization.

The chance that a crack will hit a capsule, strongly depends on the amount of capsules and their shape and size. A high amount of capsules increases the chance of healing, but also increases the costs and decreases the concrete strength. The fracture probability is higher for cylindrical capsules than spherical, due to a higher surface to volume ratio. Another important factor in the probability of capsule hitting is the type of healing agent. If the healed cracks are less strong than before damage, the crack may form again at the same place and the same (empty) capsules may be hit. If the healed cracks become stronger than before, new cracks will follow a different path and meet other (unused) capsules.

It is desirable not to weaken the concrete piece by placing capsules inside. The shape and material has to be chosen in a way that a good compressive strength is provided. On the other hand, a low tensile strength is needed for the capsule to crack when the concrete does. Big capsules modify the concrete properties more than small capsules since bigger ones introduce a more inhomogeneous structure. A cylindrical shape introduces anisotropy. "*Spherical capsules will have less influence on the mechanical properties as their shape reduces the stress concentrations around the void left from empty capsules*", Joseph et al. [22] The material may not degrade over time, nor may cause degradation reactions with the concrete components or steel reinforcement. No chemical reactions may occur with the healing agents. An example here is glass, where unwanted alkali-silica reactions may be induced when a high amount of alkalis are present in the matrix.[1]

Self-healing using a vascular system

Healing of concrete by use of a vascular system is a bio-inspired technique where a network of hollow tubes, filled with a healing agent, is embedded in the concrete matrix. The main idea is that when cracks occur in the concrete piece, these cracks will reach and break tubes allowing for the healing agent to leak into the concrete and fill the cracks. The simplest vascular system consists of a long tube or a series of parallel long tubes. This could be, for example, used in beam elements, where the tubes are installed close and parallel to the steel reinforcement. More complex networks are possible too, but are more difficult to produce.

Dependent on the used type of healing agent(s), a single or multiple vascular system is needed. If the chemical reaction is due to a one-component healing agent, the whole network (or all tubes) is filled with the same agent (Figure 2.4 A). For a multi-component healing agent, several separated networks (or tubes) are embedded so that the different networks are close to each other (Figure 2.4 B). The system can eventually get connected with the exterior of the structure. By doing so, healing agent can be added from outside. [1]

The material used for the vascular system has to satisfy several requirements, such as being chemical inert, having a high brittleness, not lowering the strength of the object (too much) and providing a good bond with the concrete. The usage of glass has already been investigated and led to good results in first instance. However, in combination with concrete, alkali-silica reactions are induced which cause damage. One of the objectives is thus searching for another material, since no ideal material has been found so far.

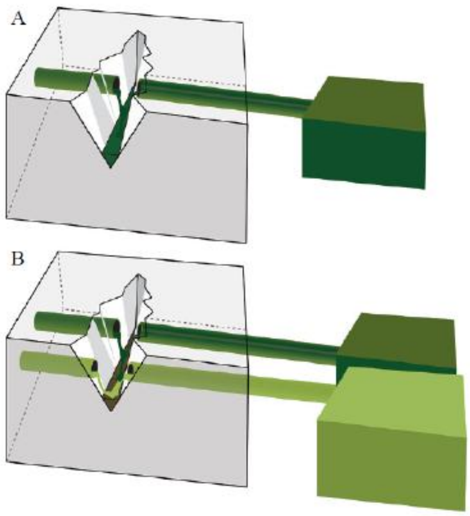

Figure 2.4: "*Vascular based self-healing approaches. Leakage of healing agent from the tank via the vascular into the crack due to gravitational and capillary forces and eventual (hydrostatic) pressure. One-channel (A) and multiple channel vascular system (B).*, Van Tittelboom et al. [1]

The healing agents are drawn into the cracks by capillary forces and gravitational forces. In case the tubes are connected with the exterior and supplied by healing agent, a pressure can be exerted to push the healing agent into the cracks and to possibly clean the system. "*Advantage is that the efficiency is not influenced by the absorption of matrix because the amount of liquid healing agent is unlimited. Therefore, there is a higher probability to realize self-healing by using a vascular system than by using capsules to supply healing agent to cracks. However, this is based on a premise that the cracks cross any parts of the vascular system. This depends strongly not only on the distribution of the vascular system in structures, but also on the depth of cracks.*", Huang H. et al. [15]. They noticed that healing cannot occur infinitely, while agents can be added from outside. After a certain amount of healing cycles, the damage to the vascular system is too high and hardening inside the system can happen, so that the network can get intermittent.
An upper limit to the crack width exists. If the cracks are too wide, the agent will just leak out of it. Mechanisms exist to reduce the crack width, but are not further discussed here.
Until now, one may have the impression that a vascular approach on self-healing has many advantages in comparison with capsules. However, there are some drawbacks that keep this technique from being applied on large scale. A first disadvantage is the existence of non-homogeneous properties of a vascular system, especially the use of a tube system. In a beam for example, place of cracking may be predicted since damage occurs in the places where tension is present. In these spots, close to the reinforcement, tubes can be installed. This is only in the theoretical case, and in more complex structures a prediction of cracking is very difficult. Healing only occurs if the cracks intersect the tubes. Cracking parallel to the vascular system excludes healing possibility. However, it should be noted that concrete properties are non-homogeneous too. An alternative could be the use of a hollow network that consists of porous concrete, as explained by Sangadji and Schlangen [23, 24]. In this technique, porous concrete cylinders, surrounded by a PVA film, are casted inside the concrete structure. The PVA film dissolves when the normal, dense concrete is casted around the porous cylinders. Exchange of fluids (healing agents) between both parts is possible, since the PVA film is dissolved. Sensors can then detect damage and healing agent can be pumped through the porous network. A second disadvantage is the embedding into the concrete. The system has to be installed before the concrete is cast. The movement of liquid concrete and the forces due to casting may result in a fractured vascular system.

Healing agents

The discussion on healing agents is mostly similar to the one in section 2.1.2. The agent should stay reactive for a long time and in the meanwhile no reactions with the vascular system may occur. A one-component healing agent tends to be more effective than a multi-component. For the latter, the different agents should mix in the same crack. The chance of fracture of the different tubes in the same location is quite small. In practise, a two-component agent may be effective only if the two different tubes lie against each other.

2.1.3 Conclusion

The research during our master thesis will focus on the two autonomous techniques discussed above. A table is made to summarize the different techniques of self-healing and some important properties are included as well as the current availability at the MeMC department of the Vrije Universiteit Brussel.

Table 2.1: Summary of self-healing processes

	Intrinsic			Autonomous	
	Autogenous	Improved autogenous	Bacteria	Capsules	Vascular system
Repeatable	Good	Good	Not known yet	Poor	Possible
Quality	Only small cracks	Bigger crack width but still limited	Self-sealing; regain of mechanical properties is minimal	Medium recovery currently	Good recovery currently
Shelf life	Long	Long	Current restriction of 6 months	Long shelf life possible	Long shelf life possible
Available	Yes	Yes	No	Yes	Yes

2.2 Self-healing measuring techniques

The question arises if we can be sure that self-healing has taken place and if yes, in what quantity and quality did it manage to heal the cracks. Therefore measuring techniques are required. In the following section some are explained.

2.2.1 Acoustic emission

Acoustic emission is a non-destructive technique (NDT) that measures the elastic energy emitted by cracking of a material. The released energy propagates as a wave through the material and will eventually reach a sensor. The arrival of a wave is registered as a hit. In post processing, when different sensors received a hit around the same time, it will be registered as an event. In this way noise and false hits are eliminated. Acoustic emisson tests have various applications. It can be used to simply count the number of events while cracking or to determine the position of a crack. In the latter case, more than one sensor is needed. The time for an event to reach the sensor is then compared for all sensors, giving the position of crack occurence.
In order to evaluate the self-healing, K. Van Tittelboom et al. [25] made use of eight acoustic emission sensors, being piezoelectric transducers, that are evenly distributed over the sample. The setup is shown in figure 2.5 and represents a three-point bending test. The sensors are represented by circles and are coupled to a computer.

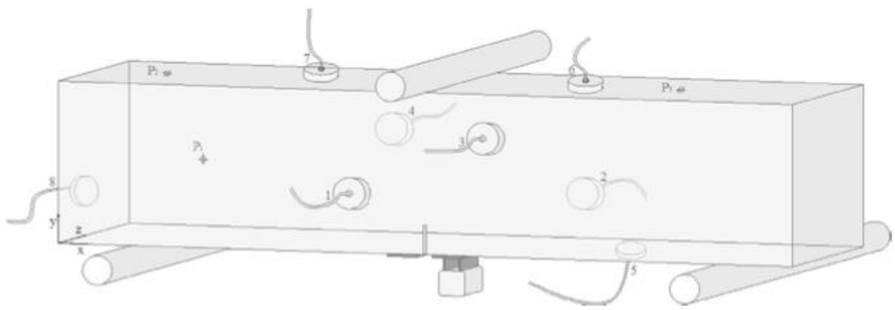

Figure 2.5: Positioning of the sensors [25]

As a conclusion it can be stated that acoustic emission has proven to be effective for knowing if tubes or capsules have been broken upon cracking. Given that it is a non-destructive technique only makes it more desirable to use.

2.2.2 Ultrasonic pulse velocity

The velocity of a propagating wave depends on the properties of the surrounding medium. A wave holds energy, that can propel or bump onto inhomogeneities of the medium. The more pores, coarse aggregates or even cracks a material possesses, the bigger the chance of energy being scattered. When energy is scattered, the velocity of the wave slows down. An ultrasonic pulse velocity test measures the velocity of the waves in a material. By comparing the value of the pulse velocity in a cracked beam with the one in a reference specimen, damage can be determined, as sketched in figure 2.6.

H. Huang et al. evaluated the self-healing efficiency by means of a UPV-test [15]. Also, a vascular system was added to the reinforced concrete beam.

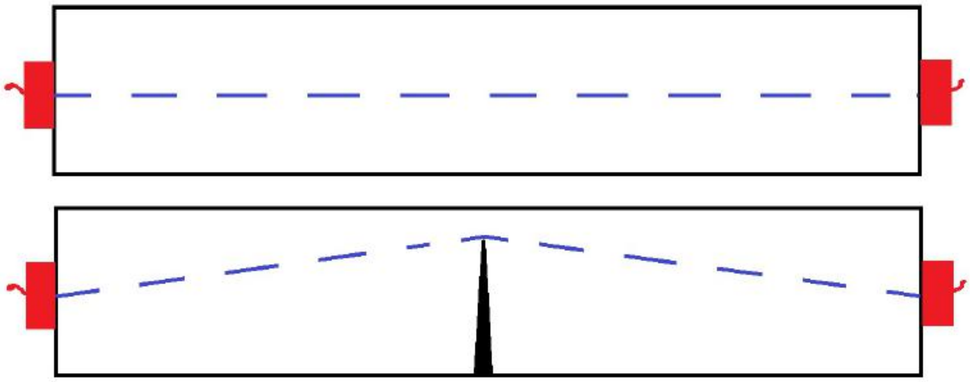

Figure 2.6: Propagation of sound through uncracked (above) and cracked (below) material

For self-healing, the main application is as following: the velocity of a longitudinal wave will be measured during the cracking and healing process. A comparison is made between a reference specimen (without self-healing capacity) and the one provided with a vascular system. We have to note here that Huang et al. made use of a vascular system that is connected with a container of $Ca(OH)_2$, which means that healing agent is inexhaustive. The results of the UPV-test are shown in the graph below.

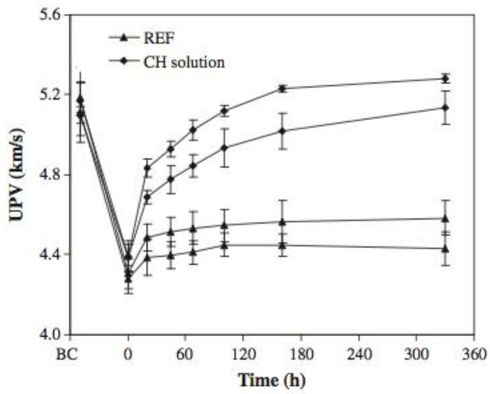

Figure 2.7: Summary graph of the measured pulse velocity in different specimens [15]

The first measured value in the graph is the velocity before cracking. After cracking, the velocity decreases strongly for the reasons explained above. Because of unloading, the curing of the specimens can start. The steel bars in the reference specimens return to their initial length and decrease the crack width. It can be seen in the graph that the UPV restores, however it does not reach the initial UPV anymore, because cracks are not fully closed. At the contrary, the UPV of the specimens with a vascular system (the two upper curves of figure 2.7) restores for more than 100%, but healing is not only due to the vascular system: further hydration of cement particles also has his part in this process.
In accordance with acoustic emission, UPV seems a good way of evaluating the self-healing efficiency. Added to that, UPV tests are non-destructive as well, which makes it a useful test for operative structures. However, UPV will not be used for this application but rather to find the depth of cracks.

2.2.3 Water permeability

The biggest problem of cracks in concrete is that they allow for aggressive liquids and gasses to enter the material, which causes corrosion of the steel reinforcement bars. To avoid this, water permeability should be kept at a low value. Therefore, a water permeability test can be done to evaluate the self-healing in concrete materials.
Homma et al. [9] performed a water permeability test on fibre-reinforced concrete. The water flow through the specimen and the difference of pressure head was measured and the water permeability coefficient k has been calculated by means of the formula:

$$k = l\frac{A'}{A \cdot t} ln\frac{h_0}{h_1} \tag{2.1}$$

where A' is the area of cross-section of the pipe, A is the surface area of the specimen, t is the time, h_0 is the initial pressure head and h_1 is the pressure head at time t. The set-up is shown in figure 2.8.

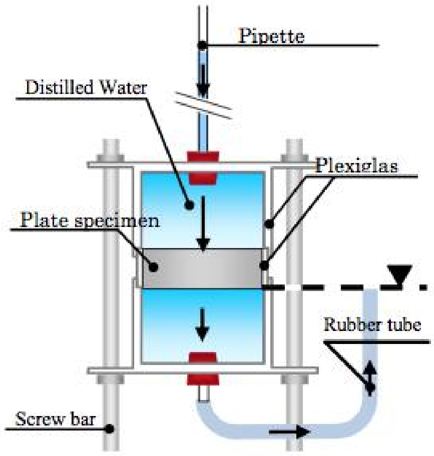

Figure 2.8: Schematic description of the water permeability test [9]

The coefficient of water permeability was calculated for different crack widths and it was seen that k increased with increasing crack width. This is as expected: larger openings cause more ingress of liquids. Homma et al. [9] also studied the time dependancy of the water permeability coefficient. Results show that k decreases strongly in the first three days after cracking. After these three days, the decrement slows down. These results were compared with the variation in thickness of cristallization products over time. Here it was seen that the thickness of cristallization products increased strongly the first three days and afterwards, the curve flattened. It was therefore concluded that the cristallization was the main cause of the decrease in water permeability, and thus that self-healing in concrete materials can be monitored by measuring the water permeability.

2.2.4 Digital image correlation

Digital Image Correlation (DIC) is, similar to acoustic emission, a non-destructive measuring technique. It offers the ability to determine in-plane displacement fields at the surface of objects under any kind of loading. It is of particular interest to study crack propagation and material deformation to check the damage during testing and the crack propagation through the known position of capsules and vascular system.

DIC is an optical measuring method that compares digital photographs of the object at different stages of deformation, which are represented by different speckle patterns. By comparing those pictures, software is able to create displacement vector fields and strain maps. In order to compare those images, a speckle pattern has to be present on the studied surface. Those speckles could be placed on the surface, but can also be the natural look of the surface itself provided that the material has a non-homogeneous appearance. It is important to have a non-repetitive, isotropic, high-contrast speckle pattern for good results (see 2.9). The change in position of those speckles is then processed by software to calculate the results.

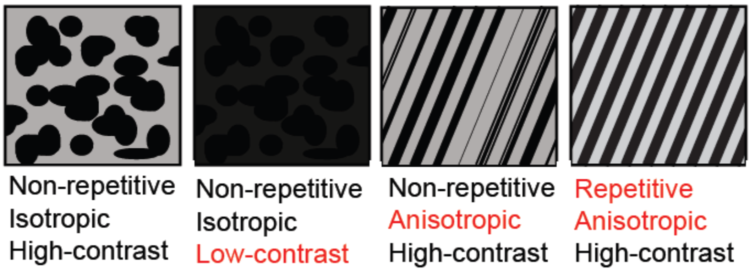

Figure 2.9: Different speckle patterns and their weaknesses marked in red [26]

The images can be made by a large variety of optical sensors, for example a CCD camera, high-speed video and several microscopes. The speckle pattern plays an important role in the accuracy of the results. Medium sized speckles with a limited spectral content tend to be the most accurate. [27] The advantages of this technique are that there is no contact between object and measuring set-up; it is suitable accurate for its low cost and it can be used outdoors.

An example is given in figure 2.10, where a reinforced concrete beam undergoes a three-point bending test. It is quite easy to see where the main crack occurs, but smaller cracks present in the beam are not very visible. By use of DIC these small cracks will be detected and given in the results. [28, 27, 29]

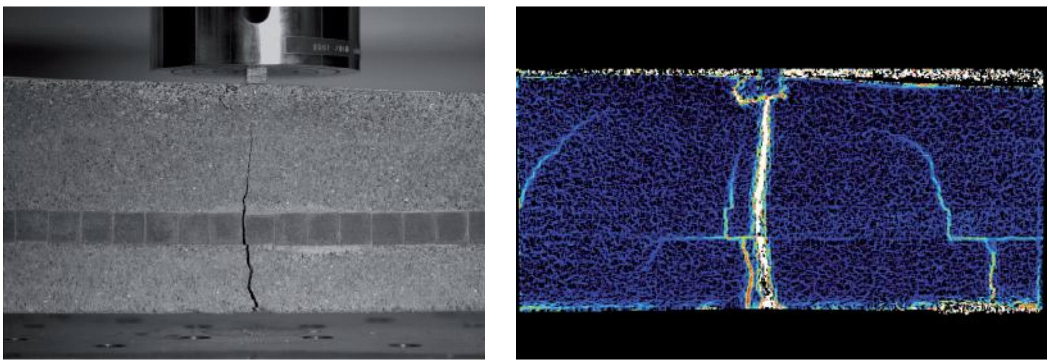

(a) (b)

Figure 2.10: (a) Main crack visible of a bar that undergoes a three-point bending test and (b) Micro cracks visible by means of DIC [28]

2.3 Extrusion process

Extrusion is a production process used to make objects with a fixed cross-sectional profile. This process is of particular interest for the production of tubes, which are used in the self-healing vascular system. One of the advantages is that extrusion is a continuous process that allows the making of very long tubes. The ability of making very complex cross-sections is another advantage. In figure 2.11, an example of an extrusion machine is shown. The design of such machines depends on the material that has to be extruded, but the main principle stays the same. At the very beginning of the process, the extruding material is supplied. For plastics, pellets is most common. Other materials are also possible, like metals and ceramics; the latter one is of particular interest with the eye on producing vascular tubes. The next step might be the heating of the material in order to increase the workability, eventually together with the mixing of the different components. If the workability of the material is enough at room temperature, no heating is required. The heating process can happen along the length of the screw, which brings the material towards the die. For solid ceramics however, the function of the screw is taken over by a ram. The ram pushes the material towards the die and can build up some pressure. Between die and screw (or ram), a breaker plate might be placed. This breaker plate helps increasing the pressure and has the ability to filter impurities. The last step of the form-giving process is the pressing of material through the die. The die is designed to give the tube the desired cross-section. The tube at the outlet of the die might not be very strong due to the increased workability as mentioned before. For heated extrusion, the tubes must be cooled in order for them to become solid and steady. This cooling process can be done by entering a (water) cooling bad. For ceramics on the contrary, an oven is installed so that the ceramics can harden.

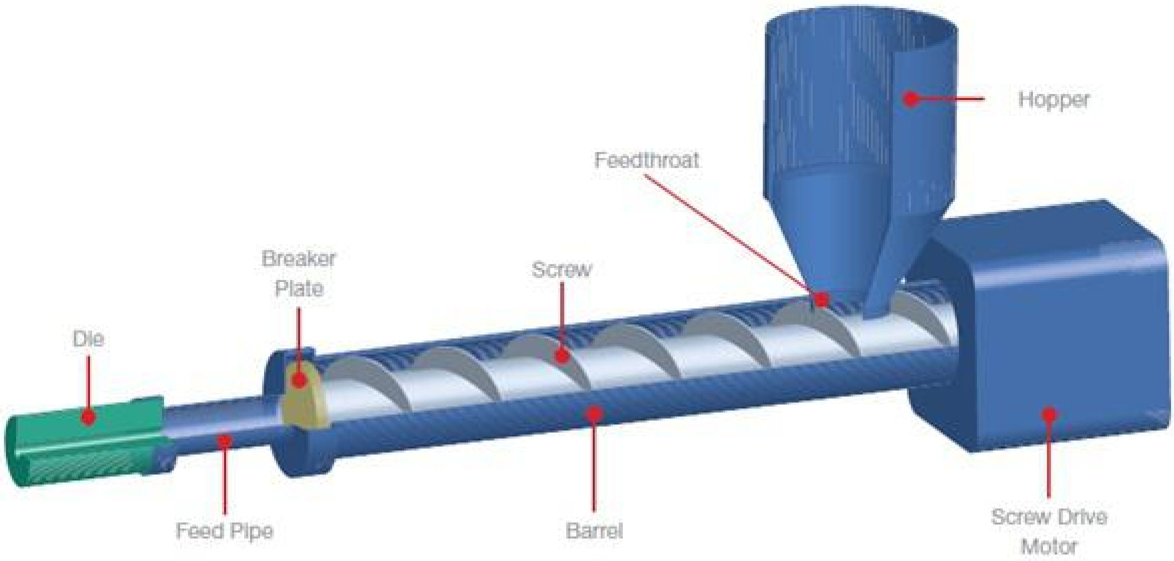

Figure 2.11: Schematical representation of extrusion machine for plastics [30]

Note that a supporting mechanism has to be provided to support the tubes, otherwise they can break under their self weight. A cutting device will cut the tubes in pieces at the desirable length. [31]

2.4 Application on large scale

For self-healing to be used on large scale, some emerging issues concerning the industrialization should be investigated. Since many of the capsules and vascular tubes break during the mixing/casting of the concrete, this will be the key issue to solve. In order to validate the results of laboratory tests, a large-scale test was set up by De Belie et al. [32] and later on by Van Tittelboom et al. [33] on beams of $150mm$ x $250mm$ x $3000mm$. The first self-healing system tested was composed of around 350 glass capsules with a polyurethane based healing agent. The glass tubes were glued on a network of wires within the mould. A second specimen using SAPs was prepared next to it. A four-point bending test was performed after 28 days of curing. Afterwards, the beams were showered with water for six weeks, everyday four times. Non-destructive testing pointed out that self-healing took place, but it can clearly be seen that this way of working is not ideal for industrialization (cfr. the network of wires with glued-on glass capsules).

Materials and methods

3.1 IPC tubes

A first material choice to produce the tubes that yield the healing agent is Inorganic Phosphate Cement (IPC). The choice is based on the material properties - such as a good bonding with concrete, brittleness and low tensile strength - and its availability at the MeMC department. It is known that IPC can be used for tube production since it does not react with the healing agent and the tubes do break upon breaking of the concrete beams.

3.1.1 Inorganic Phosphate Cement

Inorganic Phosphate Cement, short IPC, is a cementitious material developed at the Vrije Universiteit Brussel. It consists of a calcium silicate powder (wollastonite) and a phosphoric acid-based solution of metal oxides [34]. A retarding agent, to increase the workability time of the mixture is also added to the solution and the total liquid solution is called B23. The mass proportion of wollastonite to B23 is 82/100 [35]. IPC hardens at room temperature, but adding heat accelerates this hardening process, since it is an endothermic reaction. IPC has properties similar to materials that contain Portland cement. Thanks to this property, a strong bond between concrete and tubes will be created.

IPC is a ceramic material; ceramic materials originate from heating. The compressive strength decreases with increasing temperature from $105°C$, but at $800°C$ the strength increases. Identically, the stiffness starts to increase between $700°C$ and $800°C$ when reaching the glass transition temperature of some phases.

The most important properties of IPC are presented below in table 3.1. The density is calculated in laboratory. It is commonly used in composite structures, moreover textile reinforced composite laminates and shell structures. Carbon fibres or glass fibre mats are impregnated with IPC to create these composites. [36, 37, 38]

Table 3.1: Properties of IPC [36]

Density	$1950kg/m^3$
Young's modulus	$18GPa$
Compressive strength	$80MPa$
Tensile strength	6-$8MPa$

3.1.2 Production process

The correct masses of each component are weighted on a scale. Those components will then be mixed to have a uniform consistency, as seen in figure 3.1 on the right. The mixer starts at about 500 rotations per minute, to ensure the powder being taken up by the liquid solution. Then the rotation velocity is increased to the maximum of 2000 rPM and the liquid IPC is mixed for two to three minutes.

Figure 3.1: Two components of the IPC mixture (left) and the mixing process (right)

Due to the mixing process a lot of air bubbles are present in the IPC which can be reduced by vibrating and vacuuming. A pump is installed that will put the liquid in vacuum conditions. Pumping enlarges the air bubbles, which makes them rise in the liquid (figure 3.2). It is seen that at the surface large air enclosures are present, while deeper down these are smaller. After five minutes the pump is stopped and the volume of the bubbles decreases; the small ones disappear.

Figure 3.2: Vacuum pump (left) and rise of air bubbles (right)

The next step is to place the liquid on a vibrating platform, illustrated in figure 3.3 to make the bubbles pop. The time of vibration depends on the amount of air enclosures in the IPC (more or less three minutes).
Several ways are possible to manufacture the IPC tubes. Out of previous experience at the department, it was chosen to use moulds wherein the liquid IPC is casted. The moulds are made of polyvinylchloride (PVC) since this material does not react with IPC, is rather strong and is easy washable. It is important to have a smooth surface where the tubes are casted, since this will facilitate the unmoulding.

Figure 3.3: Vibrating plate (left) and IPC moulds with end pieces (right)

The moulds consist of two pieces that are laterally, along the tube's length, attached to each other by screws. The slot shapes define the shape of the tubes. Half circular and triangular slots are used, and the three different combinations lead to circular, diamond and droplet shaped tubes.
To make the tubes hollow, a removable core must be present. A PVC wire with section 2mm

is used, since this is big enough for the healing agent to pass. It is important to have the core centered so that the hole is continuous. The cores are inserted in centering end-pieces, which are inserted in both ends of the mould.

Before assembling the mould, a layer of beeswax is added on mould and core to facilitate the unmoulding process. If assembled, liquid IPC is casted by letting the fluid flow from above into the mould. Attention must be paid in order to avoid the inclusion of air bubbles. The IPC needs 48 hours at room temperature to harden. However, the core can be removed earlier, at around 24 hours, if the IPC reached adequate strength.

3.1.3 Permeability test

One of the drawbacks of IPC is its porousness and therefore perviousness. The healing agent might penetrate through the IPC tubes and fill up the pores. This is a loss of healing agent that is economically disadvantageous. On the other hand, concrete water might be absorbed that normally is used for hydration.

To verify that IPC is pervious, a permeability test is performed. A tracer - made of water with red ink as pigment - is used in order to visualize the liquid that is penetrating. Note that the healing agent is more viscous, and will therefore penetrate less (fast) than water. The set-up of the test can be seen in figure 3.4. An IPC tube is connected to two plastic jars by means of flexible tubes, some tape and silicone. The tracer is poured in one of the jars and will flow through the IPC tube to the other one, leading to an equal height of liquid in both jars following the theory of communicating vessels.

Figure 3.4: Set-up of the permeability test

After 24 hours the test is completed. The diamond saw will cut the tubes lengthwise so that the depth of penetration of the tracer is visible. Results are shown in figure 3.5 and depict that the tracer penetrated the IPC to a small extent.

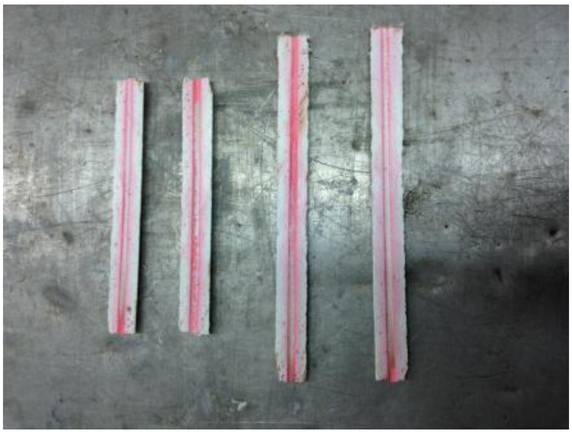

Figure 3.5: Result of the permeability test

Now the question arises if it is necessary to make the tubes impervious. Intuitively the answer is positive, because we do not want the healing agent to be spilled or the concrete to have a lower strength due to unhydrated cement. However, the properties of the sealing agent should also be taken into account and an assessment should be made whether this solution is economically justified.

3.1.4 Sealing powder

The sealing powder used, is a polyether ether ketone (PEEK). It is a thermoplastic polymer that will fill the pores of the IPC. The powder has to be added in the mixing process and after drying, the tubes need heating until $343°C$ to allow for the PEEK to fill the pores.
A point of attention is that the price of the PEEK is relatively high (ca. €200/kg). The price of healing agent is unknown because it differs along the available types, but it is thought that the price will be lower than the one of PEEK. The reservoir of the vascular system can be refilled at any time with the desired amount of healing liquid. In this context, it seems thus superfluous to use the thermoplastic for tube fabrication.
Still, the problem of decreasing the strength of the concrete remains. The question is how much water will be taken by the tubes, since the permeability test pointed out that the penetration is rather little. To know the answer, three-point bending tests are performed on eight concrete specimens (see sections 4.1 and 5.1).

3.2 Clay tubes

Another solution for making of the tubes of the vascular system is clay. At the moment, clay is already used in concrete for self-healing purposes. Jonkers et al [12] used expanded clay particles in order to protect bacteria. Tests pointed out that, even without bacteria, specimens could be healed using clay thanks to calcium-carbonate precipitation. However, including a significant volume of clay particles (here 50% of the total amount of aggregates) lowered the compressive strength of the concrete with 50%. The reduction of compressive strength is due to the adsorption of water on the clay surfaces (Budelmann [39]). This means that there is less water available for the hydration process of the cement particles and the cohesion is decreased. Due to this reason, also the tensile strength of concrete affected by the clay, is reduced. However, the tensile strength of clay itself has a higher value than the one of concrete (see section 4.3). Care should thus be taken when applying this technique onto the concrete specimens.

A problem that immediately arises, is the porosity of the material. Since the healing agent will flow through the clay tubes, a method for making these tubes watertight should be provided. In the same trend as porcelain cups are made, a glaze can be used on the inner side of the tubes to make sure the healing agent cannot intrude the clay tubes.

Clay becomes a ceramic when it is fired in stages and all water is evaporated [40]. Water evaporation already occurs at a low temperature (around $250°C$). The temperature is then increased to $573°C$, which is the temperature where the quartz changes from alpha quartz to beta quartz. During this temperature transition, the clay particles expand and tension inside the material is induced. The transition occurs in the opposite direction when cooling down and thus the particles will shrink again. When the increase and decrease in temperature around $573°C$ is applied slowly, the expansion and shrinkage of particles stays small. In this case, the transition is not of high importance. The last stage in the firing process is called sintering. Sintering happens at high temperature, dependent of the clay type, around $1000°C$. The clay minerals now stick together and form a homogeneous unit, which gives strength to the material. When the clay has sintered and cooled down to room temperature, a glaze can be applied on the desired surfaces. Heating again to a temperature according to the type of glaze (mostly $950°C$ - $1250°C$), will make the glaze become solid and the surface watertight.

3.2.1 Clay and glaze type

The type of clay used for tube production is a simple modeling clay. The maximum temperature of heating is $1150°C$, but the sintering temperature is $1050°C$. After heating, the color becomes white because of the quartz sand inside the clay. The glaze is of type Blue Midnight PC-12 from AMACO, with a glazing temperature of $1060°C$. This type of glaze is impermeable to water.

3.2.2 Production process

The production process will consist of extruding the clay tubes with a self-made extrusion device. The first prototype was made by using an empty silicone dispenser, which formed the base of the extrusion device. In order to obtain hollow core tubes, a small steel construction, that will center a fine rod inside the dispenser, was installed (figure 3.6).

Figure 3.6: Small steel construction inside the silicone dispenser

The built-up pressure will cause the clay to flow smoothly, without discontinuities, out of the dispenser. The fine rod sticks out some centimeters to guide the clay tube and to make sure that the tube stays hollow. The extrusion process is shown in figure 3.7. The length of the tubes can thus be choosen, but will still be restricted by the dimensions of the oven. This is why at maximum, a tube of approximately $40cm$ can be made.

Figure 3.7: Extrusion device and process

The drawback of this production method is that it could only be used for round tubes as the opening in the silicone dispenser is round. Also, the pressure applied on the silicon dispenser makes it to deform.
This production process is optimized by a second prototype. An aluminum tube is made which can be used together with a hydraulic pressing machine and pressing ram (piston), as seen on figure 3.8. A thread is cutted on the outside of the tube, such that a nut can be screwed on. This nut has the possibility to hold a 3D-printed die, that allows the production of different shapes, e.g. droplet- or rugby ball-shaped tubes. A centering rod which is inserted in the aluminum tube, allows the fabrication of the holes in clay tubes. The big advantage of this prototype is its robustness and reusability. It is easy to clean, possible to make different shapes, no manpower is required and a batch of approximately 10 tubes can be made at once.

Figure 3.8: Second prototype of clay extruder set-up on pressing machine (left) and nut with die (right)

Figure 3.8 and 3.9 represent the new clay extruder. The pieces are named identically as in figure 2.11.

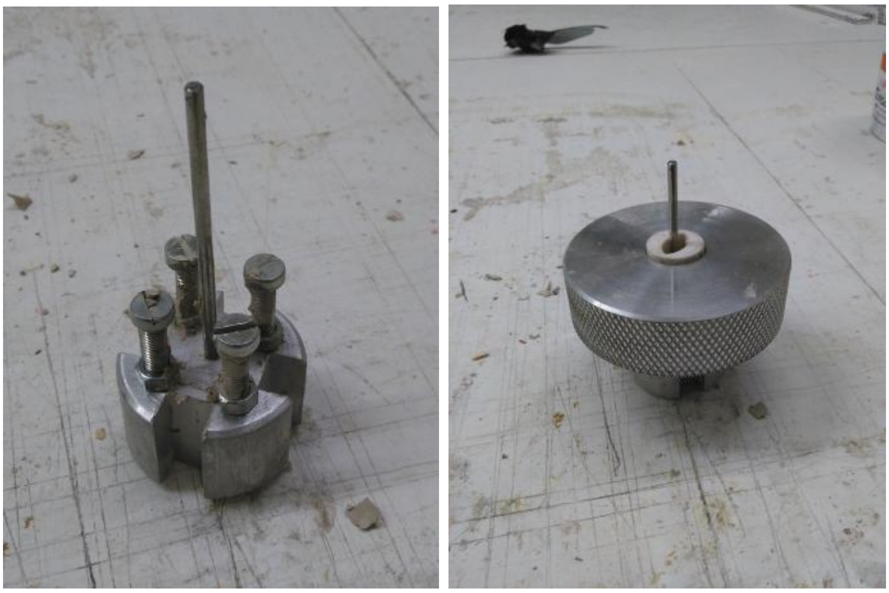

Figure 3.9: Centering rod (left) and centering rod with die in nut (right)

The clay tubes are then dried at room temperature for at least 24 hours. They should be dry before putting them in the oven, otherwise steam inside the material will expand and break the tubes [40].
The firing of clay is an important stage in the transition to a ceramic. However, it is still unknown if the high strength provided by heated clay is really necessary in our case. Of course the strength should be high enough to resist the forces of pouring the concrete, but the tubes need to break upon cracking of concrete. Another aspect is the cost of firing: if we can manage to use the tubes without firing, an important cost factor can be deleted.
Tensile tests will provide us with the answer. Three different 'types' of tubes will be tested: simply dried at room temperature, dried in the oven at $250°C$ and dried in the oven at $1050°C$. The testing procedure is described in section 4.3 and the results in section 5.3.

3.2.3 Permeability test

Identically as for IPC, a permeability test is conducted on a clay tube after heating at $1050°C$. Heating is done in stages of $250°C$ per hour. The testing method is described in section 3.1.3. The result of the permeability test pointed out that clay is pervious (figure 3.10)

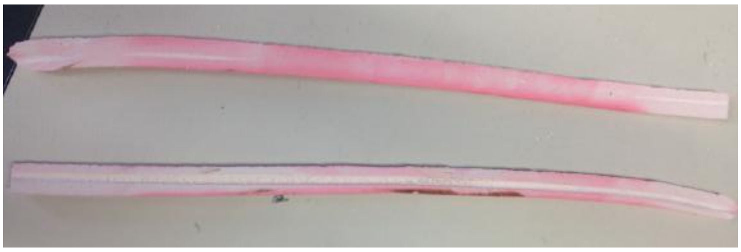

Figure 3.10: Result of the permeability test

For this reason, the inside of the clay tubes are coated with a glaze, as stated before. The same permeability test is now performed to verify its imperviousness. It can be concluded afterwards that applying a glaze coating keeps the liquid inside (figure 3.11).

Figure 3.11: Result of the permeability test with a glaze coating inside the tube

Glazing the interior of the tubes prevents the leakage of healing agent. On the other hand, water will be withdrawn from the concrete during its curing process if the external surface of tube is not glazed. It is now a matter of choice which surfaces glaze should be applied. The price of this particular glaze was €11,50 for 472ml at *Colpaert Ceramic and Sculpture Materials*. In bigger quantities and for other types, this price will sufficiently drop, which justifies its use. No chemical reaction occured between healing agent and glaze or clay in laboratory. Applying an external layer changes the interaction and bonding properties with concrete. In what follows, no glaze is used to be consistent with the testing of IPC, similarly discussed in section 3.1.4.
Note that research and price investigation should be done regarding which types of clay and glaze are optimal. Stoneware is a type of clay that is impermeable to water upon heating, without the application of a glaze, and is one example how to improve the production process.

3.3 Reservoir and connection piece

The tubes will be connected to a reservoir, which provides enough healing agent for a certain period of time. A connection piece between reservoir and tube allows the use of different types of tubes with the same reservoir.

Both reservoir and connection pieces are made of polyamide by means of 3D printing. First, a 3D drawing is made in Autodesk Inventor. The pieces are manufactured at *i.materialise* [41].

3.3.1 Polyamide

Polyamide is a polymer material made up of amide chains. This material is chosen because it is one of the cheaper materials for 3D printing. Polyamide fibers are already used inside concrete beams. A study conducted by Joong et al. [42] demonstrated that a macro-sized polyamid fibre can be used as reinforcement. The advantage these fibres have upon steel, is that they do not corrode. In this way, it can be said that polyamide does not react upon concrete. The stiffening effect of including this material is more doubtful, since the reservoirs only form a discontinuity inside the concrete material and cannot help to maintain the tensile forces.

3.3.2 Reservoir

The reservoir is the container that holds the healing agent. It is a simple rectangular box with a cylindrical tube on top and the opportunity of joining three connection pieces at the bottom (figure 3.12).

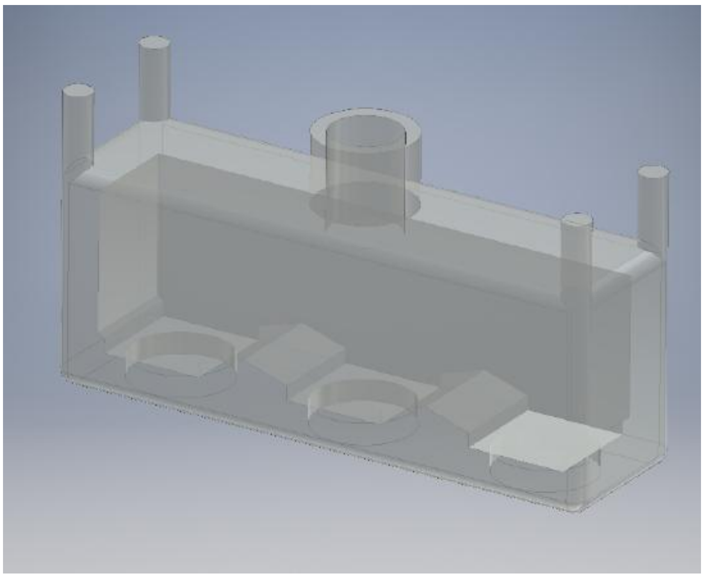

Figure 3.12: Drawing of the reservoir in Autodesk Inventor

The first improvement is the set of four bars on top of the reservoir to prevent movement of the reservoir in the fresh concrete. When the reservoir starts floating inside the concrete because of its lower density, as depicted in figure 3.13, some tubes are positioned higher than others and thus have less chance to break. The solution consists of blocking the reservoir at the upper side of the mould. However, the reservoir and connection piece did not reach the upper surface and that is why some sockets are added at the top of the reservoir.
Secondly, a sort of ramp will be added between the supply holes (leading the healing agent to the tubes) to make sure that the healing agent arrives in the holes and is not wasted.
Also, at the top there will be a longer cylinder leading to the top surface of the concrete beam. In this way the flexible tube, that will fill our reservoir or pump the liquid downward, can be deconnected in a simple way and it remains possible to fill the reservoir at any time.

Figure 3.13: Reservoir is not parallel with lower surface

3.3.3 Connection piece

The connection pieces are the links between tubes and reservoir (figure 3.14). They are designed separately from the reservoir in order to leave open the choice of how many tubes and which shape of tubes that will be used.

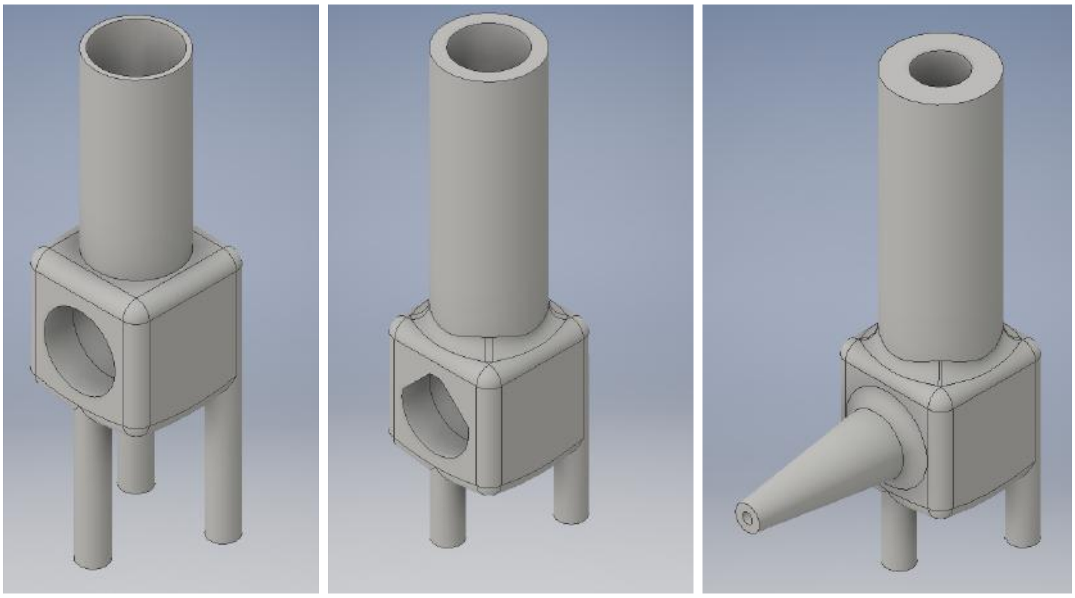

Figure 3.14: Drawings of 3 types of connection pieces in Autodesk Inventor: circular tube (left), droplet form (mid) and conical end piece (right)

To start, the distance between connection piece and reservoir (cylinder that connects both) is increased in order to have enough space for the reinforcement to fit in between.
Then, underneath the connection pieces the surfaces are rounded to minimalise the air entrapped between concrete and connection piece.
A last improvement regarding compatibility to different shapes is not yet on point. Instead of pushing the tubes into the connection piece, using a triangular piece (that will be added upon the connection piece and placed into the hollow cores of the tubes) would be more ideal. In this way, the connection pieces can be used for any type of cross section. Finally, we decided not to use this now since the hollow cores in the tubes are too small. Another idea arose to have the possibility to place the tubes under the reinforcement bars. A cutout should thus be made in the cylinder of the connection piece, in order to place the reinforcement bar in this cutout, above the tube. This cutout has a round shape, like a hollow doughnut, and permits the healing agent to flow around the reinforcement bar (figure 3.15).

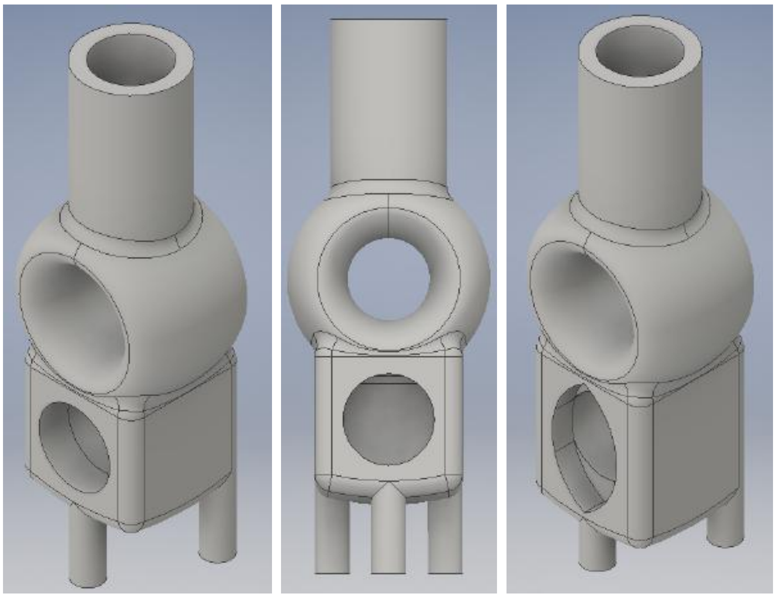

Figure 3.15: Drawings of 2 types of connection pieces with cutout for reinforcement bars in Autodesk Inventor: circular tube (left and mid) and rugby ball shape (right)

3.4 Healing agent

The healing agent used to carry out the experiments, is a yellow non-flammable polyurethane developed by De Neef Conchem[43]. It is a one-component, closed cell, phthalate free healing agent that is currently used for manually waterproofing leaking joints and cracks by injection. This specific type, namely HA Flex SLV AF, has a viscosity to work optimal for cracks <0,5mm. The technical sheet can be found in Appendix A.

3.5 Ideal form of tubes

In order to obtain the ideal cross section of the tubes in the vascular system, we are looking for the section with minimum resistance against flow of concrete. When casting the beams, the concrete is poured upon the tubes which can lead to fractures. A section that provides a minimum of resistance against this flow of concrete is thus in our best interest. Considering the translation of an inclusion in a linear elastic medium gives a theoretical model of what the shape should look like. The problem is a combination of the maximum-penetration and the minimum-drag problem [44].

Drag is the resistance that a moving object experiences, when moving through an incompressible fluid like water or air. Different shapes are shown on figure 3.16 together with their drag coefficient in %. It can be seen that a streamlined object has the lowest drag coefficient.

Shape and flow	Form Drag
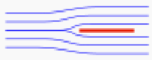	0%
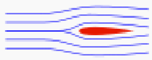	~10%
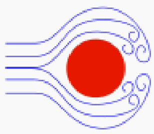	~90%
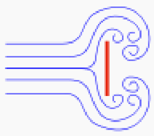	100%

Figure 3.16: Drag force around different forms [45]

Pironneau [45] found that for the flow of an incompressible medium, also called a Stokes flow, the ideal volume is the one that minimizes the drag. This volume looks like a rugby ball, symmetric on front and back.

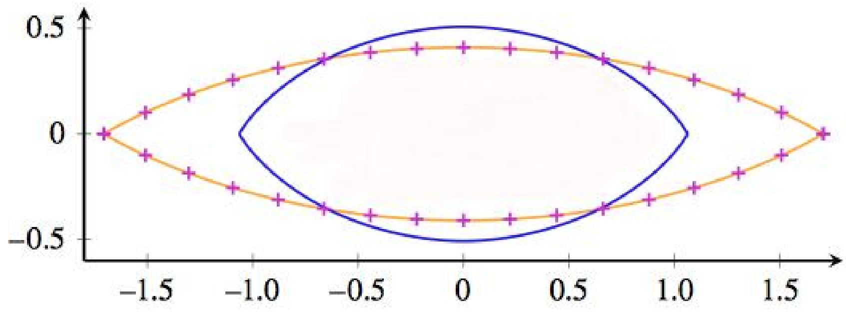

Figure 3.17: Two different types of rugby ball form [46]

Two different types can be found and are depicted in figure 3.17: one by analysis of objects with equal volume and one by analysis of equal section area. The first one has its tangent line to the cone at an angle of $60°$, while the latter one is more slender with an angle of $30°$.

On the other hand, penetration refers to the ability of a volume to make its way through a solid material. A way to find the ideal shape of a penetrating object is to look at ballistics. A study was performed by Gupta et al. [47] on the impact effect of different shapes onto thin aluminium plates. It is seen that for small thicknesses ($\leqslant 1,5mm$), the bullet has an ogive-shaped nose, while for bigger thicknesses the nose should be blunt. Another study, conducted by Shiu [48], compared the penetration depth of a flat nose and an ogive-shaped nose in a concrete wall. Results point out that an ogive-shaped nose penetrates deeper in the concrete, but only starting from a specific nose length (figure 3.18).

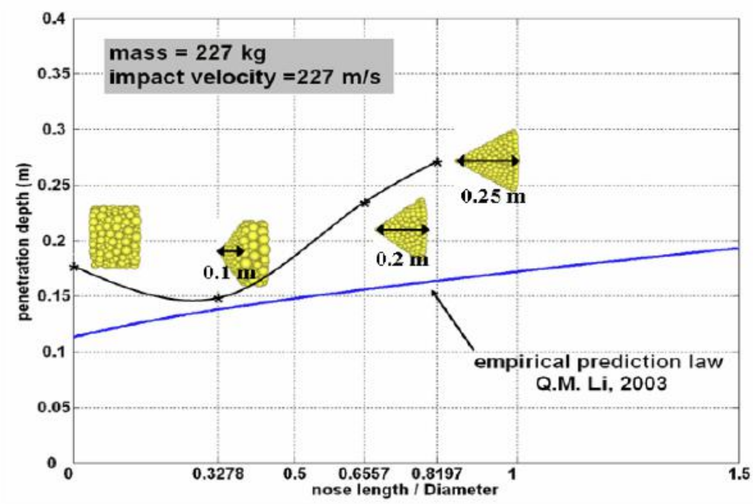

Figure 3.18: Graph showing the penetration depth vs. nose shape [48]

Solving our problem of minimum resistance means solving the Navier equations, which depend on the Poisson's ratio. As we know, for water this ratio is equal to 0,5, and then the Navier equations are equal to the Stokes equations. Zabarkin [44] studied which impact the difference in Poisson's ratio has on the ideal shape and found that for $\nu = 0,5$, the rugby ball is flatter, whereas it is more round for ν evolving to zero.
Three different shapes of tubes were already available: circular, diamond and a droplet-like cross section. By studying the problems of maximum penetration and minimum drag stated above, the ideal cross section is the droplet-like one. The latter is the most streamlined (for minimum drag) and has a pointy tip (for maximum penetration). Ofcourse, a test on the four mentioned shapes will provide us with the answer. Figure 3.19 illustrates these forms.

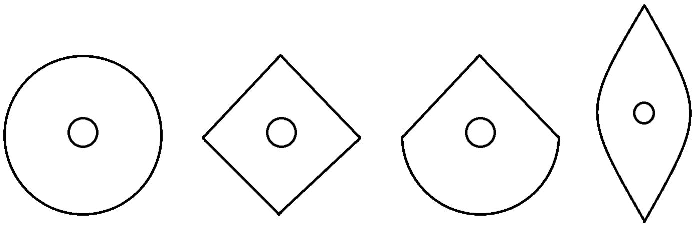

Figure 3.19: Summary of the four considered shapes of tubes, from left to right: round, diamond, droplet and rugby

Figure 3.20 shows IPC and clay tubes with the same form as mentioned above.

Figure 3.20: Four different cross sections of tubes

Experiments

4.1 Influence of PEEK on concrete strength

The influence of PEEK on the concrete strength is still unknown. If the strength without PEEK is significantly lower, it can be assumed that the IPC tubes take up too much water from the concrete mixture, which is in fact needed for hydration of cement particles. Therefore, tubes of IPC and IPC filled with PEEK are added to a concrete mixture and a three-point bending test will provide a conclusion of the influence of this component on the concrete's strength.
Eight beams are casted: two reference beams without tubes, three beams with porous IPC tubes and three beams with IPC/PEEK tubes. The result will allow us to say whether or not the decrease in strength is small enough to abandon the PEEK.

The total volume and weight of concrete needed can be determined by some simple equations. We will make use of eight identical moulds of $65cm$ x $10cm$ x $10cm$. Because of losses due to mixing and casting, the volume of concrete made will be increased by 20 percent.

$$V = 1,2 * 8 * 65cm * 10cm * 10cm = 6,24 * 10^{-2}m^3 \tag{4.1}$$

By using the density of plain concrete, which is $2400kg/m^3$, the total mass of concrete is obtained.

$$m = 2400kg/m^3 * 6,24 * 10^{-2}m^3 = 150kg \tag{4.2}$$

Table 4.1: Composition of the concrete mixture

Component	Weight percentage	Weight in kg
Sand	28%	42
Gravel 2/8	19%	28,5
Gravel 7/16	33%	49,5
CEM I 52,5 N	12%	18
Water	8%	12

The composition of the concrete mixture can be found in table 4.1. Unfortunately, it is not identical to the concrete mixture that will be used in the future, because of the unavailibility of some aggregates. It provides however no serious problem since we will not compare these results. After mixing, the concrete is casted and tubes are placed in the middle of the beams, at 2cm from the bottom of the mould. The beams are then cured at room temperature, demoulded after one day and placed in water for 12 days. Three-point bending tests take place after 15 days of curing to evaluate the strength of the beams.
The diamond saw first cutted a notch in the middle of the beams to create a weak point where the crack will initiate. Aluminium pieces are glued at 1cm distance from each other, one on each side of the notch, as can be seen in figure 4.2b. This is done to place a Crack Mouth Opening Displacement (CMOD) sensor in between which will measure the crack opening. Also, steel plates are mounted with gypsum where the beam is supported in order to straighten the beams, as in figure 4.2c. The test set-up and placement of the CMOD sensor can be seen in figure 4.2.

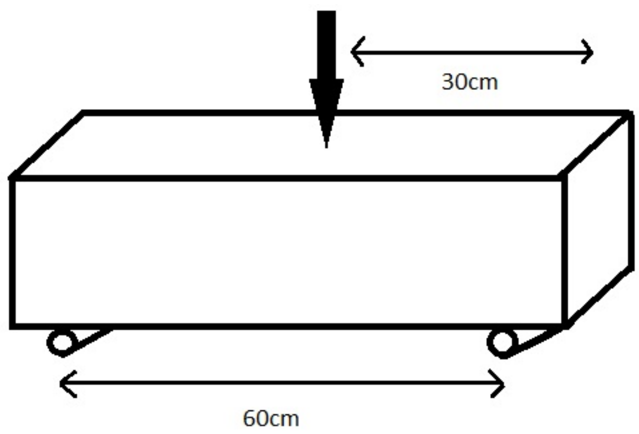

Figure 4.1: Sketch of the distances between supports

The distance between the lower supports is 60cm and the load is applied in the middle of the beam, above the notch. A small sketch in figure 4.1 clarifies these values.

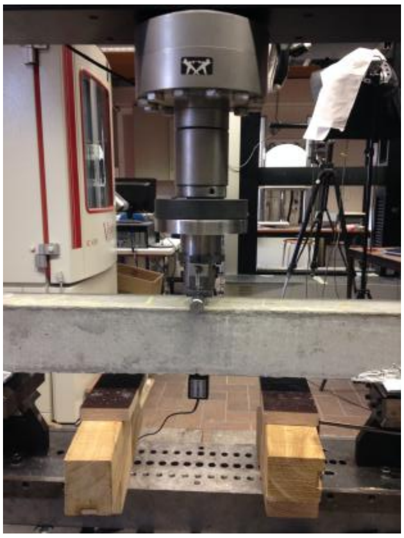

(a)

(b)

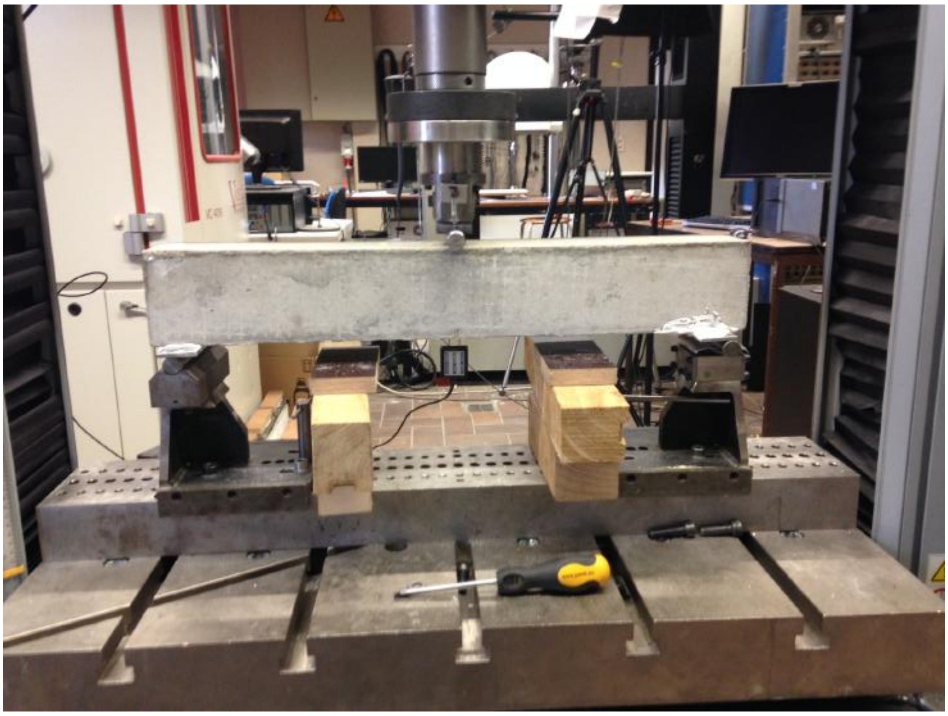

(c)

Figure 4.2: Three-point bending test set-up

4.2 Determination of crack depth

The purpose of measuring the crack depth is to provide a link between the crack opening and the depth. Also, the crack depth will show us the effective section of concrete that is still available to take up load and allows us to find the tensile load at the section of the tube. In this way, the tensile strength of clay tubes can be compared with these values to know if they will break.
In order to find the crack depth, a UPV test can be done. The principle of this test is to measure the speed of sound in a material. The sound wave is induced by means of a pencil lead break. When no cracks are present, the wave goes directly to the sensor, as can be seen on the left in figure 4.3. In the other case, the wave should go around the crack and arrives later at the sensor. The difference in these arrival times will be used to determine the final crack depth. The sensors used are piezoelectric; they produce a small voltage directly proportional to the amplitude of the sound wave.
A schematic illustration of the test is shown in figure 4.3. Two sensors are placed at a distance x and 2x with respect to the crack, one on each side. This distance is arbitrarily choosen, but it should be small enough for the signal not to diminish and large enough so that a discontinuity in the concrete is not of great importance. By breaking a pencil lead (at the position of the arrow in figure 4.3), a sound wave enters the concrete beam and travels to the sensors.

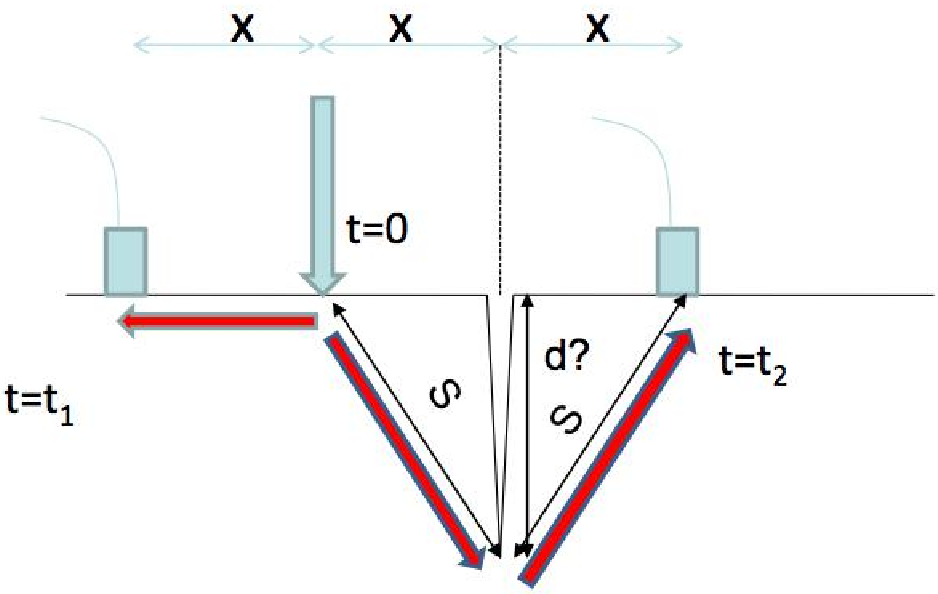

Figure 4.3: Schematic overview of an ultrasonic pulse velocity test [49]

The depth of the crack 'd' can be calculated by measuring the difference in arrival time at the two sensors. The equations to calculate d are listed below:

$$d^2 = s^2 - x^2 \tag{4.3}$$

$$c = \frac{x}{t_1} = \frac{2s}{t_2} \tag{4.4}$$

$$d = x\sqrt{\frac{t_2^2}{4t_1^2} - 1} \tag{4.5}$$

with t_1 the time of arrival at sensor 1 (direct wave), t_2 the time of arrival at sensor 2 (around the crack) and c the speed of sound in the material.

The tests are performed at two different moments. First, when the beams were already cracked, but after some days of unstressed conditions and secondly upon reloading of the beams. The set-up of both experiments is shown below.

Figure 4.4: Set-up of unloaded UPV test of sound material

Figure 4.4 shows the set-up to measure the velocity in sound concrete. The sensors are placed on an uncracked part of the beam so that the wave propagates in a straight way to the sensors. Once the velocity of propagation is known, tests can be started around the cracks.

Figure 4.5: Set-up of loaded UPV test in three-point bending

When the beams are in loaded conditions, the depth of the crack is measured again. In figure 4.5 the set-up of the sensors can be seen. The CMOD is used too, to directly relate the opening of the crack with the depth.

4.3 Tensile strength of clay tubes in relation to curing conditions

A tensile test will be performed on three different types of clay tubes: simply dried at room temperature, dried in the oven at $250°C$ and dried in the oven at $1050°C$. This test is done to find the strength and stiffness of the clay material and evaluate whether it can break at the correct moment when casted inside a concrete beam. The tubes will be placed in the testing machine and strained in tension with a speed of $0,25\frac{mm}{min}$. To have an accurate measurement of the strain, an extensiometer is placed on the sample. The load cell of the testing machine also measures the strain of the sample, but it takes into account strain in the end pieces and the clamps and it is sensitive to slipping of the sample in the clamps. The tubes are loaded until breaking. The test set-up is shown in figure 4.6.

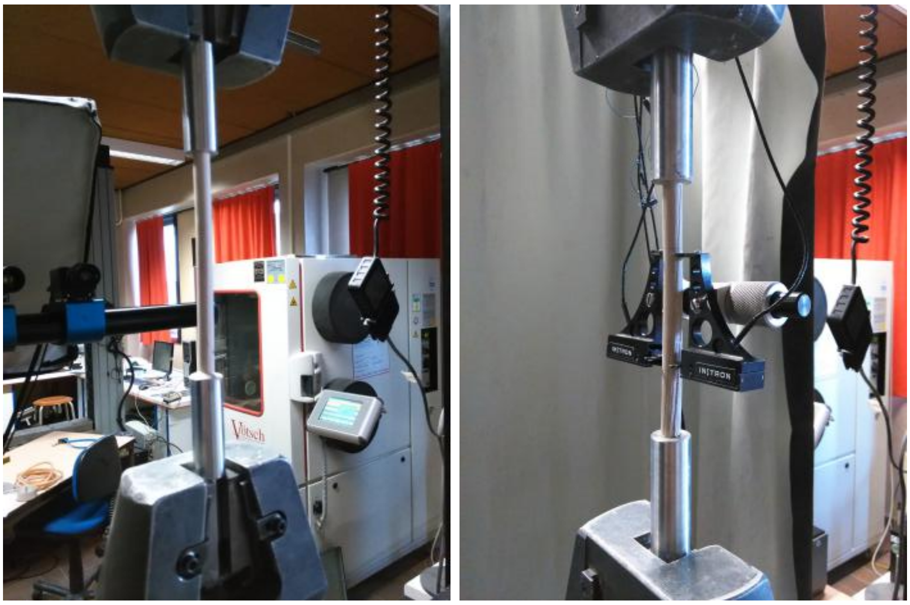

Figure 4.6: Tensile test set-up: specimen without (left) and with (right) extensiometer

A problem encountered was the clamping of the tubes in the machine. The clay material is too brittle to clamp it and would break before tests even have started. Therefore, hollow aluminium end pieces are made in which the tubes are glued. These end pieces can then be clamped in the test machine as shown in figure 4.7.

Figure 4.7: Aluminium end pieces

4.4 Influence of shape on load impact

As explained in section 3.5, there is still a problem when pouring concrete upon the vascular system. Due to the impact load, the tubes could break. Theoretically, it was seen that a rugby ball form is subject to the lowest force, since it combines maximum penetration by cutting through the concrete mixture and minimum drag because of its streamlined form. To verify this feature, four different cross section shapes will be tested by applying a uniform load. These forms are: round, diamond, droplet and rugby ball as were illustrated in figure 3.19. The test set-up is illustrated in figure 4.8.

Figure 4.8: Set-up of the test regarding the influence of shape on the impact load

The test is as following: a container yielding fine sand (figure 4.9a) will be put at two different heights. A slot underneath the container will allow to discharge the sand in a uniform way. A tube is fixed underneath the stream of sand, as in picture 4.9b and the deflection will be measured by means of a strain gauge at the place of maximum tensile moment.

(a) (b)

Figure 4.9: Detailed set-up of test regarding the influence of shape on impact load

A strain gauge of type FLK-6-11 is used, with a gauge length of 6mm and a gauge factor of 2,12. The strain gauge is glued upon the sample with a two component adhesive of type P2, as shown in figure 4.10. The technical sheet of the strain gauge is added in appendix A.

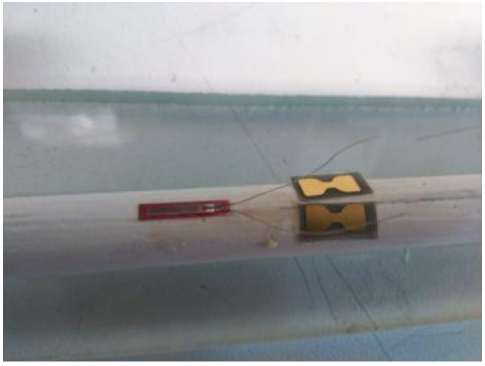

Figure 4.10: Strain gauge glued on the sample

The tubes are simply supported. The impact load is taken as a distributed load, as sketched in figure 4.11. By measuring the deflection, an approximation of the load is derived. The shape that is charged with the minimum load has the lowest resistance. The formulas needed are listed from equation 4.6 to 4.11.

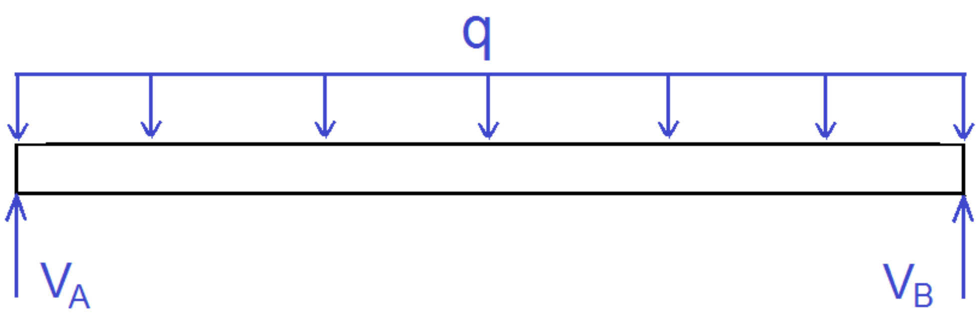

Figure 4.11: Schematical representation of the forces on the simply supported tube

$$M_{max} = \frac{q \cdot L^2}{8} \tag{4.6}$$

$$\sigma_{max} = \frac{M_{max} \cdot y_{max}}{I} \tag{4.7}$$

$$M_{max} = \frac{\sigma_{max} \cdot I}{y_{max}} \tag{4.8}$$

$$\frac{q \cdot L^2}{8} = \frac{\sigma_{max} \cdot I}{y_{max}} \tag{4.9}$$

$$\sigma_{measured} = E \cdot \epsilon \tag{4.10}$$

For $\sigma_{measured} = \sigma_{max}$:

$$q = \frac{8E \cdot \epsilon \cdot I}{y_{max} \cdot L^2} \tag{4.11}$$

with:

- M_{max}: maximum moment (i.e. in the middle of the beam)
- q: uniformly distributed load
- L: length between the supports
- σ_{max}: maximum stress (i.e. in the middle of the beam)
- y_{max}: location of the outermost fibre
- I: moment of inertia
- $\sigma_{measured}$: measured maximum stress

- E: Young's modulus
- ϵ: measured strain

The moment of inertia of the different forms are summarized in table 4.2. They are calculated by means of formula 4.12.

$$I_y = \int_A z^2 \, \mathrm{d}A \tag{4.12}$$

Table 4.2: Moment of inertia of different forms

	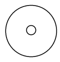	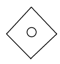	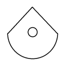	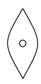
Moment of inertia	$490mm^4$	$211mm^4$	$445mm^4$	$1103mm^4$

For practical reasons, it was not possible to attach the strain gauge at the extreme fibre of the diamond and rugby ball (pointy end). The strain gauge is attached on the flat surface, as close as possible to the edge. Since the strain is linear over the cross section, the strain at the tip can be found by a linear interpolation between the measured strain and the neutral line (no strain), which is in the middle of the cross section due to symmetry. It was measured that the strain gauge is positioned at 4,3mm from the neutral axis for the diamond form. The distance to the outer fibre is 5mm, which means that the strain gauge will show $\frac{4{,}3mm}{5mm} = 84\%$ of the strain at the outer fibre. For the rugby form, the strain gauge measures 93% of the strain at the outer fibre.
In order to calibrate the tests, different known point loads are applied on the middle of the sample. The strain is then measured by the strain gauge. By means of theoretical formulas, the applied load should be found. The load situation looks similar to figure 4.11, except that the applied load is now a point load F in the middle of the tube. Following formulas are used together with equations 4.7, 4.8 and 4.10:

$$M_{max} = \frac{F \cdot L}{4} \tag{4.13}$$

$$\frac{F \cdot L}{4} = \frac{\sigma_{max} \cdot I}{y_{max}} \tag{4.14}$$

For $\sigma_{measured} = \sigma_{max}$:

$$F = \frac{4E \cdot \epsilon \cdot I}{y_{max} \cdot L} \tag{4.15}$$

4.5 Four-point bending test with IPC vascular system

In this test, a vascular system containing the reservoirs, connection pieces and IPC tubes will be embedded inside a concrete beam. Both circular and droplet-form tubes are used and self-healing efficiency will be compared. Also, steel reinforcements are added to the beams.
The connection pieces are glued to the reservoir with a two-component glue of brand *Araldite*. When dry, the tubes are placed in between two systems and glued to them (figure 4.12). Then, the supply pipe at the top of the reservoir is covered with duct-tape, so that no concrete can flow inside.

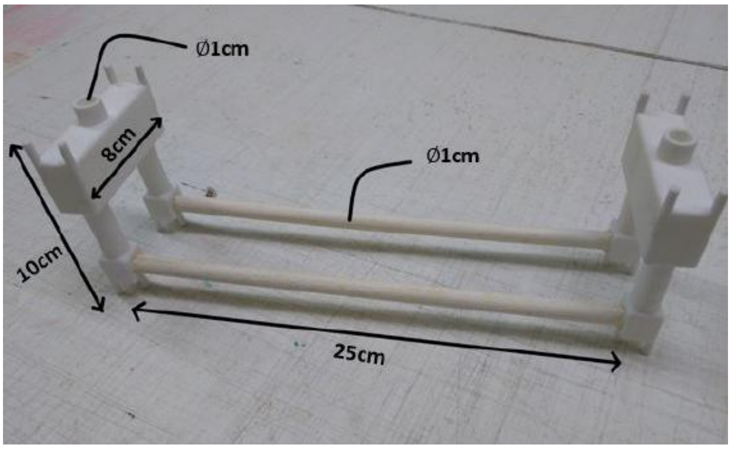

Figure 4.12: Assembly of the vascular system

First, steel reinforcement is placed in the mould, consisting of 1 bar, 6mm in diameter and 600mm in length. At the ends, two inclined steel pieces are welded as footage so that the reinforcement bar is at 2cm of height. This reinforcement bar is placed in the tensile zone of the beam and helps to distribute cracks over a longer zone. When a crack occurs, steel takes over the load so that also other cracks are induced rather than the opening of only one crack. The vascular system is placed on top, which is shown in figure 4.13.

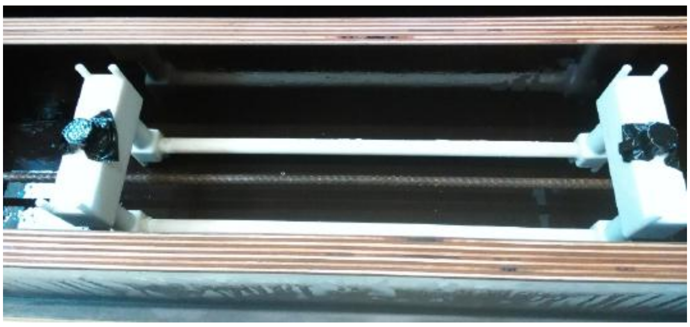

Figure 4.13: Steel reinforcement and vascular system in the mould

In reality, beams are loaded with a distributed load. To approach this load situation as close as possible, four-point bending tests will be performed. Acoustic emission and DIC will be used to find the location of cracks. Eight piezoelectric AE sensors will be placed upon the beam with vaseline for a good surface contact, and some tape. The sensors are 13mm in diameter, which states that the source of signals can be determined with an accuracy of 13mm. The layout of the sensors is drawn in figure 4.14.

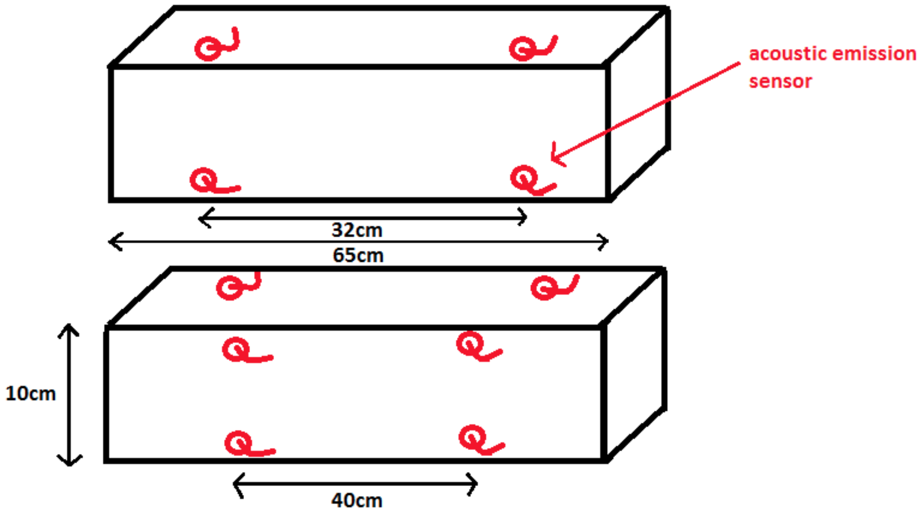

Figure 4.14: Lay-out of the eight acoustic emission sensors on front (above) and back (below) side

On the front side, in between the two acoustic emission sensors, a speckle pattern is applied on the surface. An example of one of our beams is depicted in figure 4.15

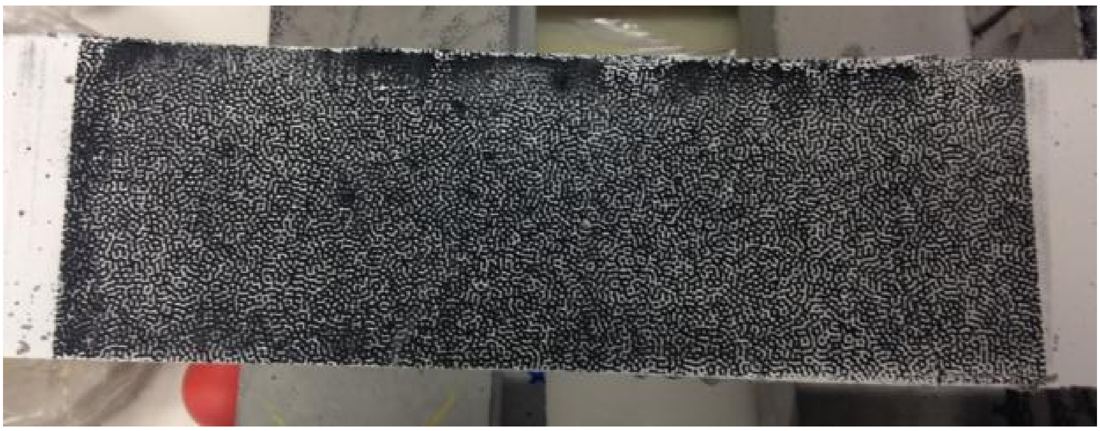

Figure 4.15: Speckle pattern on one of the beams

First, the concrete beam is painted white to have enough contrast between the black speckles and background. The speckles are added afterwards by means of a sieve and a platelet. Black viscous paint is pulled over the sieve, which has a particular pattern, and in this way a unique speckle pattern is created on the surface. The methodology followed can be seen in figure 4.16. For some beams, the speckle pattern was not totally perfect. Black dots were added by hand and care was taken to differentiate the size and shape of the dots.

Figure 4.16: Application of speckle pattern on the beam

Before testing, the DIC system had to be set up. Two cameras are placed in front of the concrete specimen at the correct height. A lamp, providing appropriate light, is placed behind the cameras. The cameras should now be positioned in a way that the total speckle pattern can be seen and that the angle between both cameras is not too big. Next, a calibration should be done by using a dotted plate. The plate is held in different directions and moved over the speckled area while pictures are taken with VIC SNAP. Using VIC 3D, the system is calibrated and as soon as the calibration error is below 0,036, testing can start. The test set-up is depicted in figure 4.17.

Figure 4.17: Four-point bending test set-up front (above) and back (below)

On the first picture of the figure above, the specimen is captured from the front side. Two DIC cameras are focused on the speckle pattern of the beam. The beam is simply supported on the sides and the load will be applied by two supports at the top. In the second picture of figure 4.17, the four acoustic emission sensors at the back side can be seen. The healing agent is added to the vascular system by means of a funnel, which can be seen in the lower picture of figure 4.17. It is tried to start the DIC at the same time as the acoustic emission and the Instron machine. The self-healing efficiency will be measured by comparison of stiffness. The stiffness k is defined by:

$$k = \frac{F}{\delta} \tag{4.16}$$

In formula 4.16, F is the applied load on the beam and δ is the displacement in the vertical direction. The formula for the self-healing efficiency is given by equation 4.17 and is the percentage of stiffness regain. The value is used as a quantification of healing.

$$\eta = 100 \cdot \frac{Stiffness_{afterhealing}}{Stiffness_{original}} (\%) \tag{4.17}$$

4.6 Four-point bending test with clay vascular system

In the previous section, four-point bending tests are explained for the vascular systems using IPC tubes. A difference is made between the beams with clay tubes since a new vascular system is designed and used for these tests. The vascular system in question can be seen in section 3.3. A cutout is made in the connection pieces to be able to slide the steel reinforcements through it. In this way, the tubes are somewhat protected by the steel reinforcements while casting. The new vascular system with tubes is depicted below.

Figure 4.18: Vascular system and reinforcement bars inside the mould

The improvement in vascular system in figure 4.18 is assumed to increase the survivability of the tubes while casting. From a height of 40cm, the concrete will be poured over the system and it shall then be seen whether or not it proves its effectiveness.
Also, different forms of tubes will be used in this test: droplet and rugby form. In this way, it can simultaneously be checked whether a rugby ball form provides a benefit over droplet form in case of pouring concrete.

Results and discussion

5.1 Influence of PEEK on concrete strength

The testing procedure is described in section 4.1. A three-point bending test is performed at a speed of 0,2mm/min. A summary table of the test results, giving the ultimate load, the mean value per type of beam and the standard deviation per type, is included below in table 5.1. The standard deviation is calculated by:

$$s = \sqrt{\frac{1}{n-1} \cdot \Sigma(x_i - \mu)^2} \tag{5.1}$$

Table 5.1: Summary of results on influence of IPC/PEEK on concrete bending strength

	Ultimate load (N)	Average strength per type (N)	Standard deviation per type (N)
Reference 1	3 801	4 109	435
Reference 2	4 416		
IPC 1	4 090	4 006	281
IPC 2	4 235		
IPC 3	3 693		
PEEK 1	3 638	3 984	342
PEEK 2	3 992		
PEEK 3	4 321		

To draw a conclusion, a Gaussian curve showing the normal distribution around the mean value is sketched in figure 5.1. The tolerance interval of $2 \cdot s$ is added, which shows the interval in which 95% of the data lies. The mean values lie closely together and between all three tolerance intervals: the differences in mean value of strength are so small that the statistical uncertainty about these values is bigger. In this way it can be concluded that the tests are trustworthy and the strength of the concrete beams is not changed by adding neither IPC, neither IPC with PEEK.

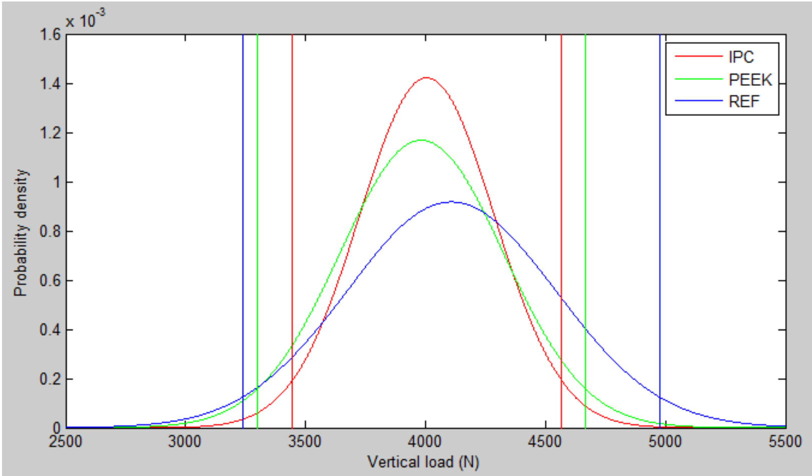

Figure 5.1: Gaussian curves and $2 \cdot s$ intervals

5.2 Determination of crack depth

The UPV test as described in section 4.2 will be performed on the five remaining (unbroken) beams. The other three were unavailable, since one broke and two others were cut open to verify if the tubes were at the desired place. The idea of a UPV test came up after cutting the beams and that is why there were only five left.
A table showing the crack opening and related depth can be found below, for both the unloaded and loaded experiment.

Table 5.2: Determination of crack depth

	Crack width (μm)	Crack depth (cm)	Sound velocity (m/s)
Unloaded			
Reference 2	477	5,6	3722
IPC 2	238	5,7	3289
IPC 3	263	6,8	3623
PEEK 1	183	4,6	3036
PEEK 2	237	4,7	3198
Loaded			
Reference 2	/	/	3722
IPC 2	315	6,2	3289
IPC 3	356	7,8	3623
PEEK 1	295	5,0	3036
PEEK 2	413	7,5	3198

As expected, the crack depth increases with the crack width. However, a clear relationship regarding the different beams is not visible. Note that the crack depth certainly reaches a higher level than the position of the tubes for a crack width of $300\mu m$, which is a standard value for self-healing. It can thus be said that there is a high chance, but not a certainty, that the tubes broke.

5.3 Tensile strength of clay tubes in relation to curing conditions

The set-up of the tensile test can be found in section 4.3. This tests are performed at a speed of 0,25mm/min. The results are summarized and represented below. While testing, it became clear that the tubes cured at $250°C$ and room temperature were not able to withstand any load. These ones could thus not be tested.

Table 5.3: Summary of tensile strength of clay tubes heated at $1050°C$

	Ultimate load (N)
Specimen 1	918,4
Specimen 2	889,6
Specimen 3	835,4
Specimen 4	469,1
Mean value	881,1

The last value will not be included for calculating the mean value of the tensile strength, since we believe that the value differs too much and may be due to a flaw. Finally, a mean value of $881,1N$ is received which gives a stress in the tube equal to:

$$\sigma_{tube} = \frac{881,1N}{0,66cm^2} = 13,35MPa \tag{5.2}$$

To be sure that the clay tubes break upon loading inside the concrete beams, some calculations are done as can be found from equation 5.3 until 5.9. We assume perfect fixation between tube and concrete, which means that the strains should be equal. The Young's modulus of concrete is taken as 40GPa. For clay, a mean value of the Young's moduli of the different specimens is taken. The E-modulus can be found by fitting a linear trendline to the stress-strain curve as shown in figure 5.2 for specimen 2. The slope of this line is equal to the Young's modulus. The calculated mean value is equal to 22,8GPa.

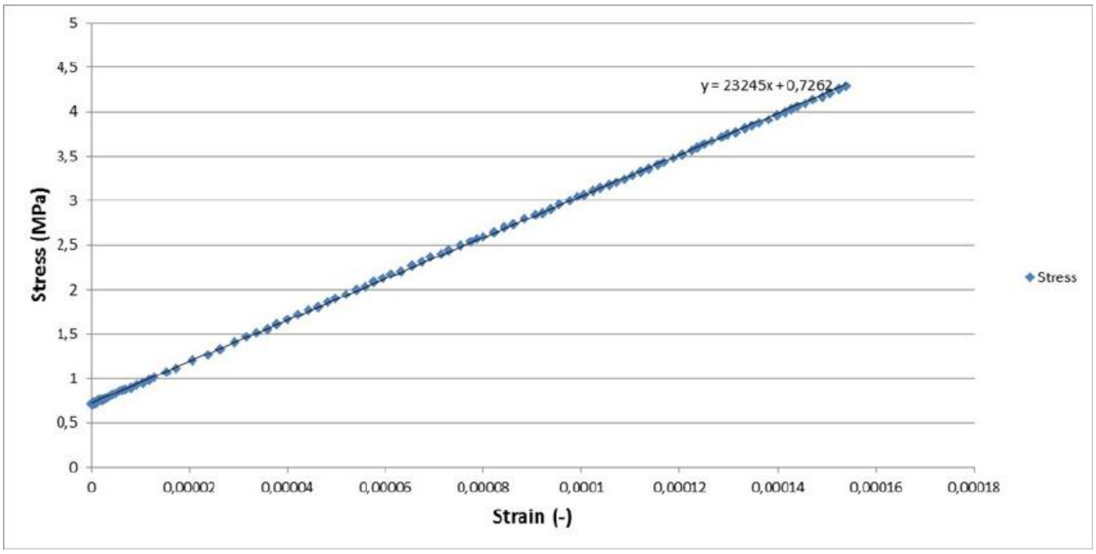

Figure 5.2: Determination of the Young's modulus from the stress-strain curve

Due to the difference in Young's modulus, both materials will carry a different load. The stiffer the material, the more load it will carry, as shown below in figure 5.3.

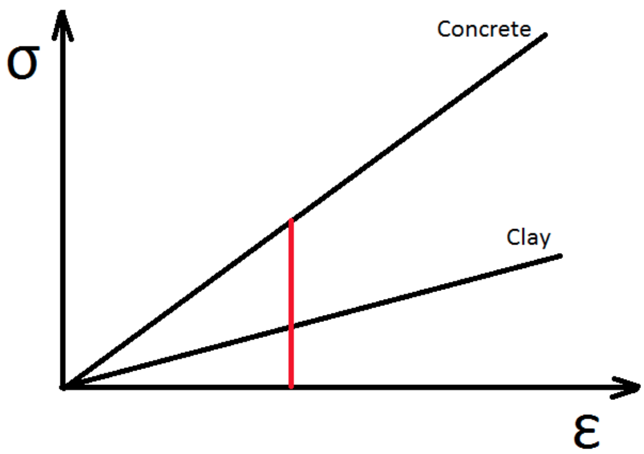

Figure 5.3: Difference in stress due to different Young's modulus for equal strain

$$\epsilon_{clay} = \epsilon_{concrete} \tag{5.3}$$

$$\frac{\sigma_{clay}}{E_{clay}} = \frac{\sigma_{concrete}}{E_{concrete}} \tag{5.4}$$

$$\frac{\sigma_{clay}}{\sigma_{concrete}} = \frac{E_{clay}}{E_{concrete}} = 0,575 \tag{5.5}$$

The cross section is however not constant, since we have a clay tube inside the concrete. If we look at the horizontal line crossing the center of the tube, it can be said that the total stress at this height of the cross section is composed of stress in the clay tube and stress in the concrete. The clay tube represents 10% of this line (1cm/10cm) while the concrete represents the other 90%.

$$0,1 \cdot \sigma_{clay} + 0,9 \cdot \sigma_{concrete} = \sigma \tag{5.6}$$

The total stress σ at this height in the cross section is calculated by formula 5.7, by assuming that the stress just above the crack tip is equal to the ultimate stress in the concrete beam (just before a first crack occurs) as shown in figure 5.4.

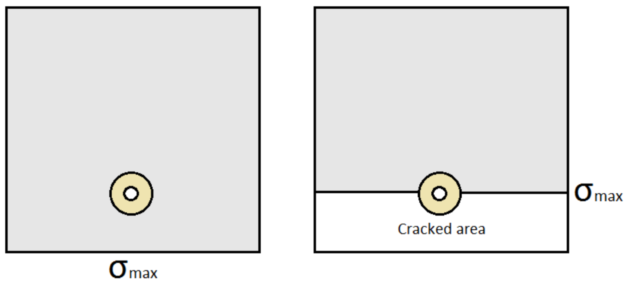

Figure 5.4: Constant maximum stress: before cracking (left) and during cracking (right)

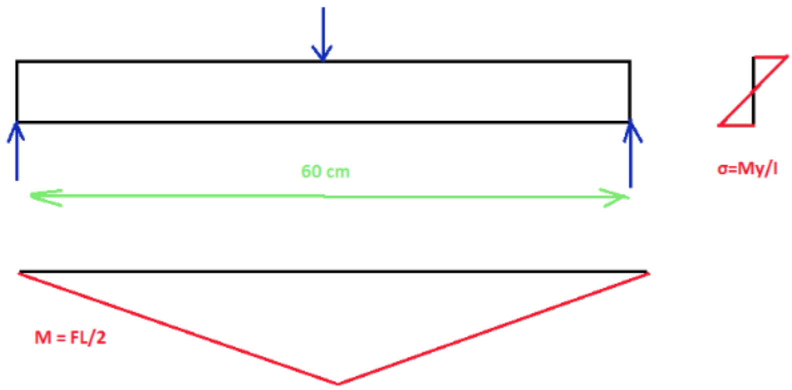

Figure 5.5: Maximum moment due to a centered vertical force (used in formula 5.7)

$$\sigma = \frac{My}{I} = \frac{F \cdot \frac{L}{2} y}{I} \tag{5.7}$$

In this equation, y is equal to 5cm, L is equal to 60cm (length between supports) and I is $\frac{10^4}{12} cm^4$. The ultimate load F is taken as the mean value of ultimate load of all eight beams and is equal to 4023N. Now, the stress in the clay tube can be calculated as:

$$0,1 \cdot \sigma_{clay} + \frac{0,9}{0,575}\sigma_{clay} = \sigma = 724\frac{N}{cm^2} \tag{5.8}$$

$$\sigma_{clay} = \frac{\sigma}{1,67} = 434\frac{N}{cm^2} = 4,34MPa \tag{5.9}$$

If we compare this value with the ultimate tensile stress measured in the clay tube, it seems that the tube will not break simultaneously with the concrete. To be sure, the tubes will be embedded in concrete for a new experiment, providing us with a more accurate answer.

5.4 Three-point bending test with clay tubes

The set-up for the experiment will be the same as the three-point bending test in section 4.1. The speed of testing is 0,5mm/min. Eight acoustic emission sensors are placed on the beam, identical as for the four-point bending tests in section 4.5. The purpose of these sensors is to see a difference in released energy, that will be correlated to the breaking of concrete and the breaking of the clay tubes. This information is used together with DIC to investigate whether the clay tubes break at a crack width of $200\mu m$ or $300\mu m$, measured by the CMOD.

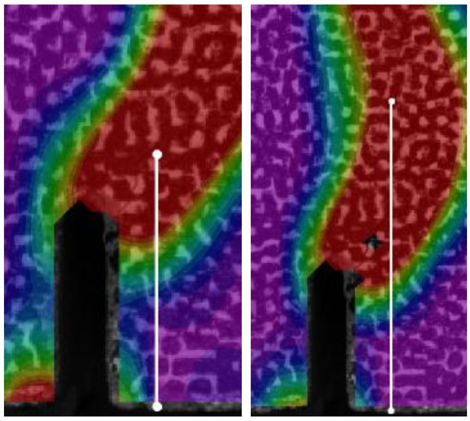

Figure 5.6: Cracking of the first beam at a crack width of 200μm (left) and 300μm (right)

The images taken by the DIC cameras, reveal that the crack indeed starts at the premade notch (figure 5.6) for the first beam. The absence of other increased strain fields evince that there is only one crack. With the software, crack depth on the images are measured. A depth of 19mm is found corresponding with 200μm of crack width; a depth of 33mm is found corresponding with 300μm of crack width. At 200μm the clay tube inside the beam is not cracked yet, but at 300μm the crack surely passes the tube.

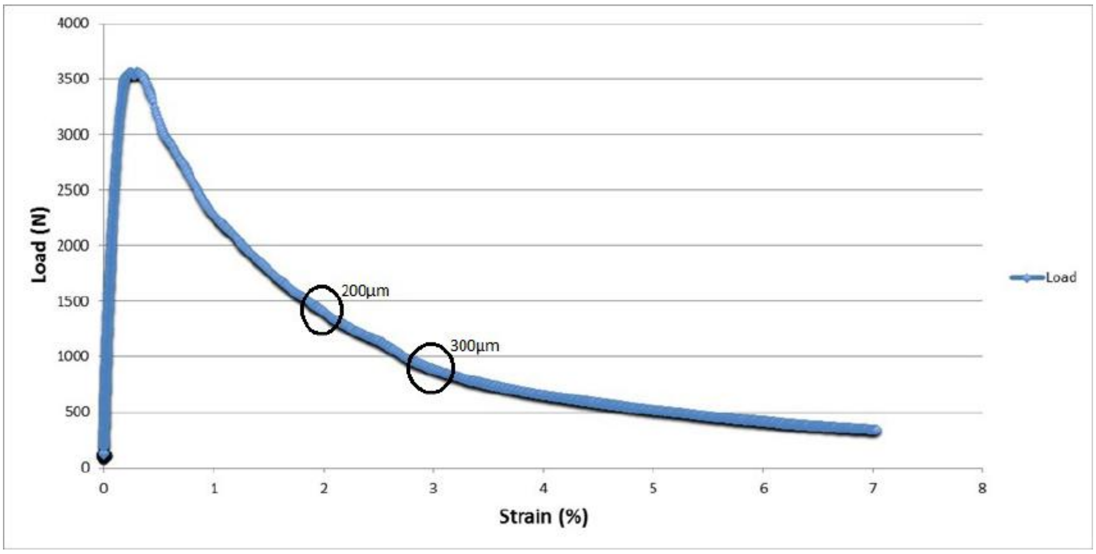

Figure 5.7: Load curve of first beam with clay tube

The loading curve of the first beam with clay tube is represented in figure 5.7, where the two considered crack widths are indicated. No load drops are visible at these stages, so no information is revealed about cracking of the beam or clay tube.

After analyzing the acoustic emission data, no particularities are seen and as well no information about cracking of the clay tubes is retrieved. The assumption is made that the clay tubes break if the cracks pass them, although this cannot be taken for granted.

To be representative, a second beam with clay tube was made and tested in the same manner. Also here the beam is only cracked in the middle. A depth of 49mm is found corresponding with 200μm; a depth of 51mm is found corresponding with 300μm. No big difference in crack depth between those two widths occurs, but the crack already passed the tube at 200μm. Here too, we assume the tube to be broken.

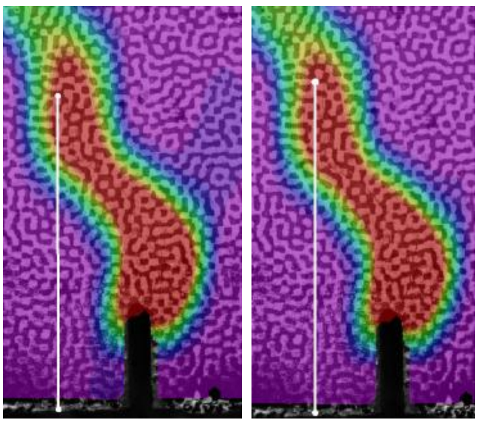

Figure 5.8: Cracking of the second beam at a crack width of 200μm (left) and 300μm (right)

The loading curve of the second beam with clay tube is represented in figure 5.9, where the two considered crack widths are indicated. At the point of ultimate loading, a load drop occurs.

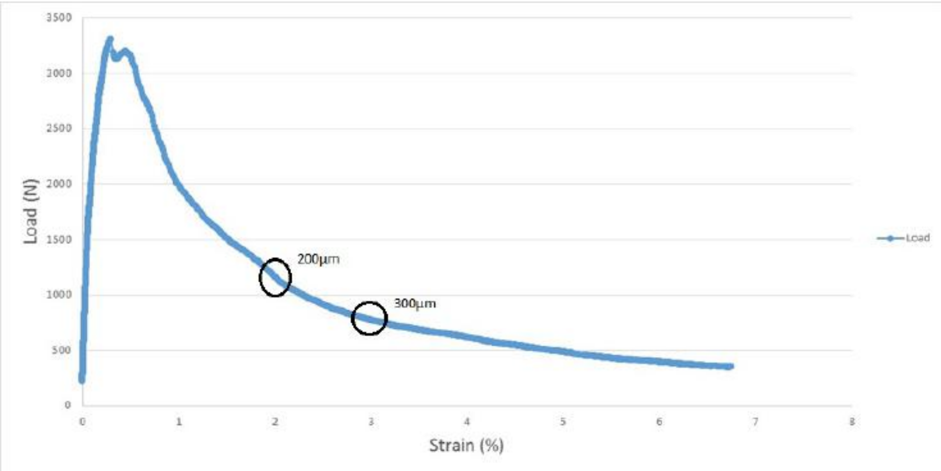

Figure 5.9: Load curve of second beam with clay tube

Out of the acoustic emission data, clear events are found for cracking of the beam, located in the middle. Since this is already seen on the DIC pictures, further analysis is not needed.
Comparing the load curves shows that a similar behaviour is found. The difference lies in the fact that for beam 1, the crack had not passed the clay tube at $200\mu m$ of crack width, while this is the case for the second beam. A crack opening of $200\mu m$ is already mentioned as being a normative value for self-healing, however the common value is $300\mu m$. It can thus be concluded that for this value, the crack passed both tubes. Following our assumption, the clay tubes will break, but there is still an uncertainty about this. These results show the potential of clay as a material for vascular self-healing.

5.5 Influence of shape on load impact

The differences in load impact on various cross sectional shapes will be tested as explained in section 4.4. By means of the equations listed in that section, the impact load on the tube can be calculated by using the maximum strain recorded during sand falling. To check whether these values are correct, a calibration is performed on each of the tubes by applying a point load in the middle of the tube. Comparing the theoretical loads (by filling in the strain in equation 4.15) with the applied load shows a significant difference (more than 20%). Therefore, a linear equation relating load and strain is matched to the strains and applied loads. The obtained graph is depicted in figure 5.10 in case of the round tube.

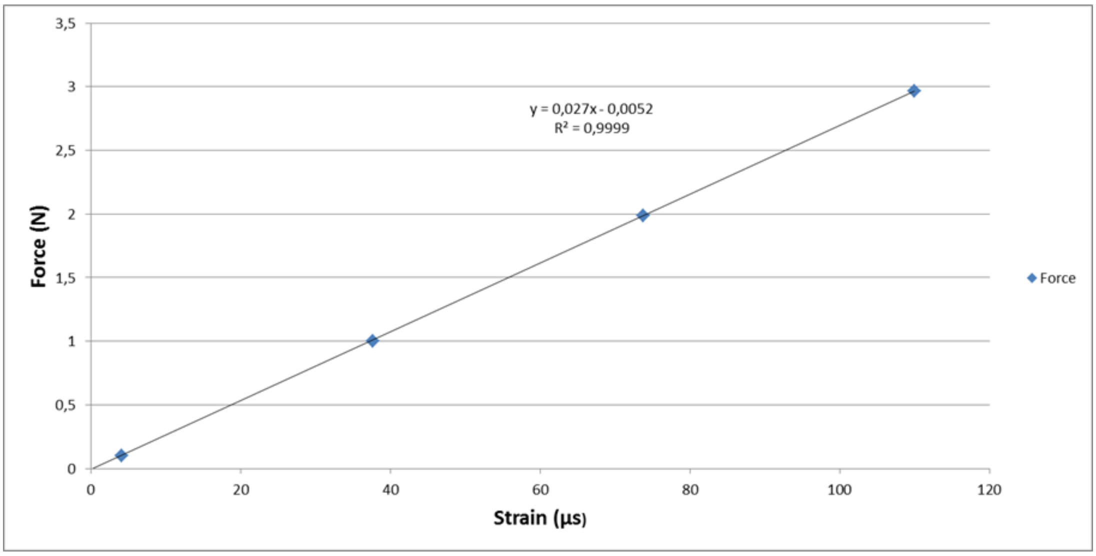

Figure 5.10: Linear relation between applied load and measured strain

The obtained relation can now be used to calculate the distributed load that comes from the sand impact. However, a conversion should be done since the equation is derived for a point load and is thus only correct for the same load situation. By saying that the strains at the extreme fibre with largest bending moment are equal for both distrubuted and point load, the distributed load can be linked to the point load, which is linked to the strain by the equation in figure 5.10.

$$\frac{q \cdot y_{max} \cdot L^2}{8E \cdot I} = \frac{F \cdot y_{max} \cdot L}{4E \cdot I} \tag{5.10}$$

thus the load by calibration is given by:

$$q = \frac{2F}{L} \tag{5.11}$$

The load by theory is then given by:

$$q = \frac{8E \cdot \epsilon \cdot I}{y_{max} \cdot L^2} \tag{5.12}$$

Below, a table summarizes the measured maximum strains and the loads calculated by both the theoretical equations and the calibration on the IPC tubes.

Table 5.4: Summary table of influence of shape on load impact on IPC tubes

	Droplet				Circle				Diamond
Weight sand	19kg		25kg		19kg		25kg		25kg
Height	50cm	92cm	50cm	92cm	50cm	92cm	50cm	92cm	50cm
Maximum strain (μs)	72	112	148	166	133	141	158	230	355
Load by theory (N/m)	20,8	32,3	42,7	47,8	40,9	43,4	51,2	71,0	40,7
Load by calibration (N/m)	13,9	28,5	21,6	31,9	33,5	35,5	40,4	58,1	58,3

When comparing the strain and load for identical volume of sand and testing height, the droplet shape has a serious advantage over the circular and the diamond one. Also, testing with higher volume and/or pouring from increased height gives a larger strain.
Afterwards, a test with two clay tubes is done. Since the rugby form could not be made in IPC yet, this one is tested in clay together with a droplet form tube in order to compare with the IPC results. These tests are performed using a volume of 25kg of sand, pouring from a height of 50cm, since the link between strain vs. pouring height and strain vs. volume of sand is already proven. The values of strain and load can be found in table 5.5.

Table 5.5: Summary table of influence of shape on load impact on clay tubes

	Droplet	Rugby
Maximum strain (μs)	158	89
Load by theory (N/m)	56,6	67,0
Load by calibration (N/m)	44,2	34,8

It can be seen from the table above that, in theory, the rugby cross section has a disadvantage over the droplet form. However, the theoretical formula does not take into account the flow of sand, as the impact is taken as a static, distributed load. As seen during the experiment, the sand flows smoothly over the rugby form. The value of the load by calibration states that the rugby form experienced a lower impact than the droplet form, and this with an almost equal amount of material used. The cross sectional area of the droplet form is equal to $82,6mm^2$ while the one of the rugby form is $82,8mm^2$. It is therefore concluded that the theoretical approximation about minimum drag and maximum penetration, as explained in section 3.5, is correct and that the ideal shape to minimize the load impact is found.
A critiscism should however be made about the flow around this shape: in concrete beams, only few centimeters of cover are present underneath the reinforcement. Since tubes are placed under these bars, only a small space is available between tube and bottom of the mold. When pouring concrete, the flow around the tubes will quickly be stopped by the fact that the space beneath the tube is filled up. Question then arises if a cross section that minimizes the drag is necessary.

5.6 Four-point bending test with IPC vascular system

As explained in section 4.5, four-point bending tests are used to evaluate the efficiency of self-healing. The speed of the Instron machine is set at 2mm/min. Regarding the theory already presented, two notes should be made before representing the results. First, during some tests a small pause (or two) is made. When the loading stops, the beam relaxes and the load on the beam will be decreased. On the graphs representing the load cycles, such points in time can be seen by straight vertical lines in between two measurements, as in figure 5.11. Secondly, it was said that eight sensors are used. However, due to a problem, only two sensors captured signals during the first load cycle. For these loading steps, only a linearized location of events could be found between sensors 5 and 6, which are on the top left and top right on the concrete beam, as showed in figure 4.14. To be consistent in analyzing and comparing the data captured by the sensors, localization of events will only be checked linearly for all beams of this set. This direction is the longitudinal axis of the beam, in our case called the x-direction.

5.6.1 Reference

First, two reference beams are loaded in four-point bending. When cracking occurs, the test is stopped and the beams are put aside. Afterwards, the beams are reloaded to obtain the difference in stiffness. These values will be used to compare the stiffness and strength after reloading of a beam with self-healing mechanism. An analysis regarding the cracking of one reference beam, being reference 1, is discussed. The acoustic emission energy is plotted together with the load-time curves.

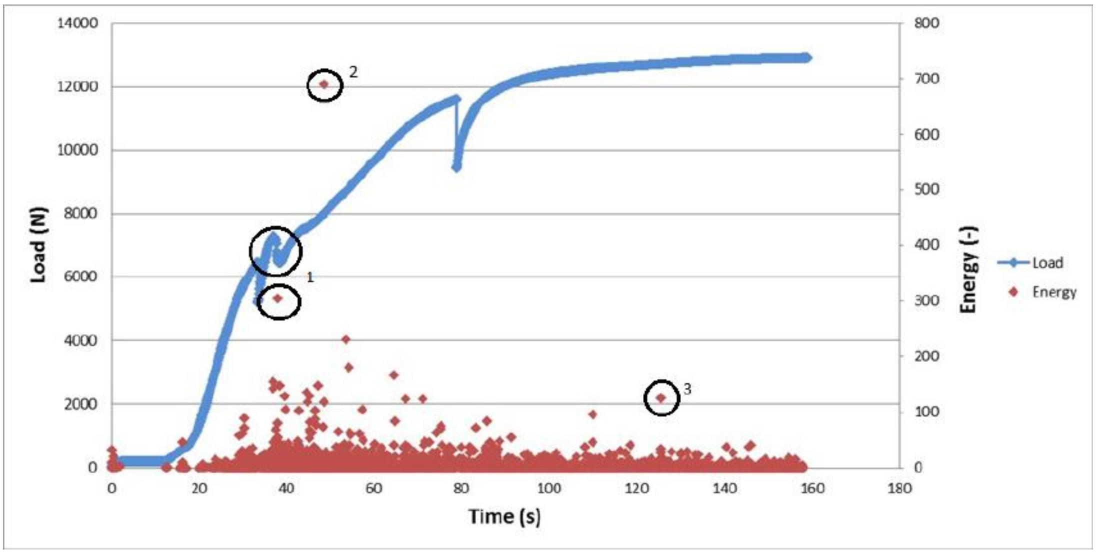

Figure 5.11: Load vs. time and energy vs. time of reference specimen

Figure 5.11 shows the similarities between load and energy at a specific moment in time. Comparing high energy events with load drops on one side and DIC data on the other side provides information about the cracking of the beam. Three moments are chosen where a clear relation is found between at least one of these measured parameters. The number of events is then plotted over the longitudinal axis of the beam to locate the chosen points. In this way, a closer look on the DIC pictures can be taken at the areas with high number of events or a particular point in energy. These locations normally tend to be the same as the locations with high strains as seen in the DIC data, as cracking is expected to take place where high strains are measured. A global view of the strain field on the beam is given in figure 5.12 and afterwards the location of events is depicted.

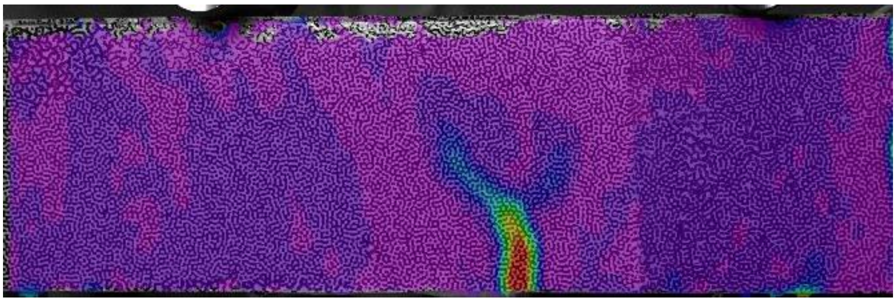

Figure 5.12: Global strain field on reference specimen before first event

Figure 5.12 depicts the strain field on the beam before specific points are seen on the loading curve or in acoustic energy. In the middle, there is already a strain field available, which gives high chance to allocate a crack at further loading.

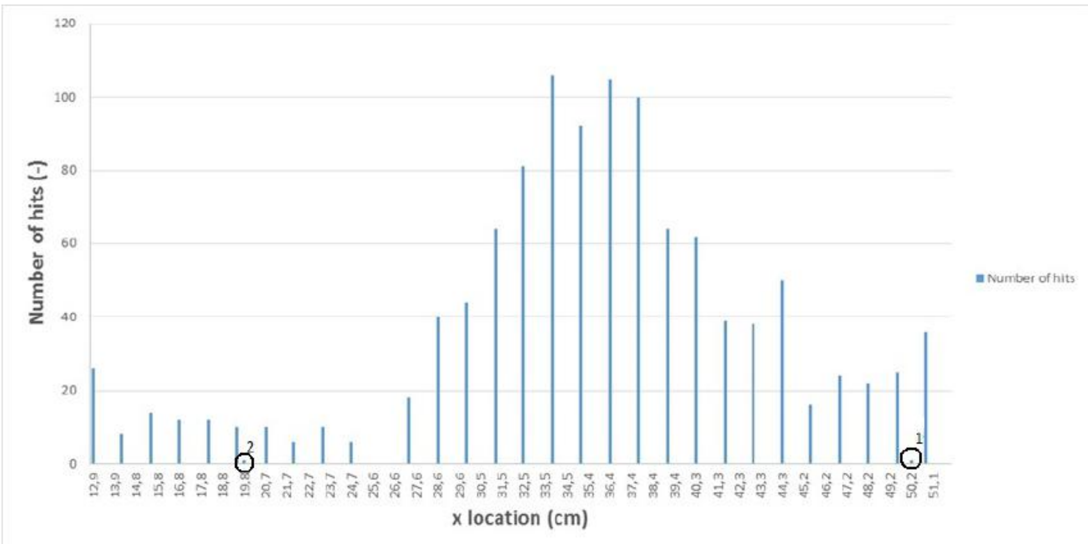

Figure 5.13: Location of events in the x-direction of reference specimen at first loading

The location of moments 1 and 2 are found using *Noesis*, a program for analysis of acoustic emission data and shown on figure 5.13. For the third one, no specific location could be found.
The three chosen points on figure 5.11 are now individually discussed. For number 1, there is a relatively high energy seen at the same moment a load drop takes place. This clearly proves that something has happened inside the beam. To clarify whether a sudden increase in strain or the beginning of cracking has occured, a comparison with the DIC data is made. Picture 5.14a shows the initiation of a crack, simultaneously with the initiation of the strain field on the right side of the speckle pattern. It is the strain field associated with the first moment in time.

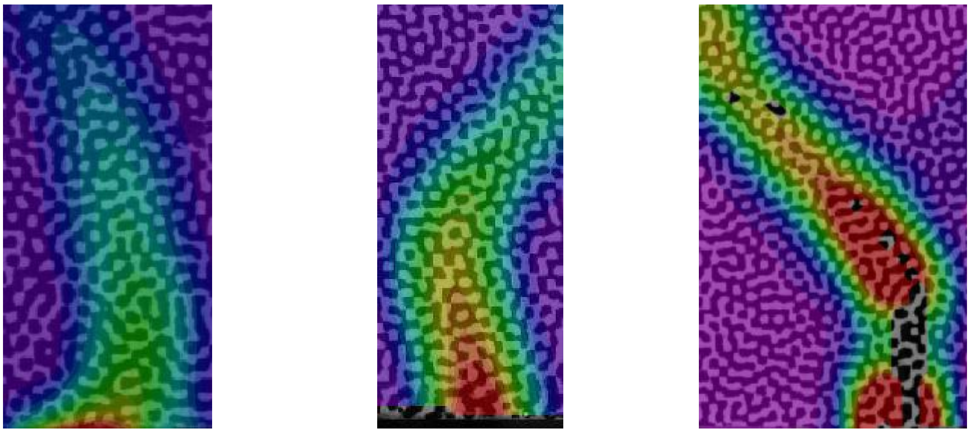

(a) Moment 1 (b) Moment 2 (c) Moment 3

Figure 5.14: Pictures of the DIC data for the different events on reference specimen at first loading

At the next point in time, being point 2, only a high energy event occurs in abscence of anomalies in the load curve. Analyzing the DIC pictures, reveals the beginning stage of cracking on the left side, shown in figure 5.14b.
The third event shows a high value in energy, but lower than in the previous events. It can be linked to the start of cracking in the middle increased strength field (figure 5.14c). For this event, no location was found by use of AE. It can however be seen in figure 5.13 that a high number of events occurs in the middle of the beam. The strain field of figure 5.12 has now changed into the one of the figure below.

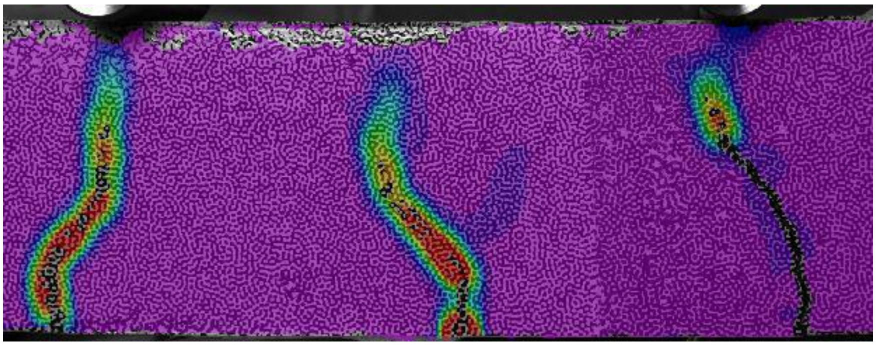

Figure 5.15: Ultimate strain field on reference specimen

The ultimate strain field after first loading is shown in figure 5.15. Three cracks are visible in the speckle pattern, showing the weak points of the beam. The crack widths after first loading are tabulated below in table 5.6. No healing mechanism is present, but the values give a good idea of typical widths reached for the following experiments containing a vascular network.

Table 5.6: Crack widths of reference beams at ultimate loading, as seen on DIC (accuracy $\pm 70\mu m$)

Crack widths (μm)	Left	Middle	Right
Reference 1	/	405	620
Reference 2	135	/	/

As already explained in paragraph 5.4, it is very important for the vascular system to release healing agent at the proper crack width. In other words, the healing agent should infiltrate as soon as possible, preferable before the crack reaches the tensioning bars such that water and/or gasses can infiltrate and reach these. In practice, the target is set to heal around 200μm to 300μm. To quantify, the crack widths at ultimate loading are measured on the DIC pictures by means of pixels. Since one pixel corresponds to a length of 135 μm, more precise values could not be given and the accuracy is thus rather low. In addition, only the cracks visible on the side with speckle pattern are taken into account. Caution should be taken for the fact that cracks can be smaller and generally wider on the surface not facing the DIC cameras of the beam, a feature that is enhanced by the reduced visibility on the side with speckle pattern (due to the coating of paint).

A summary graph of the two reference beams in their loading and reloading cycle is depicted below in figure 5.16. This graph shows the load vs. displacement curves for the two reference beams.

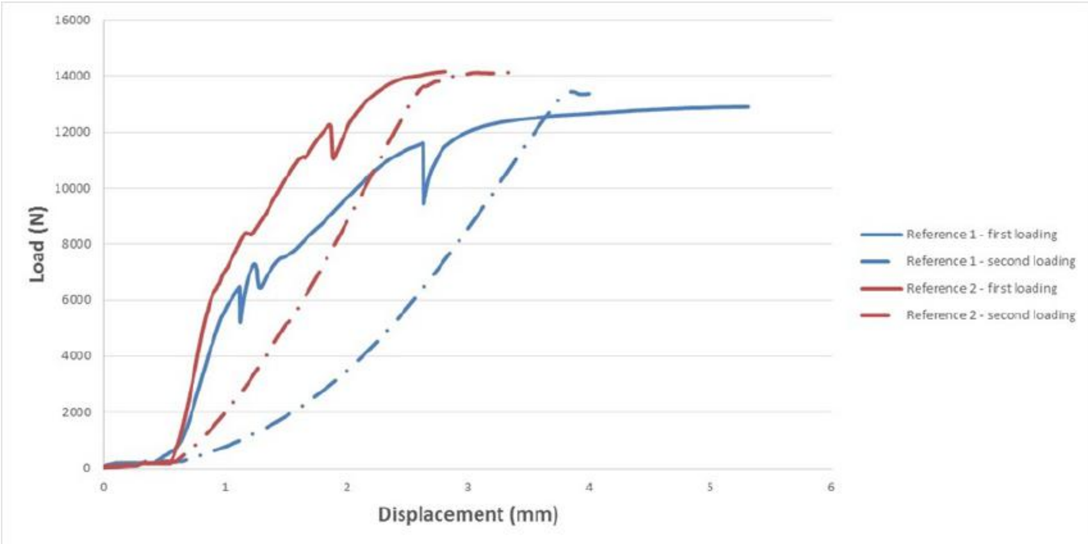

Figure 5.16: Loading and reloading curves of the two reference beams

In the first loading cycle, the stiffness is significantly higher (steeper slope) than for reloading. The exact values, found by plotting a trendline through the straight part of the curves, are tabulated.

Table 5.7: Stiffness of the reference beams in loading and reloading cycle

	Stiffness	Mean stiffness per load cycle	Standard deviation
Reference 1 - first loading	13800N/mm	13844N/mm	61,5N/mm
Reference 2 - first loading	13887N/mm		
Reference 1 - second loading	5103N/mm	5910N/mm	1141N/mm
Reference 2 - second loading	6717N/mm		

Table 5.7 states that the stiffness of the first load cycle is significantly higher than the one for the reloading cycle. Also, it is seen that the onset stiffnesses of both beams lie very close to each other. This can be a coincidence, but makes the tests more representative. A mean value in stiffness of both load cycles will be used to compare the stiffness after self-healing. These values are: $13844 N/mm$ for first loading and $5910 N/mm$ for reloading.

5.6.2 Round tubes

A vascular system, consisting of round tubes, is put inside the concrete beams. An evaluation of the self-healing efficiency will be done by applying three load cycles to the beams, with at least 24h of healing time in between. At the first loading stage, the healing agent is added to the vascular system. Before second loading, the vascular system is refilled. The healing agent flows into the cracks and reacts with the concrete. Cracks are then sealed upon hardening of the healing agent. Using DIC, the depth of the cracks is revealed and assures us that tubes are broken. By using both DIC and acoustic emission, the position of cracks is found. These are important to investigate whether cracks reopen upon reloading. If not, the healing agent has not only cut off the steel reinforcement from external humidities, which is most important, but also strengthened the beam. Four beams of this type are tested. Only one representative specimen is discussed in this section, being nr. 3. In the same way as for the reference specimen, particular points are picked from the loading curve and the acoustic energy. A strain field before these points is depicted below.

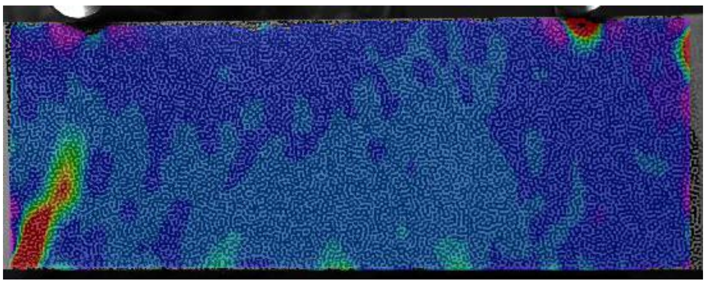

Figure 5.17: Global strain field before first event

The strain field on the left in figure 5.17 announces the position of a possible crack. Three other strain concentrations are starting to the right of this one.

First load cycle

For the first load cycle, two load drops reveal a particular happening inside the beam. Both of them go together with a highly energetic acoustic event. In between these load drops, another event is chosen, because of its relatively high value in comparison with other captured events.

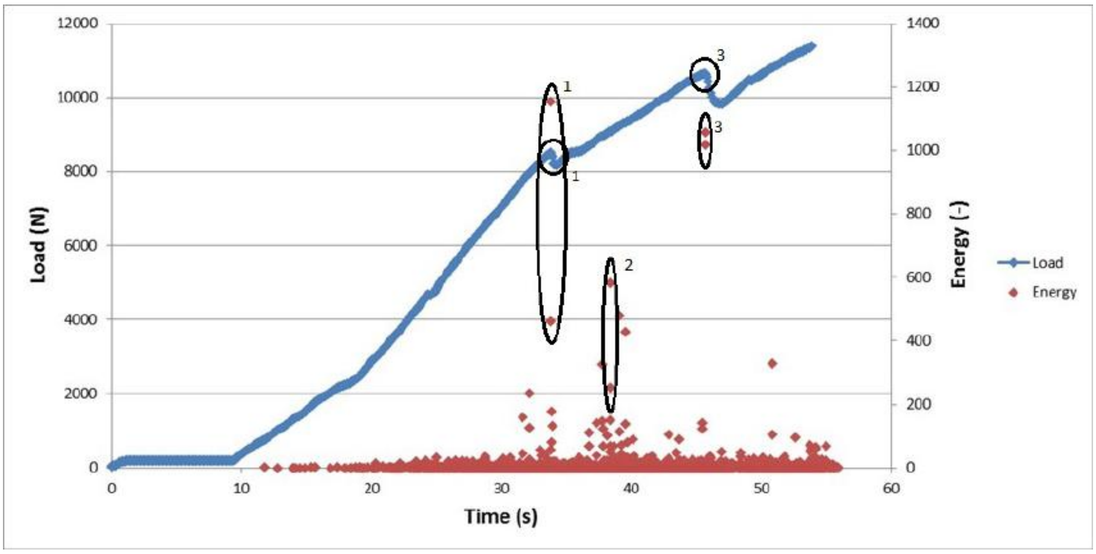

Figure 5.18: Load vs. time and energy vs. time before healing

For all three moments in time, the location is searched by analyzing the acoustic emission data. A histogram showing the number of events at different positions on the longitudinal axis is shown in figure 5.19.

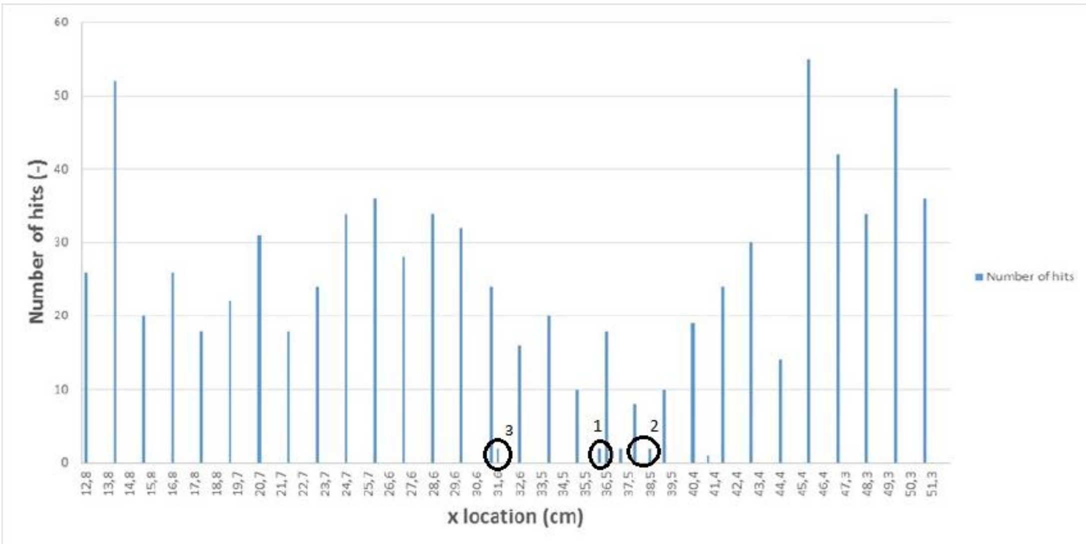

Figure 5.19: Location of events in the x-direction before healing

The location of all three points on figure 5.18 are found. A closer look is now taken on the different features and their DIC pictures.
As can be seen in figure 5.18, the first load drop comes together with an event of acoustic emission. This event also shows the highest energy during this cycle. The location of this event is in the

middle of the speckle pattern, being at the right initiating strain field in figure 5.17. DIC data show that, around this moment, a crack occurs at the same spot, as shown in figure 5.20a.

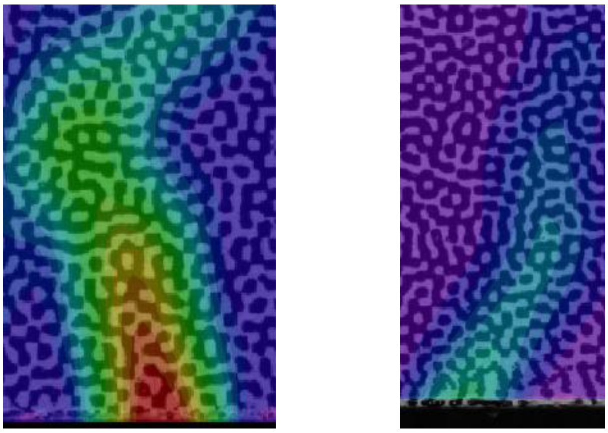

(a) Moment 1

(b) Moment 3

Figure 5.20: Pictures of the DIC data for the different events before healing

Secondly, there is an event of relatively high energy seen between the load drops. Locating this event shows that it is around the crack that just occurred. The picture of the DIC does not show any difference with the previous one.

At the second load drop there is again an event with a high energy. This event is located more or less in the middle of the beam, being at the second strain field spot in figure 5.17. This is confirmed by the DIC picture in figure 5.20b and a new crack initiates at the center.

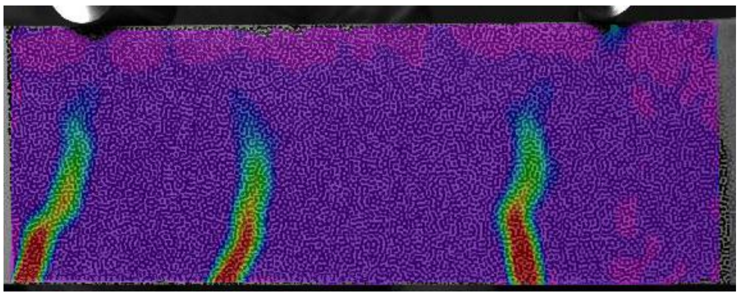

Figure 5.21: Ultimate strain field before healing

On figure 5.21 three strain fields with related cracks are visible. For the left crack, no acoustic emission events were captured. Since this crack is close to one of the sensors, the other sensor probably did not capture a hit. The crack can then be dislocated, which means that the acoustic emission sensors 'think' that it comes from elsewhere. However, at the moment that the DIC pictures show a crack on the left, no hits of increased energy are seen. Identically as for the reference beams, a list of crack widths after first loading is available in table 5.8.

Table 5.8: Crack widths of beams 'round' at ultimate loading, as seen on DIC (accuracy $\pm 70\mu m$)

Crack widths (μm)	Left	Second from left (or middle)	Third from left	Right
Specimen 1	/	/	/	/
Specimen 2	311	446	324	310
Specimen 3	378	351	/	392
Specimen 4	877	1040	/	580

The table above represents the crack widths for the different beams. In one of them, four cracks were seen, while in the other only three cracks were present. The middle crack is therefore placed in the column 'second from left (or middle)'. In order to be sure that healing could take place in this first set of healing experiments, the beams are bended sufficiently to have wide cracks. All cracks that intersected the vascular tubes, were filled with healing agent. A width of 300μm to 400μm proved succesfull to break the tubes. No data is retrieved from the first beam with round tubes, since the cracks were only visible on the back side of the beam, and not on the speckle pattern. Note that, in all specimens, three to four clear cracks occured, from which two at the location of the reservoirs. These reservoirs are located just outside the zone of maximal bending and introduce thus local weaknesses. No healing can be retrieved from these cracks.

Second load cycle

Since cracks were already present in the beam, the same denomination for them will be used as in the first load cycle. One load drop is seen in the second load cycle.

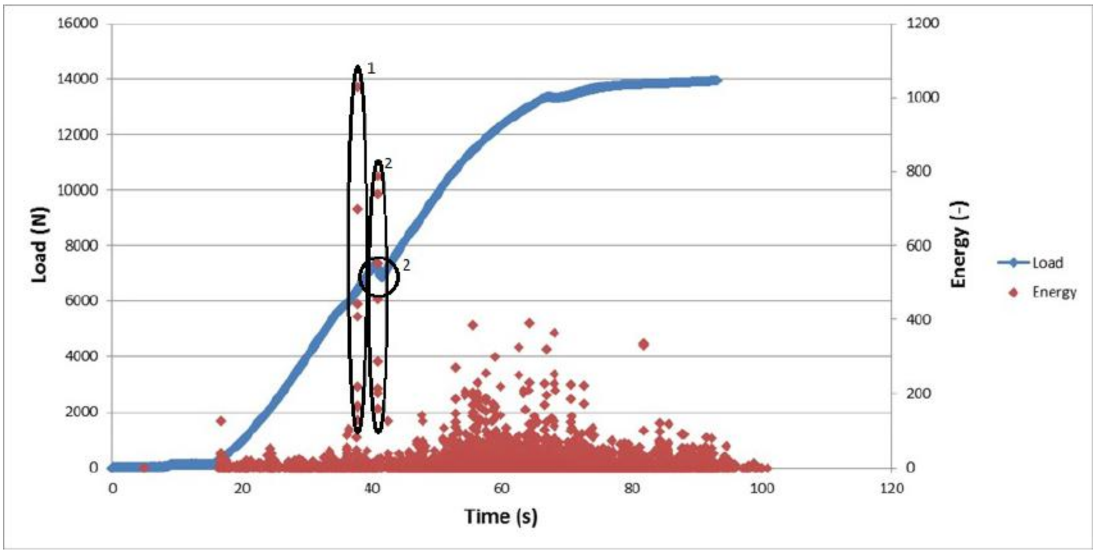

Figure 5.22: Load vs. time and energy vs. time after first healing

Some seconds before the load drop, a high energy event is captured by the sensors as shown in figure 5.22. Only two spots in time are discussed for this load cycle. As the figure above depicts, there are some raised energy events besides the ones chosen. Since their values are not significantly high and nothing happens in the load curve, these will not be discussed in depth.

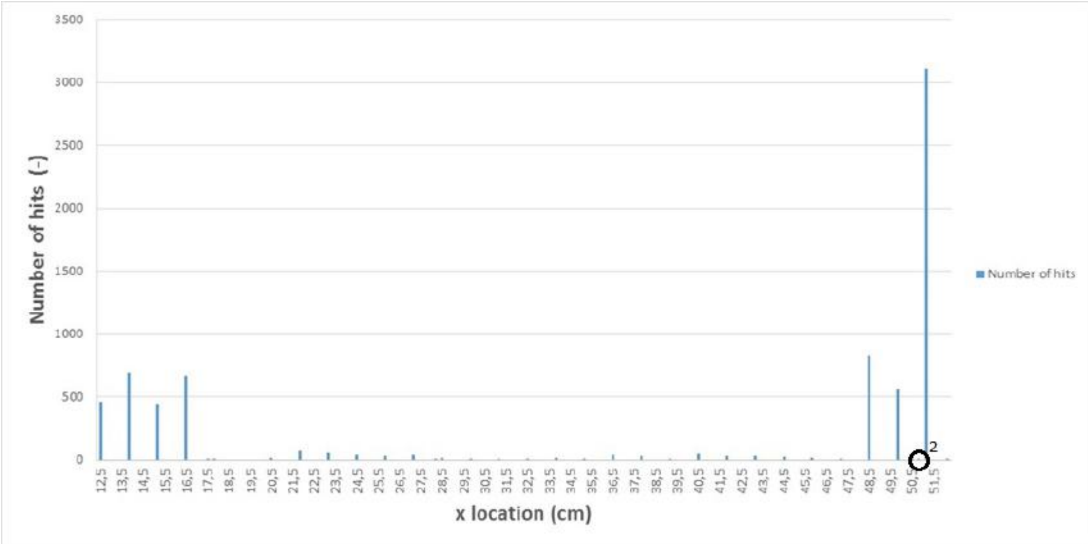

Figure 5.23: Location of events in the x-direction after first healing

Figure 5.23 shows the location of moment number 2. For the first one, the location of the event could not be found in the acoustic emission data. Also, pictures from the DIC do not show any particularity, neither a reopening of a present crack.
At the load drop, a second high energy event is seen. This event is localized at the right side of the beam. Comparison with the picture taken at that moment shows that the right crack, which was already there in the first loading cycle, reopens.

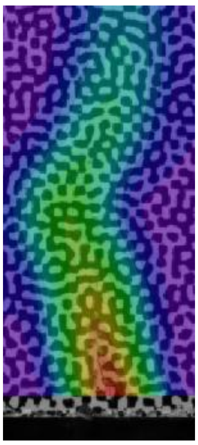

Figure 5.24: Picture of the DIC data for the event at load drop after first healing

Figure 5.24 represents the reopening of the right crack. A new crack initiated at the right side of this one, but can not clearly be seen since it is outside the speckle pattern.

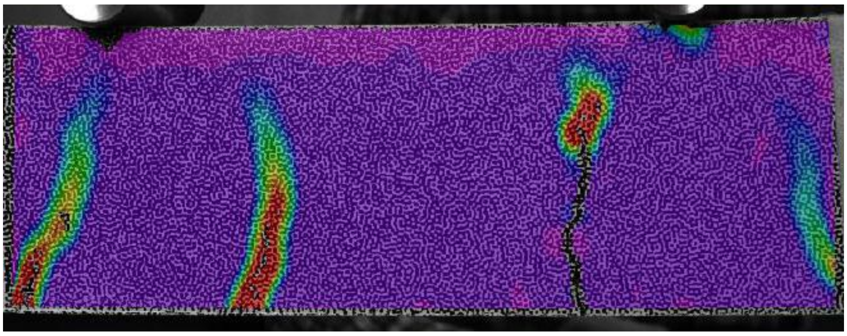

Figure 5.25: Ultimate strain field after first reloading

The final strain field in figure 5.25 shows that the third crack from the left, the one that has been talked about before, opened and extended deeply in the beam.

Third load cycle

In the third load cycle there is no load drop. The chosen points in time are merely based on the acoustic events.

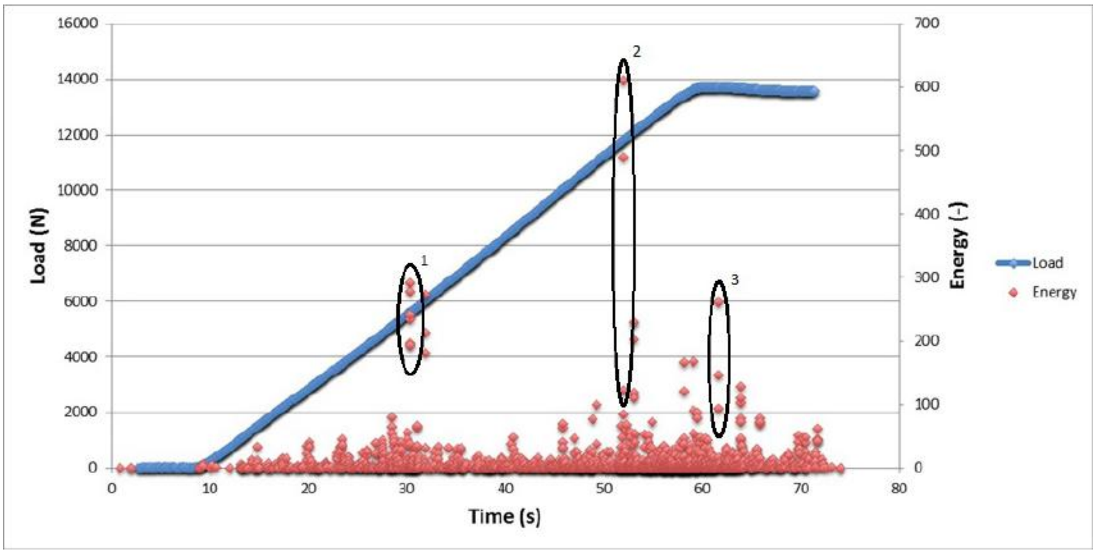

Figure 5.26: Load vs. time and energy vs. time after second healing

The first point in time on figure 5.26 represents an event of medium high energy. Localizing this point based on AE data was however not possible and the DIC showed no particular changes in strain around this event. Therefore, the event just after is also not taken into account for further analysis.

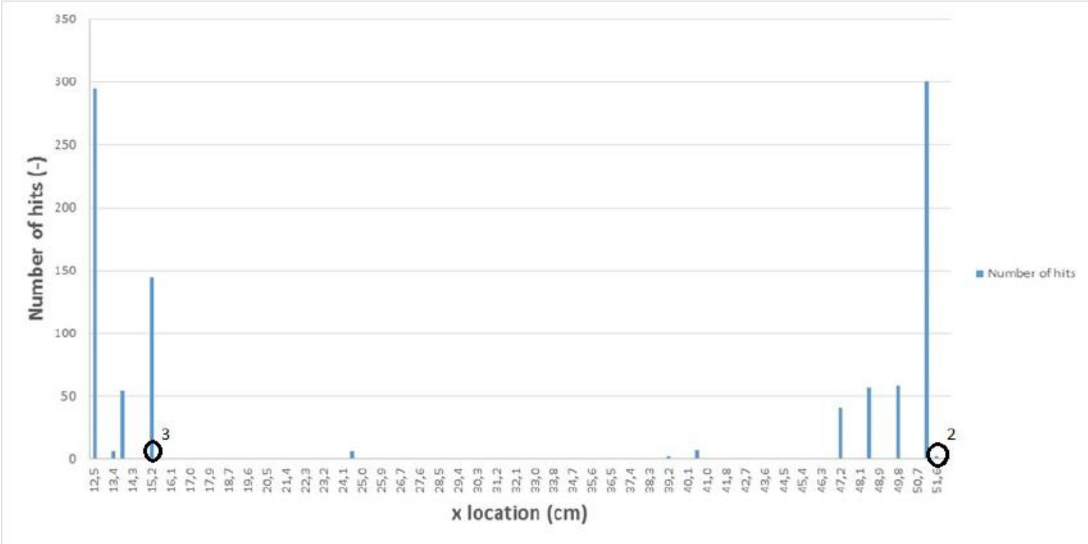

Figure 5.27: Location of events in the x-direction after second healing

The highest energy event is the second point of interest in 5.26. Following the AE data in figure 5.27, the location of this event is totally on the right of the beam. Probably it is linked to the outermost right crack which initiated in the second load cycle. However, this could not be checked on the DIC pictures, since the speckle pattern stops there.
The third and last designated point is at the end of loading, where the load stays constant. Event location is on the left extremity of the pattern. No particular changes are seen in the DIC and are therefore not depicted.

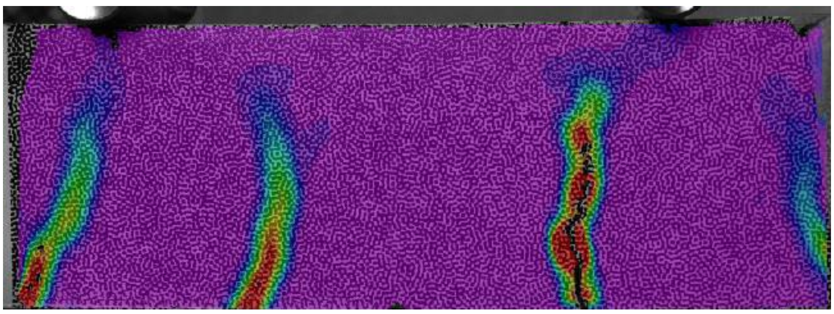

Figure 5.28: Ultimate strain field after second healing

Figure 5.28 holds the final strain field of beam round 3 after 3 loading cycles. Four strain concentrations are visible with cracks inside.

Discussion

A plot of the three load cycles is shown in figure 5.29. The stiffness during the different load cycles will be compared hereafter.

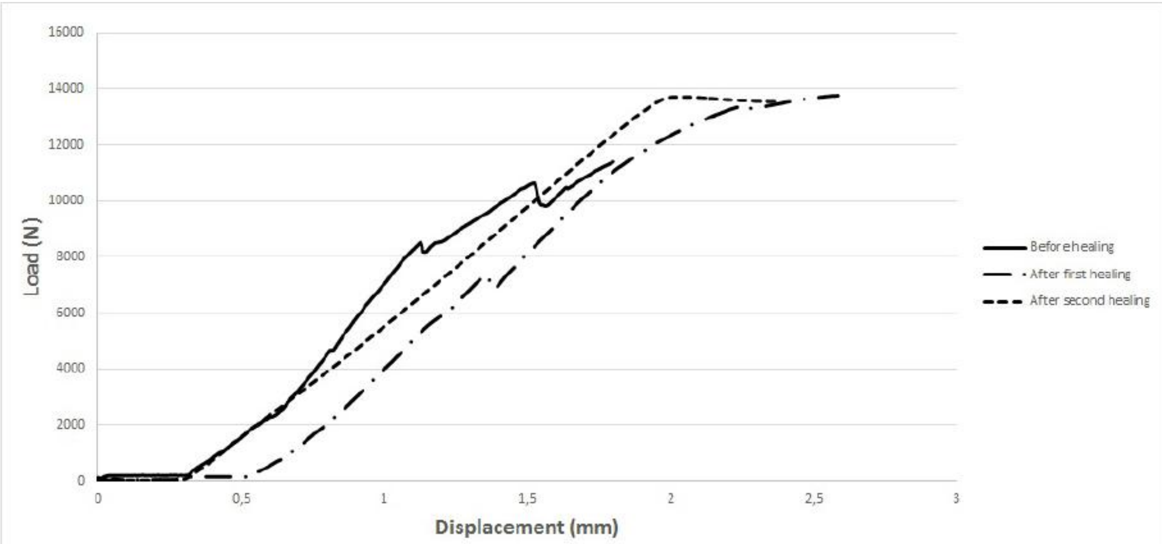

Figure 5.29: Load vs. displacement of the three load cycles

As expected, the stiffness of the beam before healing is the highest and decreases per load cycle. To make an evaluation about these stiffnesses, a trendline is plotted and the values of the bending stiffnesses are tabulated.

Table 5.9: Stiffness of specimen in different load cycles

	Stiffness (N/mm)
Before healing	10577
After first healing	9112
After second healing	8290

Table 5.9 details the values of the stiffnesses. It is thereby seen that these values decrease per loading cycle. Comparing these values to the stiffness of a reference beam, at first and second loading, shows a particular feature: the stiffness before healing is smaller than the one obtained for the reference beams. We assume that this is due to the vascular system that provides a large discontinuity inside the beam and debonds at higher load. However, after first healing, the stiffness only lowered by 10% whereas for the reference beams this is more than 50%. This is a clear proof that healing occurred. Even after a second healing and loading cycle, the stiffness is still higher than for reloading of a reference beam.

The values of stiffnesses for all beams with round tubes are listed in table 5.10 and a mean value of the stiffness and the standard deviation is calculated.

Table 5.10: Stiffness of the beams with round tubes in different load cycles

	Stiffness before healing	Stiffness after first healing	Stiffness after second healing
Specimen 1	13589N/mm	11922N/mm	7907N/mm
Specimen 2	12255N/mm	10165N/mm	7759N/mm
Specimen 3	10577N/mm	9112N/mm	8290N/mm
Specimen 4	8958N/mm	7699N/mm	6598N/mm
Mean stiffness	11345N/mm	9725N/mm	7639N/mm
Standard deviation	1743N/mm	1541N/mm	631N/mm

Using the stiffnesses in the table above, the self-healing efficiency is calculated by formula 4.17. The values are shown in the table below.

Table 5.11: Self-healing efficiency of beams with round IPC tubes

	Regain after first healing (%)	Regain after second healing (%)
Specimen 1	88	58
Specimen 2	83	63
Specimen 3	86	78
Specimen 4	86	74
Mean efficiency	86	68

Table 5.11 denotes the percentages of remaining stiffnesses compared with the original ones. After the first healing cycle, the remaining stiffnesses lie in between 80% and 90% of the specimens at first loading. Looking at the second healing cycle, the results are more widespread, but always lower than in the first healing cycle. This means that healing truly happened, at least for the first cycle. The healing efficiencies of the second healing cycle do not really prove if healing is achievable after the first cycle. During second healing tests, most beams did not bleed healing agent. Only a few exceptions had new healing agent visibly drawn into one or two cracks. However, the regain after second healing stays higher in comparison with the reference beams (table 5.7) where those values are beneath 50%. It is not said that a second healing occured, but rather expected that it is still an influence of the first healing cycle where stiffness regain is still notable in following loading cycles.

5.6.3 Droplet form tubes

In this section, the beams with vascular system using droplet form tubes are investigated upon three loading cycles. Both width and position of cracks are examined.
Three beams with vascular system and droplet tubes are tested. Hereafter, specimen nr. 1 with droplet tubes will be discussed. The load curves of all three specimens were first compared to choose a representative one. Again, some particular points will be chosen for analysis. The strain field at the start of the test, after applying a small load, can be found in figure 5.30. Two strain concentrations are seen in the figure above, at the extremities of the speckle pattern.

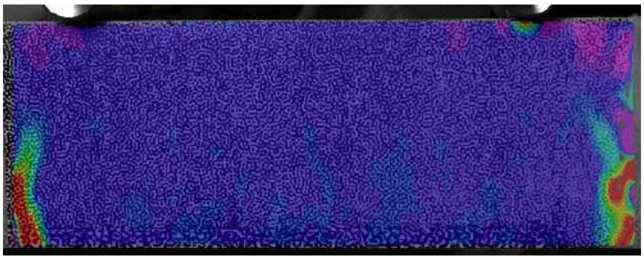

Figure 5.30: Global strain field before first event

First load cycle

Two load drops with coincident high acoustic emission energy are found by analyzing the load curve of the first beam. Besides these two points, no significantly interesting data are seen on figure 5.31

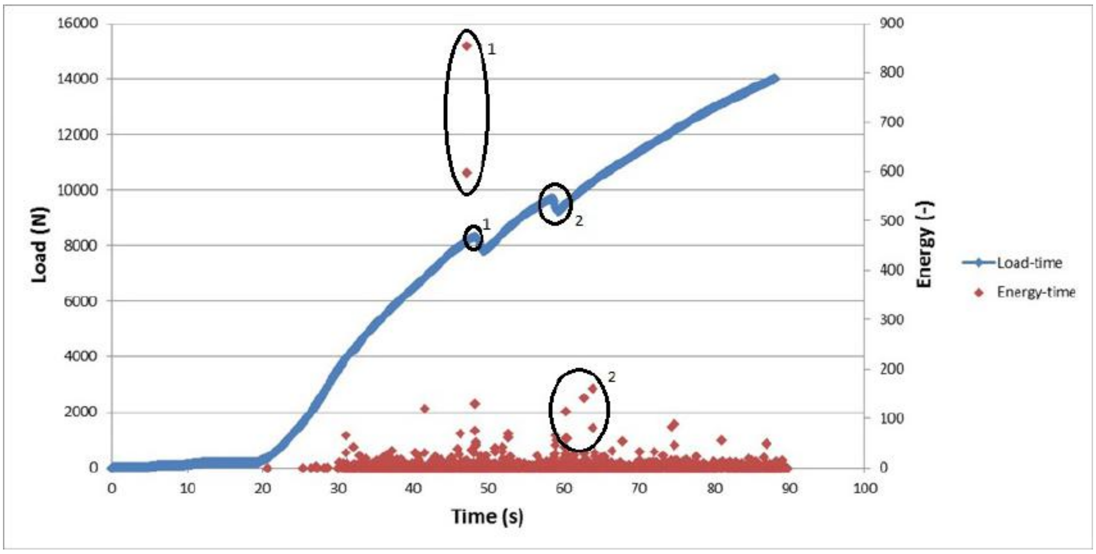

Figure 5.31: Load vs. time and energy vs. time before healing

The first load drop occurs at ca. 8,2kN. The acoustic emission energy belonging to this drop is classified as an event since both sensors received a signal. The location of this event is in the middle of the concrete beam, in between the two strain fields of figure 5.30, slightly more to the right as showed in figure 5.32.

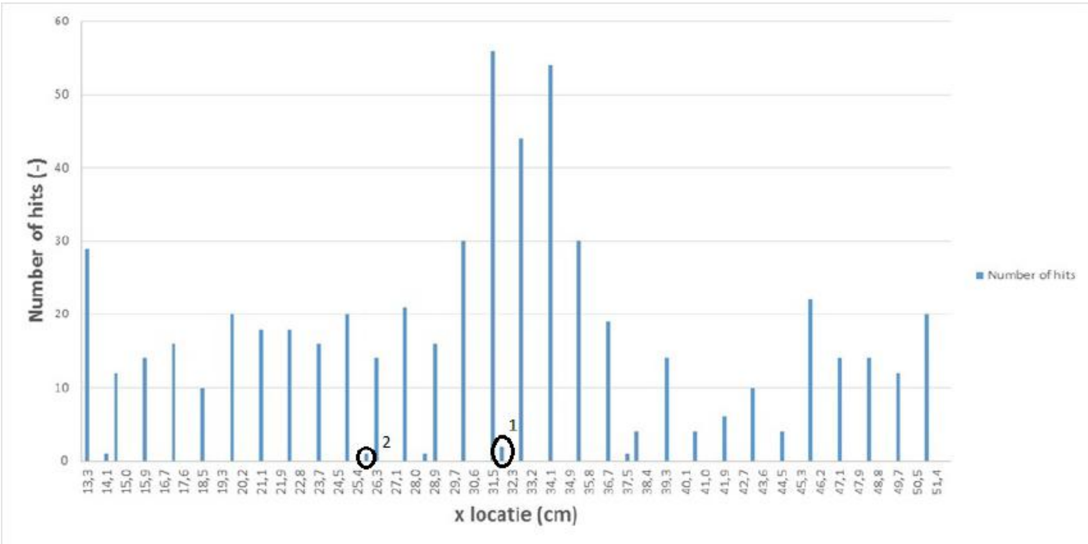

Figure 5.32: Location of events in the x-direction before healing

Linking this first event to the DIC, a sudden increase in strain and simultaneous cracking can be seen on figure 5.33a. It corresponds with the third crack from the left on figure 5.34.

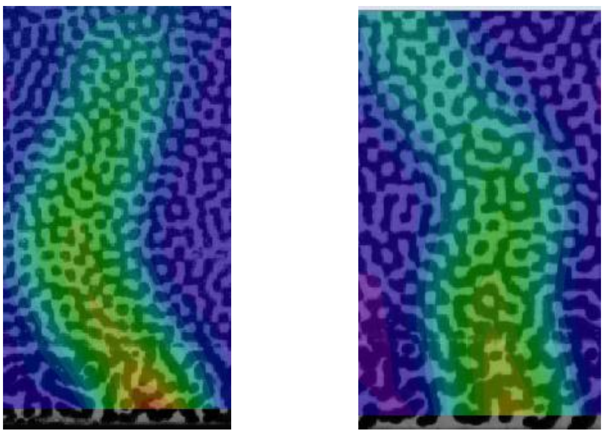

(a) Moment 1 (b) Moment 2

Figure 5.33: Pictures of the DIC data for the different events before healing

For the second point of interest, being the second load drop, another AE event can be linked to the increase in strain, to the left of the previous crack. This strain concentration is depicted in figure 5.33b. The other encircled energy dots, represent the crack origination and further opening.

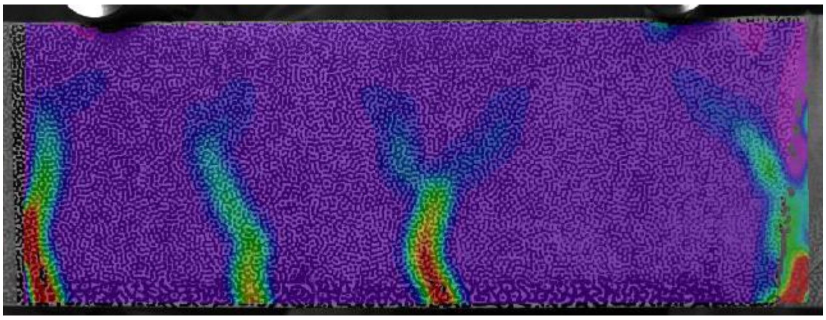

Figure 5.34: Ultimate strain field before healing

In figure 5.34, the final strain situation of the first load cycle is depicted. One can distinguish four strain concentrations whereof two cracks are noticed with acoustic emission and loading data. However, the third crack, being the one on the left extremity, could not be linked with AE or loading curve. The crack widths can be found in the table 5.12 below.

Table 5.12: Crack widths of beams 'droplet' at ultimate loading, as seen on DIC (accuracy $\pm 70 \mu m$)

Crack widths (μm)	Left	Second from left (or middle)	Third from left	Right
Specimen 1	311	270	364	/
Specimen 2	/	338	/	/
Specimen 3	419	432	/	526

The applied bending moment was increased in order to reach at least one crack of 300μm or more. Done so, healing liquid is already observed in cracks of around 300μm and even one crack of 270μm.

Second load cycle

Again, as for the first load cycle, two load drops are seen. At the first load drop, no high energy acoustic events are seen. By analyzing the hits at the time of this load drop, it could be seen that something happened at the right extremity of the speckle pattern. Correlating this with the DIC data gave the reopening of the right crack and a new crack close to this one, as to be seen in figure 5.37a. Identically, no high energy is linked to the second load drop, but just afterwards. The location of hits at the load drop is both left as right.

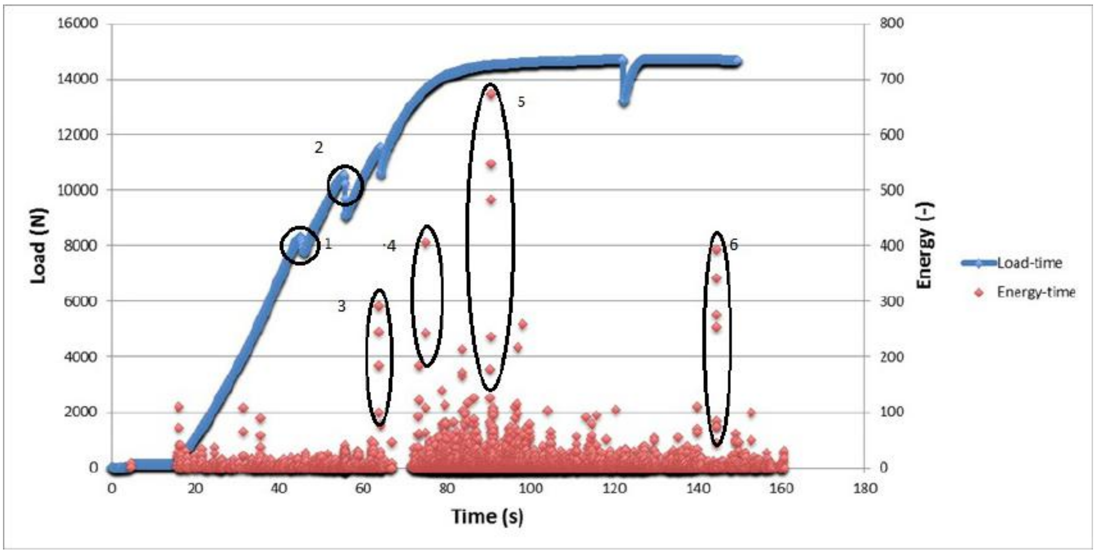

Figure 5.35: Load vs. time and energy vs. time after first healing

After the load drops, four high energy events are picked up by the sensors. These are designated by circles in figure 5.35 and their location can be seen below.

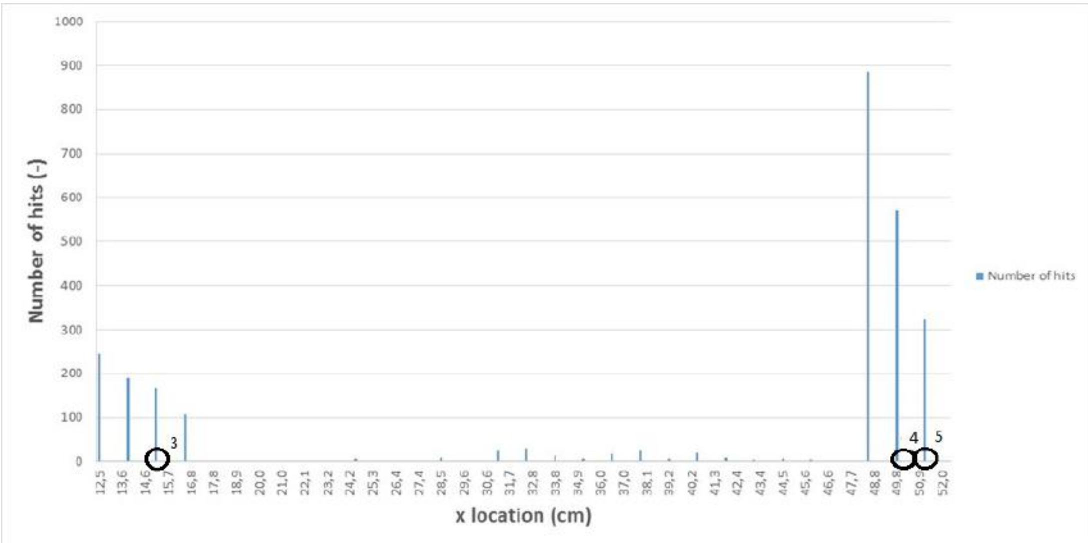

Figure 5.36: Location of events in the x-direction after first healing

The first high energy event is quite close after the second load drop. AE localization points out that this event occurs at the left extremity of the beam, as shown in figure 5.36. However, following the DIC picture at this moment, the second crack from the left reopens, as shown in figure 5.37b. The event is thus probably not captured in a right way. Next, the high energy event of moment 4 can be related with a sudden increase in the strain field (5.37c), and this at the

crack position third from the left as seen in figure 5.38.
For the fifth chosen point, the energy comes again from the right end of the pattern. In the DIC picture, the opening of the two cracks is revealed, as depicted in 5.37d. Finally, at the end of loading, a last high energy event is captured. The location could not be specified by the acoustic energy and the DIC data did not give a decisive answer too.

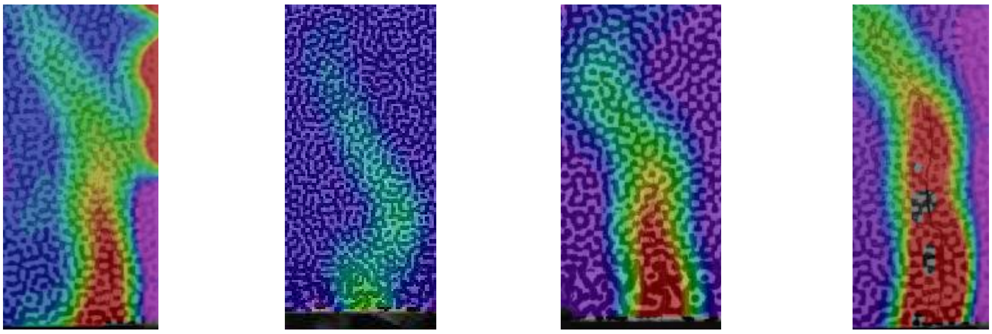

(a) Moment 1 (b) Moment 3 (c) Moment 4 (d) Moment 5

Figure 5.37: Pictures of the DIC data for the different events after first healing

Only the pictures of moments 1,3,4 and 5 are shown in figure 5.37. For both 2 and 6, no new flaws are observed.

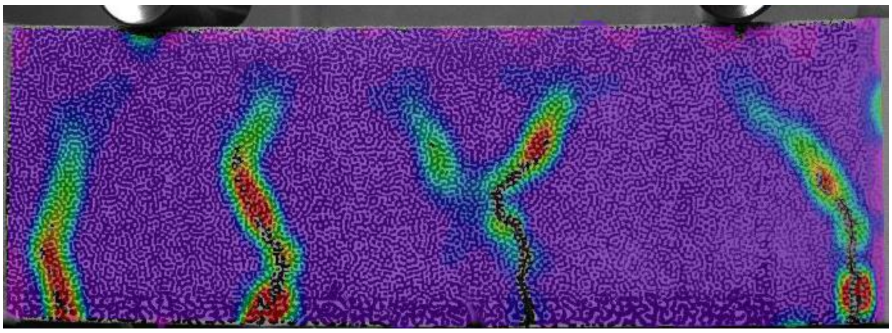

Figure 5.38: Ultimate strain field after first reloading

After the first healing period, it can be concluded that, at the same four crack positions as after the first load cycle, strain fields reappear and thus the same cracks reopen. The only difference between the beam before healing and at reloading, is that a new crack appears next to an old one. The self-healing efficiency will be discussed after the analysis of the third load cycle in section 5.6.3.

Third load cycle

The third and last load cycle does not show any load drops. Three points of interest are investigated more deeply.

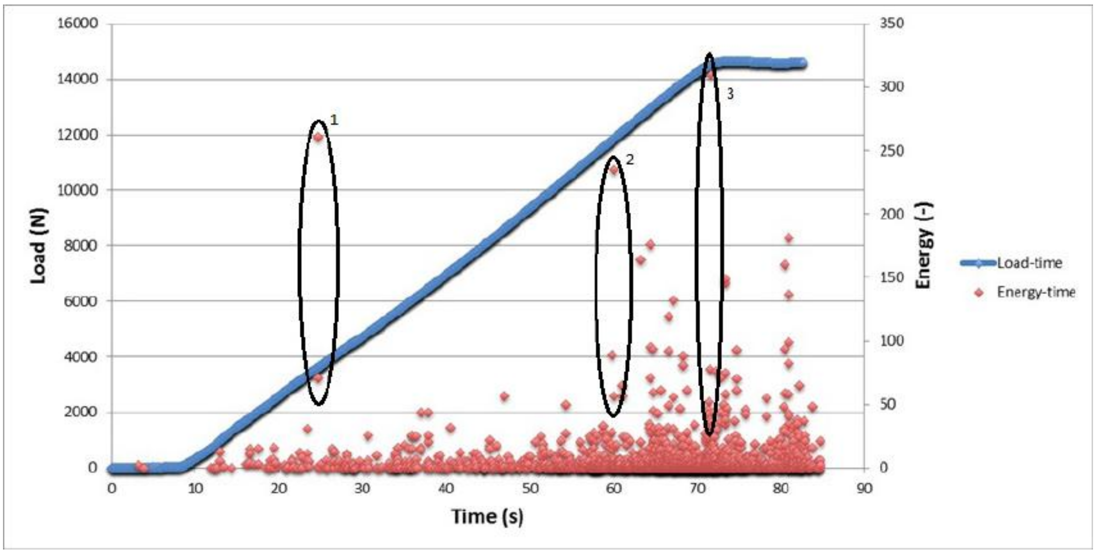

Figure 5.39: Load vs. time and energy vs. time after second healing

A first point of interest in figure 5.39 has relatively high energy compared to the other hits. However, both the loading curve and the DIC data don't show anything specific. Analysis of the AE data tells us the location of this event, which is totally left on the pattern, as depicted in figure 5.40. The load at this stage is 3,6kN and already around all cracks a strain field is visible.

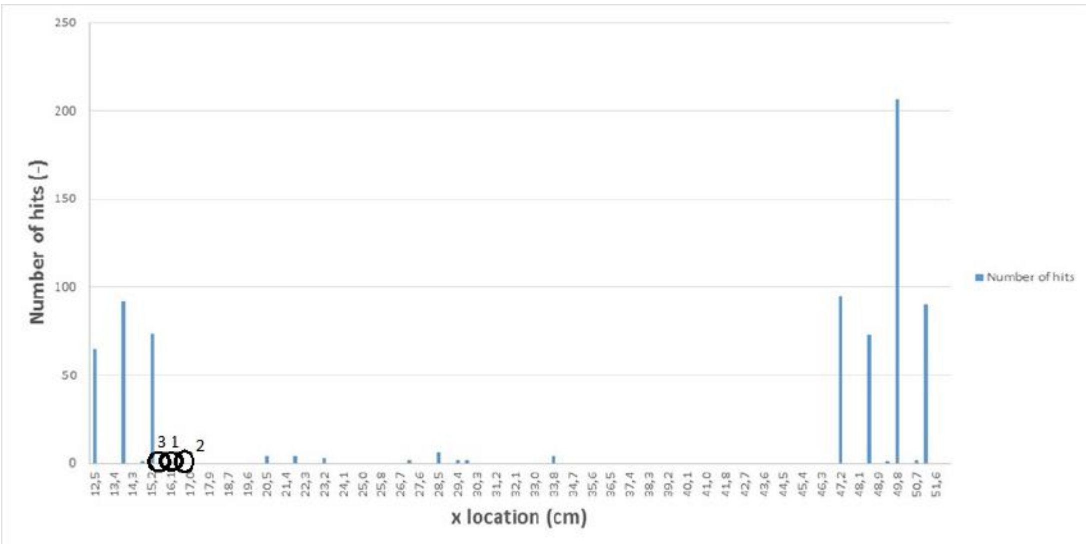

Figure 5.40: Location of events in the x-direction after second healing

Somewhat further, a second event of high energy is seen. The location of the event is found to be, again, totally at the left side. The DIC data however does not show any particularity on this side, neither somewhere else. Idem dito as for previous point in time, there is a new event of high energy at moment 3 which cannot be linked to a specific crack. At this moment, the highest load is reached. Following the acoustic emission data it should still be located on the left.

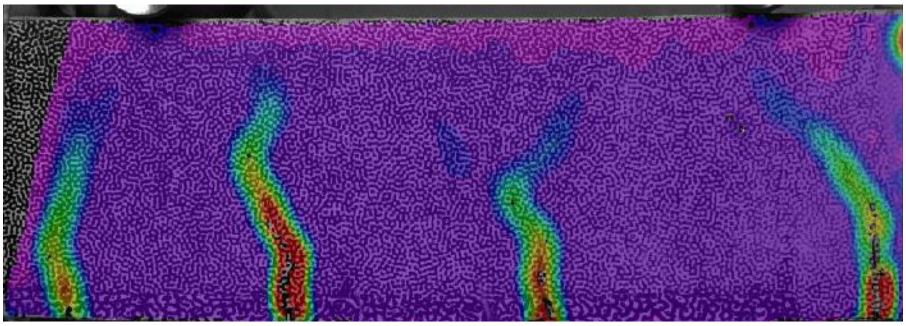

Figure 5.41: Ultimate strain field after second reloading

The strain field observed in figure 5.41 is almost identical to the one of 5.34 and 5.38. It is then concluded that the points of weakness are at the same locations during the three loading cycles.

Discussion

The three load cycles are now compared to evaluate the self-healing efficiency. This is done by examining the differences in stiffness of the beams.

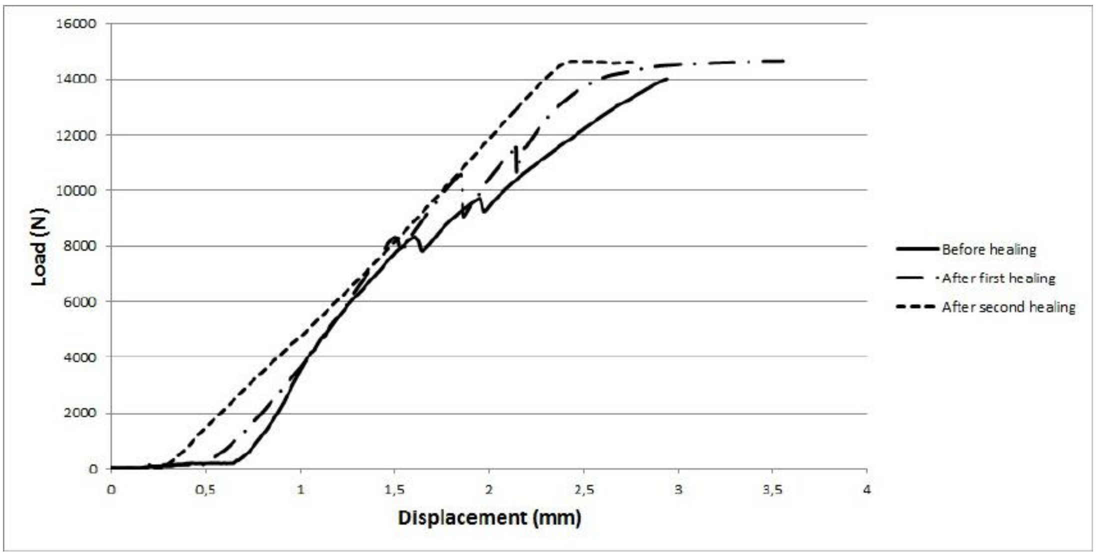

Figure 5.42: Load vs. displacement of the three load cycles

It can immediately be seen from the graph that the bending stiffness in the first load cycle is the highest. The values of stiffness are summarized below in table 5.13.

Table 5.13: Stiffness of specimen 1 in different load cycles

	Stiffness (N/mm)
Before healing	8849
After first healing	8202
After second healing	6931

The stiffness of the undamaged beam is the highest. The sound concrete shall, due to cracking under loading, lose stiffness. The bending stiffness after the first healing, had a higher value than the one after second healing. This is explained by the fact that self-healing occured, and stiffness is regained. Comparing these values with the ones of beam round 3 shows that the stiffness is systematically lower. This could be due to the higher stiffness of tubes inside the beam or a possible flaw. Regarding the reference beams, the stiffness of the sound concrete seems incredibly low. Before healing, the stiffness of beam droplet 1 is only 2/3 of the one for the references. But, after a healing cycle, the beam only lost 8% of its stiffness. As already said in section 5.6.2, this is more than 50% for either of the reference beams. A table summarizes the stiffnesses for the three droplet beams, together with the mean values for every load cycle and the standard deviation.

Table 5.14: Stiffness of the beams with droplet form tubes in different load cycles

	Stiffness before healing	Stiffness after first healing	Stiffness after second healing
Specimen 1	8849N/mm	8202N/mm	6931N/mm
Specimen 2	7718N/mm	11795N/mm	6823N/mm
Specimen 3	12777N/mm	9370N/mm	6745N/mm
Mean stiffness	9781N/mm	9789N/mm	6833N/mm
Standard deviation	2168N/mm	1496N/mm	76N/mm

It should be noted here that the value of stiffness after first healing in table 5.14 is higher than before healing. The self-healing efficiency of all stages is tabulated below for the three droplet beams.

Table 5.15: Self-healing efficiency of beams with droplet IPC tubes

	Regain after first healing (%)	Regain after second healing (%)
Speciment 1	93	78
Specimen 2	153	88
Specimen 3	73	53
Mean efficiency	106	73

Table 5.15 denotes the percentages of the remaining stiffnesses compared with the original ones. An anomaly is the behaviour of the second beam with droplet shaped tubes. High healing efficiencies are reached here, with the first efficiency even bigger than 100%. A possible explanation can be that there is a flaw or crack before loading. The stiffness during the first load cycle will then be lower than expected. Due to cracking of the tubes, healing agent will flow out and could heal the flaw as well. The particular high value in stiffness at the second load cycle is thereby not totally explained, but an efficiency of more than 100% can be possible. The high value is then rather explained by a wrong choice in data to plot a linear trendine.

5.6.4 Summary

The main conclusion that is drawn from these results is that the stiffness of the references at first loading is the highest of all, which means that the vascular system softens the beams. On the other hand, the stiffness of the references at reloading is the lowest, such that self-healing surely occurred. No significant difference in stiffness between round and droplet- shaped systems is seen.

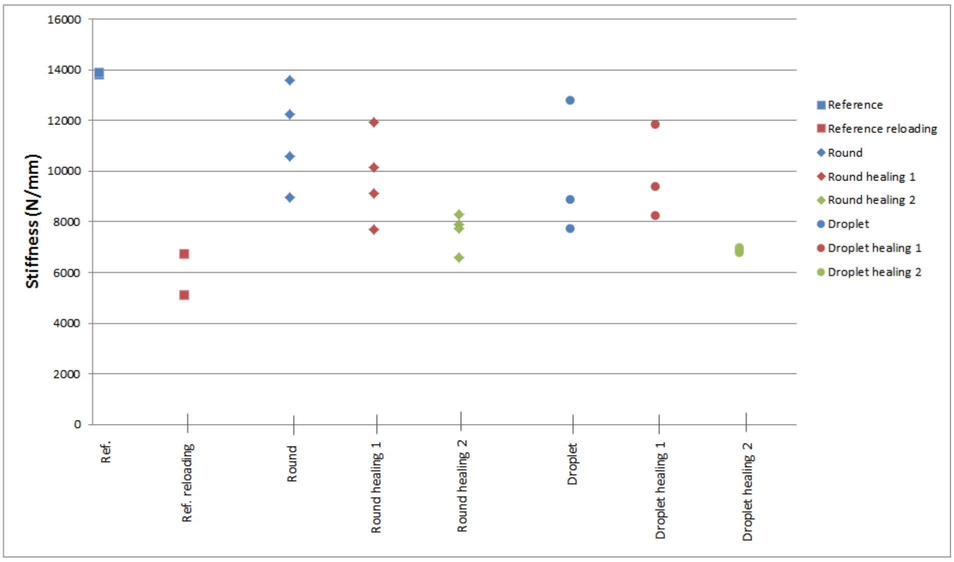

Figure 5.43: Summarizing chart representing stiffnesses of all beams during their load cycles

Regarding the cracks, it may be concluded that cracks of ca. 300μm break the vascular tubes and are wide enough to draw healing agent into them.

Further, looking at the healing efficiencies of both sets of beams, no remarkable difference is found except for beam droplet 2. As explained, these values in stiffness are rather a particularity than a nomality. Therefore, this beam is said to be non-representative for the whole and shall not influence the final conclusion about self-healing.

Finally the beams are cut through at the place of a crack and at the place of a reservoir. Figure 5.44 depicts the sections near a reservoir of a beam with round tubes (left) and one with droplet tubes (right).

(a)

(b)

Figure 5.44: Cross sections of the beams with IPC tubes: round (a) and droplet (b)

It can be seen that the systems are still positioned the right way, parallel to the bottom surface. Also the reinforcement is well placed, visible between and just above the connection pieces. There are no little cracks or cavities in the concrete surrounding the system, indicating that a good bond between system and concrete was achieved. However, there is still a rather large amount of healing agent present in the system, despite the attempt to pump out the agent after testing. This can explain why multiple healing in most cases didn't occur. The resulting healing agent possibly hardened before the new healing agent was added, blocking it to flow in the system. Fortunately no healing agent was absorbed by the IPC tubes, which confirms that IPC is not porous to healing agent.

5.7 Four-point bending test with clay vascular system

Identically as for the beams with IPC tubes, four-point bending tests are performed on beams with a vascular system made up of clay tubes as described in section 4.6, with a speed of 2mm/min. The goal of these tests is to demonstrate self-healing ability by using clay tubes. Clay is a cheap solution for IPC and the production process is faster. Therefore, it is of particular interest that these vascular systems provide self-healing as well.
The outline of this section will be similar to the one above, section 5.6. Two reference beams, four beams yielding droplet tubes and four beams holding rugby ball tubes are tested. Only one of each set will be discussed in detail and afterwards a summary of stiffnesses of all the beams is given and the healing efficiency is calculated.
First, during casting of the beams, concrete was manually poured from a higher height, being some 40cm. None of the tubes were broken and the vascular system stayed in place. To verify this, air or liquid could be pumped into the system on one side. An intact system would allow the air or liquid to flow out on the other side. Furthermore, it is seen that the concrete bumps onto the reinforcement bars and then slowly slides off. The impact on the tubes will thus be lower, which means that the protection works. A difference between pouring over droplet or rugby ball form could not be stated.

5.7.1 Reference

Two reference beams are loaded and reloaded. Their change in stiffness will be evaluated and later on compared with the beams containing vascular systems, and this to see whether there is a regain in stiffness for the self-healing beams. For deeper investigation, only reference 1 will be used.
The global strain field before the discussed events is depicted below and gives a good idea of where cracks will occur in the end.

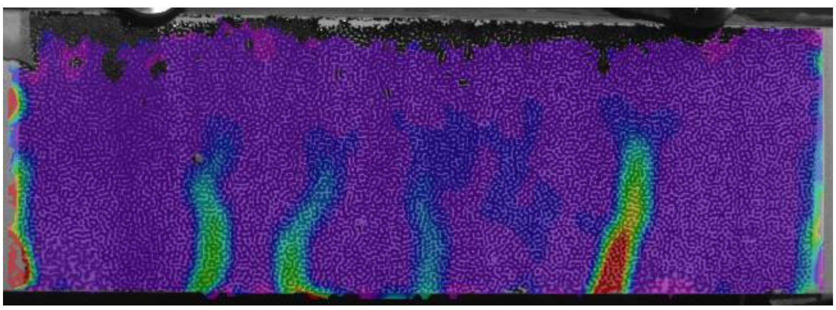

Figure 5.45: Global strain field on reference specimen before first event

Six strain concentrations are seen on figure 5.45. The spots at the sides can probably not clearly be analyzed by DIC, since the speckle pattern stops there. The load curve and acoustic emission energy are shown in the graph of figure 5.46. Five moments on the graph are chosen to discuss. For all five, something happens in both loading curve and acoustic emission energy.

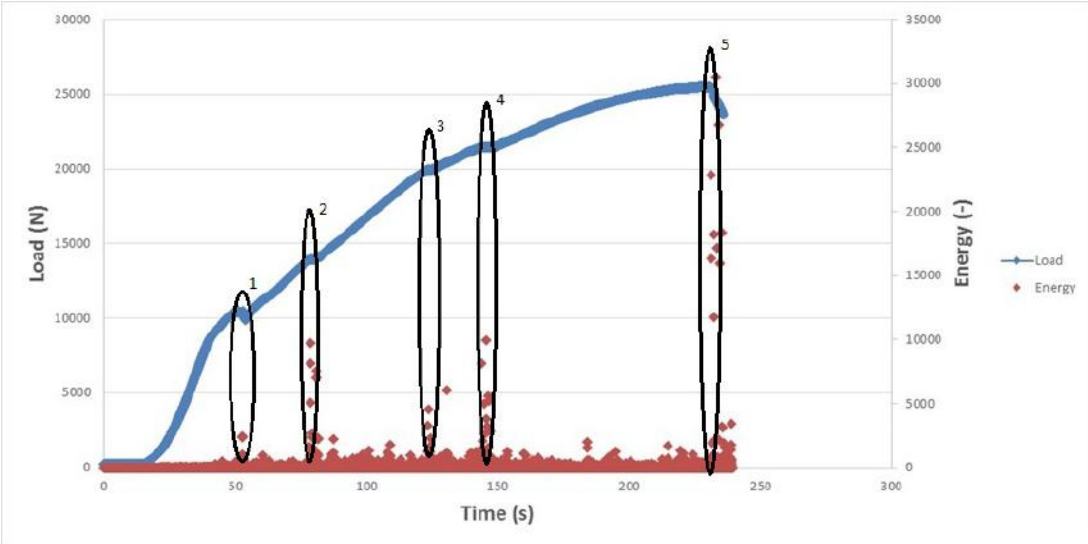

Figure 5.46: Load vs. time and energy vs. time of reference specimen at first loading

The first picked acoustic emission event comes together with a small load drop. Following the acoustic emission data, as in figure 5.47, this event occurs on the left side of the beam. The exact position is at the second strain field from the left in figure 5.45, and is shown in figure 5.48a.

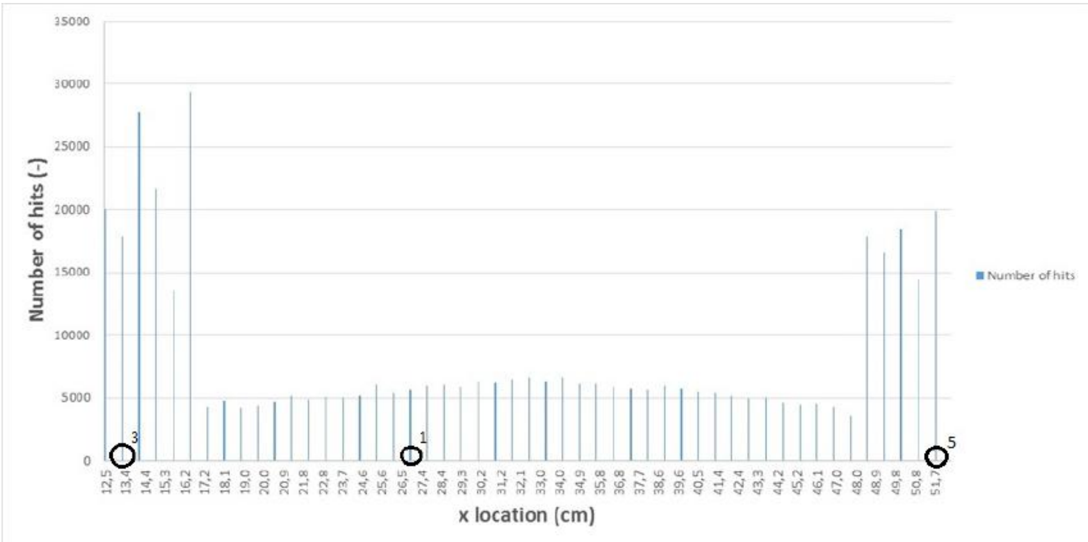

Figure 5.47: Location of events in the x-direction of reference specimen during first loading

The second point of figure 5.46 shows an acoustic event with high energy, together with a plateau in the load curve. This event could not be located by using AE data and DIC did not reveal any particularities.

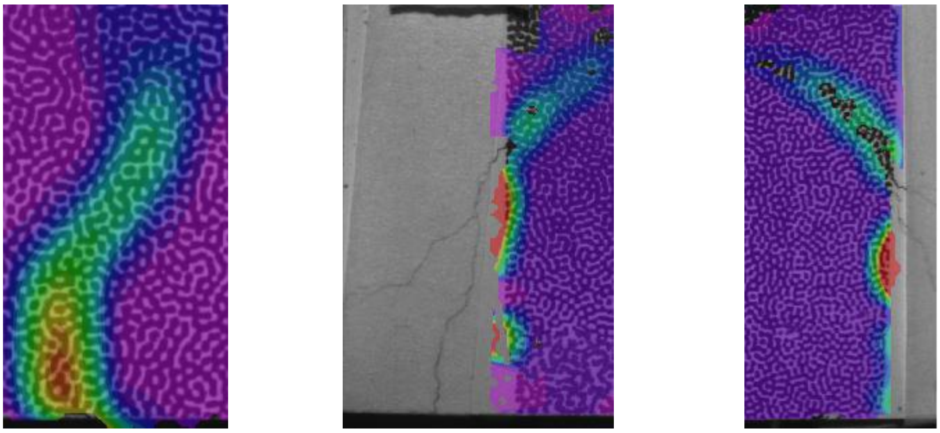

(a) Moment 1 (b) Moment 3 (c) Moment 5

Figure 5.48: Pictures of the DIC data for the different events on reference specimen at first loading

At the third moment in time, the same kind of information is retrieved as for the previous one. The location is found to be at the left extremity, just outside the speckle pattern. A crack is clearly visible, but strains cannot be found. The crack can be seen in figure 5.48b

For the fourth event, no exact location could be determined. The acoustic emission shows events at different locations, which indicates that several cracks induce energy at the same time. In addition, no specialities are seen on the DIC images.

Lastly, the highest emitted energy is captured at the same moment as a load drop occurs. The event is located at the right extremity of the beam and falls thus outside the speckle pattern. On figure 5.48c, this crack is shown in detail. The final strain field after the first load cycle is depicted below in figure 5.49.

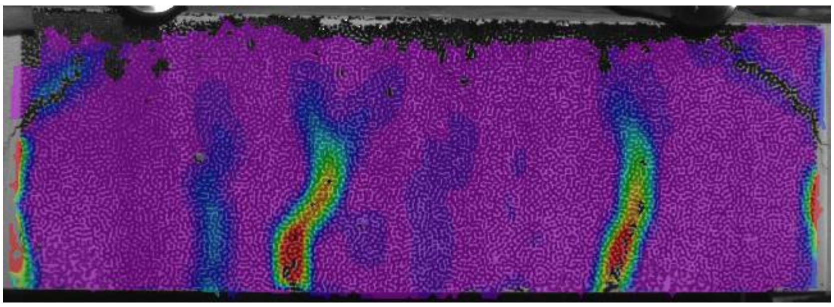

Figure 5.49: Ultimate strain field on reference specimen at first loading

On the figure above, four cracks are visible. The opening of the third one from the left has not been captured by the acoustic emission data. At the moment of opening of this crack, lower energy events are available but no localization was possible. The widths of the cracks in figure 5.49 and the ones of the second reference beam after first loading are listed below.

Table 5.16: Crack widths of reference beams at ultimate loading, as seen on DIC (accuracy $\pm 70\mu m$)

Crack widths (μm)	Left	Second from left (or middle)	Third from left	Right
Reference 1	1100	688	578	/
Reference 2	1265	1100	/	688

The values of crack widths in table 5.16 are very high, although during loading this was not observed. Because other cameras were used and the pictures are a bit fuzzy, no clear distinction of cracks was observed. The pixels around the cracks go from white to black, with different grey scales in between. It is therefore difficult to pick out the darker ones, which correspond to the cracks. Caution should be taken with these calculated crack widths, since we have the feeling that they were smaller in practice.
The loading and reloading curves of the reference beams are plotted in figure 5.50. This graph represents the load vs. displacement, because the stiffness can be taken from it. Again, as expected, the stiffnesses at the first load cycle are higher than the ones of the second loading.

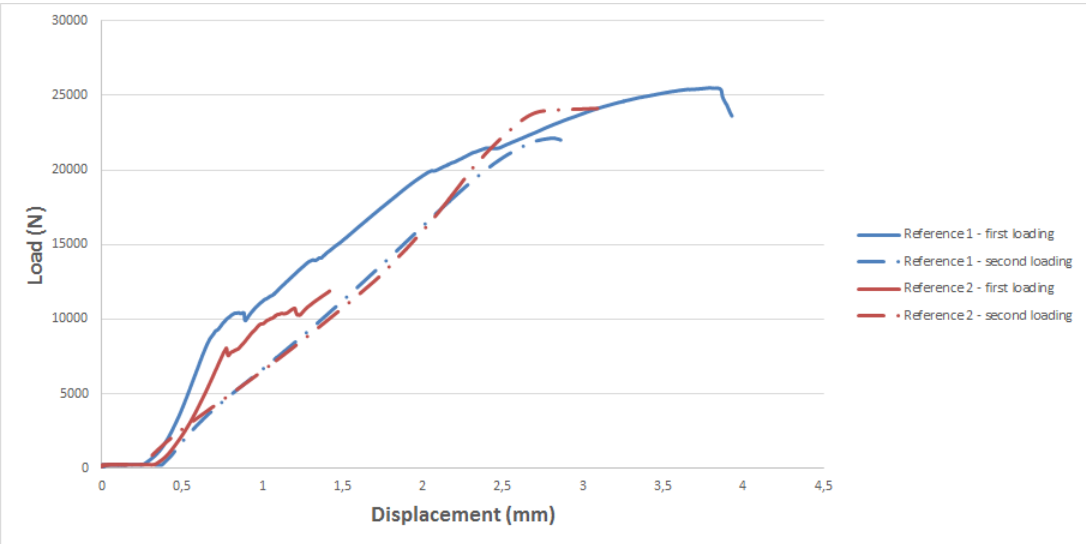

Figure 5.50: Loading and reloading curves of the two reference beams

It can already be seen in figure 5.50 that the curves for the reloading of the beams lie closely to each other. The exact values are summarized in table 5.17.

Table 5.17: Stiffness of the reference beams in loading and reloading cycle

	Stiffness	Mean stiffness per load cycle	Standard deviation
Reference 1 - first loading	24769N/mm	22584N/mm	3090N/mm
Reference 2 - first loading	20399N/mm		
Reference 1 - second loading	9479N/mm	9098N/mm	540N/mm
Reference 2 - second loading	8716N/mm		

Table 5.17 shows the difference in stiffnesses during both load cycles. In the same trend as for the previous set of beams with IPC, the stiffness lowers drastically after first loading. Now, the results of the beams with vascular system can be analyzed and compared with these values.

5.7.2 Droplet form tubes

Four beams with a vascular system, made up of clay tubes, are tested in four-point bending. Identically as in section 5.6.2, the beams will undergo three load cycles. A period of 24 hours is left in between the cycles so that self-healing can take place. The cracks in the beam will be found using AE and DIC. This method of analysis gives information of the exact location of events, which are possibly linked to crack occurrence.
One beam is investigated in depth, being beam droplet 3. A full analysis of all particularities in load curve, acoustic events and DIC pictures is described below. To start, a global strain field at the beginning of the test is shown in figure 5.51.

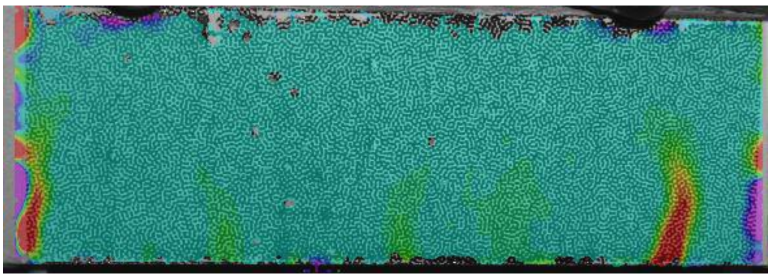

Figure 5.51: Global strain field before first event

On the figure above, five spots can be distinguished. The strain fields at the left and the right already have a higher value. In the middle, three smaller strain concentrations are seen.

First load cycle

For the first loading cycle, picking acoustic events was not that easy. The treshold for capturing hits was decreased regarding to the previous tests, in order to localize the events more clearly. This means however that the sensors will capture more hits, which makes the graph less clear. One particular point has been choosen from the load curve in figure 5.52: the load drop at moment number 5. Four other events are picked by looking at the DIC data. These four all represent different crack initiations.

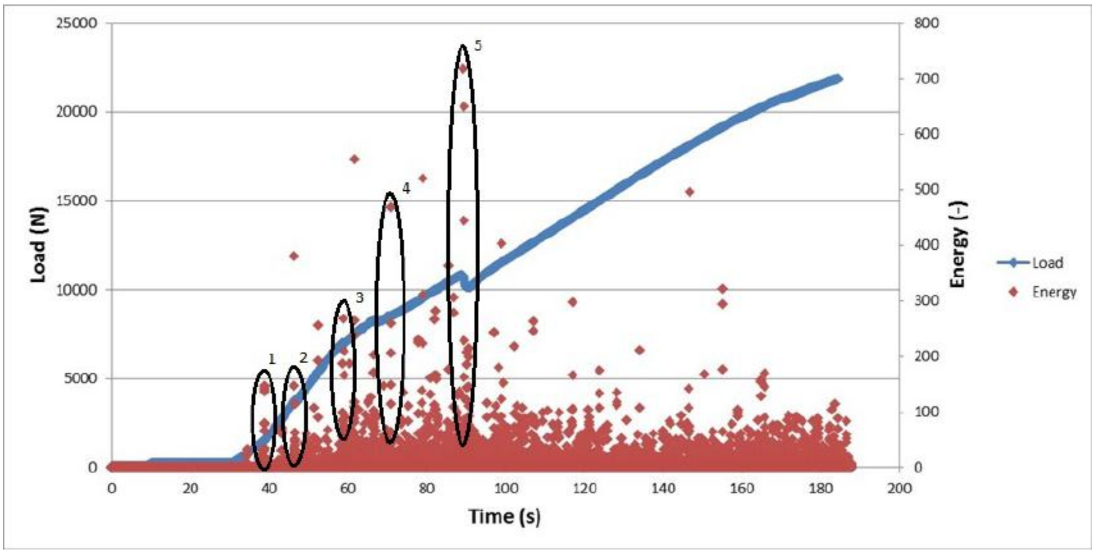

Figure 5.52: Load vs. time and energy vs. time before healing

The first event of increased energy is taken from figure 5.52. Nothing happens at this moment in the load curve, but the DIC picture reveals a part of an increased strain field. Despite, this strain field is at the border of the speckle pattern and can thus not totally be seen. A crack initiates here, but lies underneath the tape used for attaching the AE sensors. The moment when the crack becomes visible for the DIC equipment is shown in figure 5.54a. This is in fact the moment number 2 chosen in figure 5.52. Acoustic emission data could not clearly locate this event. The locations based on acoustic emission are shown in figure 5.53.

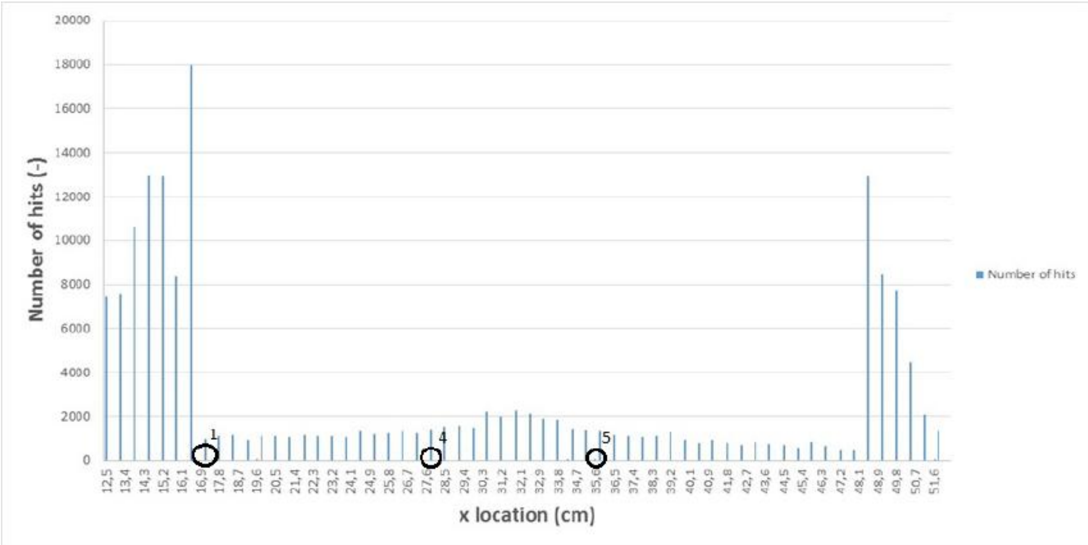

Figure 5.53: Location of events in the x-direction before healing

For the third moment, there is an inflection point in the load curve. A crack initiates at the strain concentration third from the left. Again, AE could not define the exact position of the event. The crack is shown on picture 5.54b.

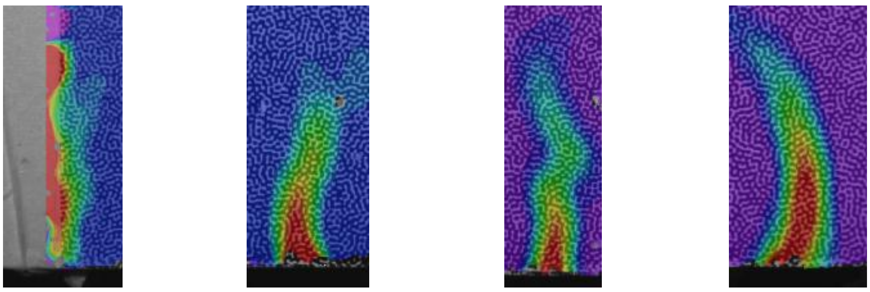

(a) Moment 2 (b) Moment 3 (c) Moment 4 (d) Moment 5

Figure 5.54: Pictures of the DIC data for the different events before healing

The fourth event chosen also comes together with an inflection point in the load curve. In figure 5.53, the location of this event is encircled. The position corresponds to the second strain concentration on the left of figure 5.51.

At the load drop in figure 5.52, an event of high energy occurs. This event is linked by the acoustic emission to the strain concentration third from the left. On the DIC pictures, the opening of this crack is seen, but also the initiation of the crack on the right, which is shown in figure 5.54d. The final strain field is depicted below.

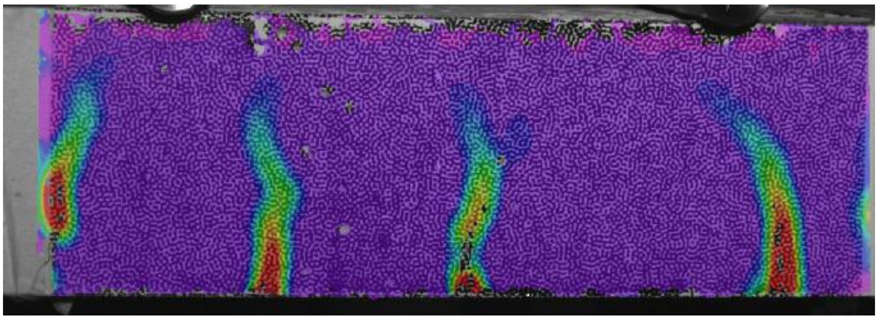

Figure 5.55: Ultimate strain field before healing

Figure 5.55 shows the strain field after the first loading cycle. Four cracks are available, but only two of them are in the self-healing zone underneath the vascular system. Crack widths can be found in table 5.18.

Table 5.18: Crack widths of droplet beams at ultimate loading, as seen on DIC (accuracy $\pm 70\mu m$)

Crack widths (μm)	Left	Second from left (or middle)	Third from left	Right
Specimen 1	729	839	/	564
Specimen 2	433	/	/	523
Specimen 3	963	564	660	523
Specimen 4	399	371	399	413

Identically as for the reference beams, the values of crack width are higher than expected. The healing agent did flow out of the crack, so that it can be stated that healing took place for these crack widths. It is however not sure if the values are correct. A determination of healing at smaller crack widths cannot be verified.

Second load cycle

The curve of the second load cycle, shown in figure 5.56, exhibits two load drops. Together with these, no high energy events are seen. Close to the end of loading, two high energy events are found and designated on the graph in figure 5.56.
At the first load drop, a lot of low energy events are captured by the sensors. Following the acoustic emission data, the location could not be defined. Signals are detected from everywhere. The DIC picture shows the opening of the second crack from the left.

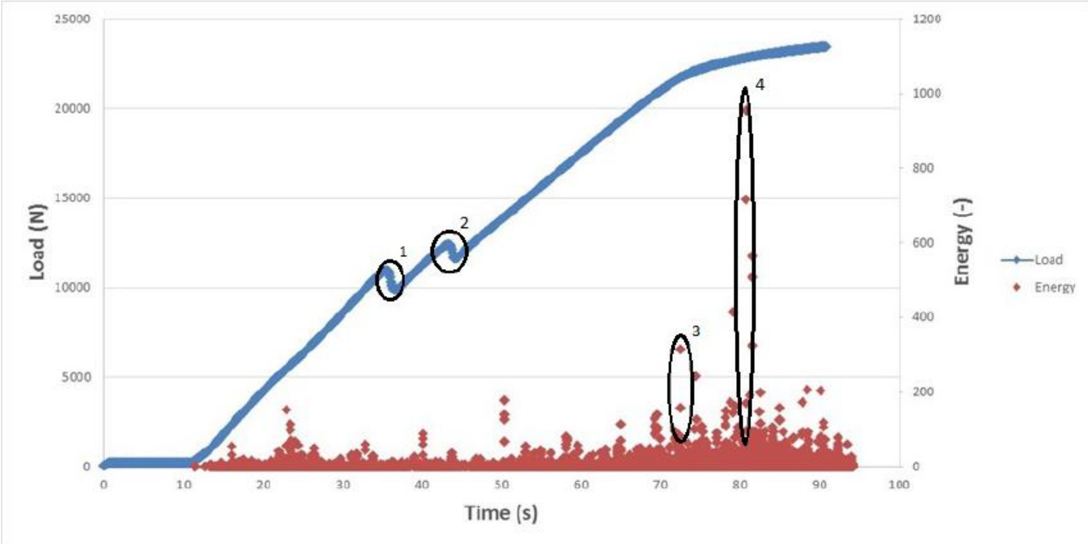

Figure 5.56: Load vs. time and energy vs. time after first healing

At the second load drop, no particular high energy events were seen. Locating the events at the moment of this load drops shows that they are both left as right on the beam. In the DIC pictures all cracks open, but the ones at the sides on speckle pattern are wider. The location is depicted in figure 5.57.

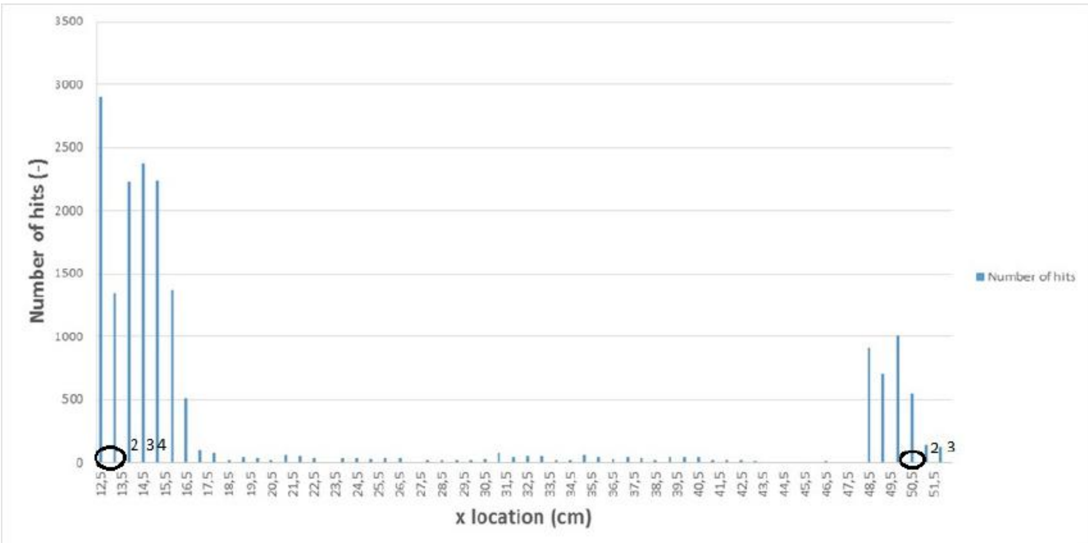

Figure 5.57: Location of events in the x-direction after first healing

Identically as for the second chosen moment, the event at number 3 is localized on the sides of the beam. Event nr. 4 is localized only on the left. The final strain field after the first healing step is shown on figure 5.58, indicating the increased strains at the same positions as for first loading.

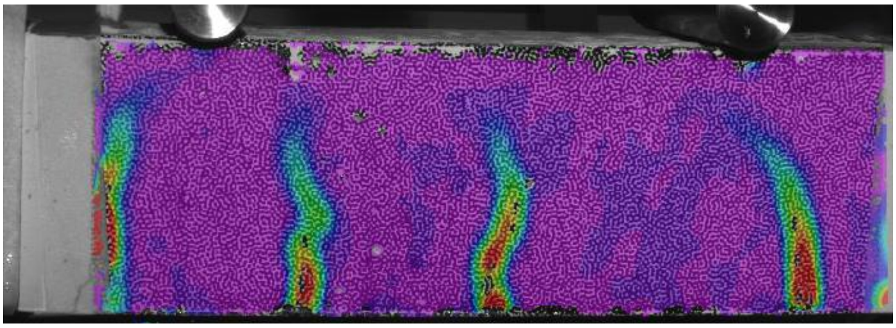

Figure 5.58: Ultimate strain field after first healing

Reloading thus causes reopening of the cracks. The final DIC image learns that the left crack is wider than the other three, which is nicely linked with AE data where on the last three discussed events, activity is localized in this area. Concerning the reopening of the middle two cracks, low AE information is provided. Looking closer at the first DIC images, the cracks induced by the first loading cycle are very small, smaller than they were at maximal loading of the first cycle. When unloading, the elastic bending capacity - mainly caused by the tensioning bars - closes the cracks.

Third load cycle

The curve of the second load cycle, shown in figure 5.59, exhibits no load drops but a straight line until the beam's strength is reached. Three events of high energy are chosen out of the AE data, but no correlation matches the behaviour in loading curve. However, the last two events occur simultaneously with a decrease in stiffness, namely where the beam reaches its maximal strength.

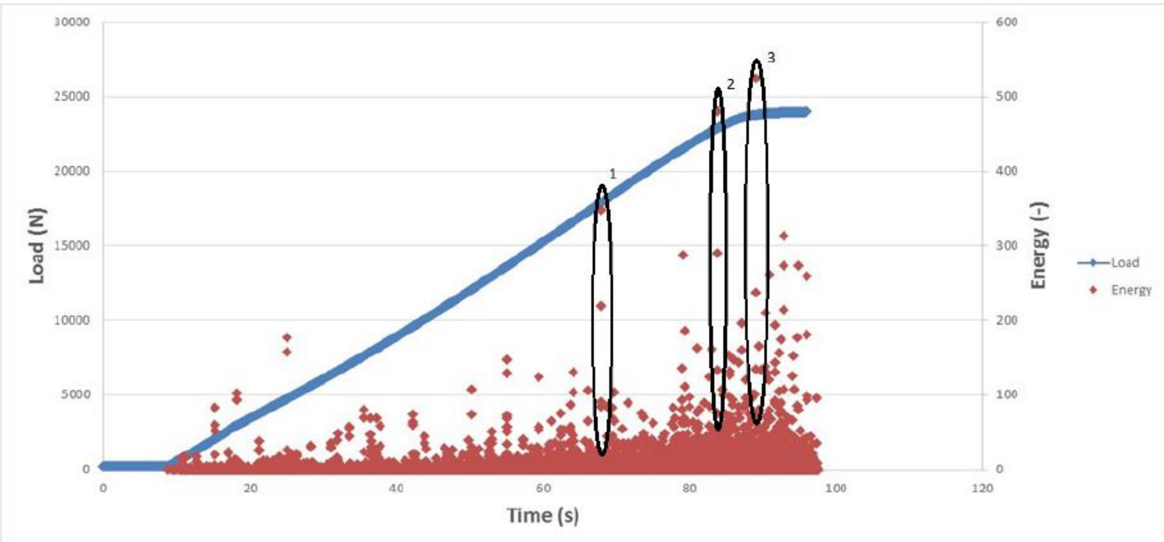

Figure 5.59: Load vs. time and energy vs. time after second healing

Now the locations of those three events are examined; all of them refer to activity on the left side of the beam, very close to each other (encircled on figure 5.60). Noticeable, a new branch of the currently present crack emerges and originates from right above to left under.

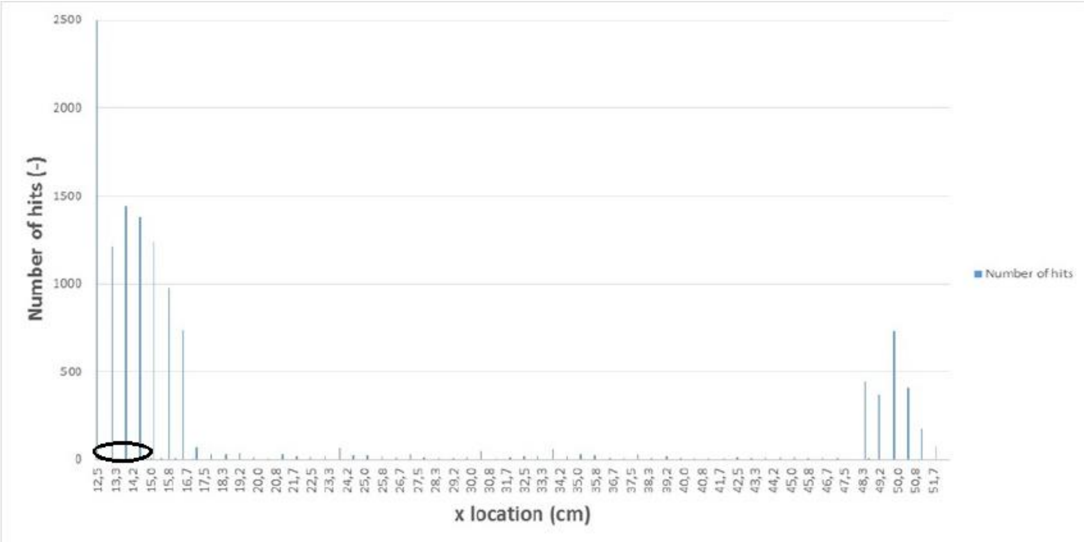

Figure 5.60: Location of events in the x-direction after second healing

The three events are associated with the DIC pictures, and shown at different times on figure 5.60. The same newly induced branch extends towards left under.

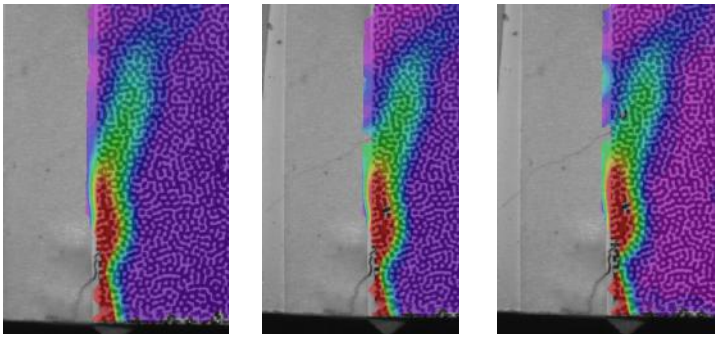

(a) Moment 1 (b) Moment 2 (c) Moment 3

Figure 5.61: Three different stages of newly arised crack branch after second healing

When the ultimate strain field (figure 5.62) is compared to the previous two loading cycles, the same locations of increased strain fields are seen. Nonetheless a new branch occurs at the left crack. It is however just beside the speckle pattern, otherwise this would lead to a differently shaped strain field.

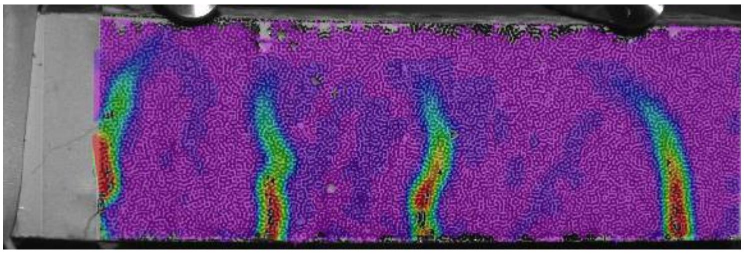

Figure 5.62: Ultimate strain field after second healing

Discussion

The three load cycles are plotted together on the graph in figure 5.63.

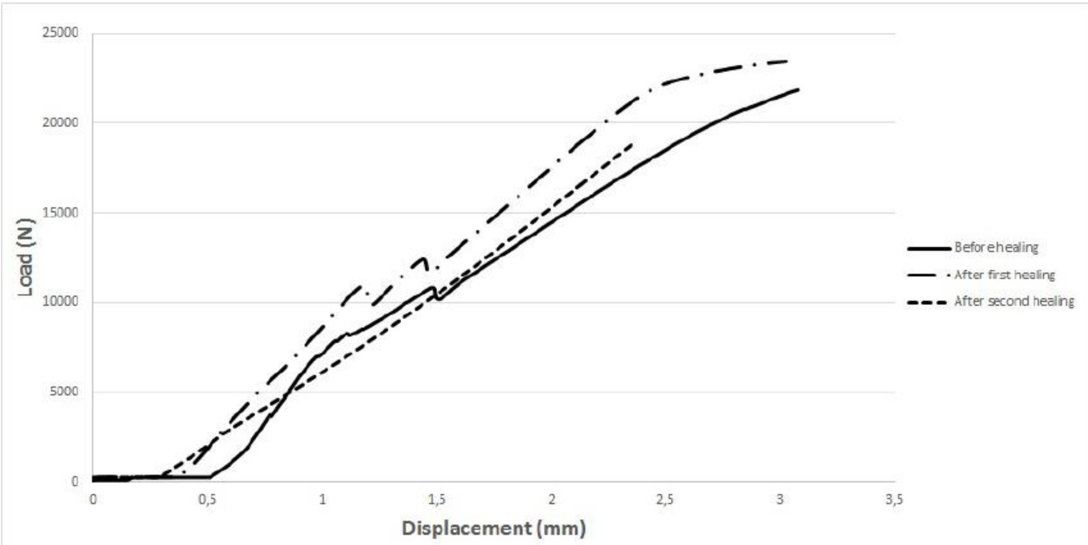

Figure 5.63: Load vs. displacement of the three load cycles

The slopes of the curves in the graph above are changing. During first loading, the stiffness is the highest because the beam is still undamaged. The stiffness lowers then per load cycle. Exact values of stiffnesses are described in table 5.19.

Table 5.19: Stiffness of the beam in different load cycles

	Stiffness (N/mm)
Before healing	17028
After first healing	13248
After second healing	9430

The values of stiffnesses for al the beams containing a vascular system with clay droplet tubes are summarized in table 5.20. Also, the mean stiffness for every load cycle and the standard deviation is added.

Table 5.20: Stiffness of the beams with droplet tubes in different load cycles

	Stiffness before healing	Stiffness after first healing	Stiffness after second healing
Specimen 1	21639N/mm	12873N/mm	11419N/mm
Specimen 2	12873N/mm	14592N/mm	8746N/mm
Specimen 3	17028N/mm	13248N/mm	9430N/mm
Specimen 4	15466N/mm	12587N/mm	10424N/mm
Mean stiffness	17118N/mm	13563N/mm	10005N/mm
Standard deviation	4343N/mm	852N/mm	1168N/mm

A first remarkable point in the table above is the variance between the stiffnesses before healing. The beam with the highest stiffness is almost two times as stiff as the one with the lowest. The cause of this phenomenon is yet unknown. Also, this beam provides a self-healing efficiency larger than 100% after first healing, as will be seen in table 5.21.

When comparing the stiffnesses after first and second healing with the ones of the reload of the reference beams, it can be seen that the values still overpass the ones of the reference beams, except for droplet 2. Since the stiffnesses are lower for the beams with this vascular system before healing, it can surely be said that healing took place in between the load cycles. The efficiency of self-healing is calculated and listed in table 5.21.

Table 5.21: Self-healing efficiency of beams with droplet clay tubes

	Regain after first healing (%)	Regain after second healing (%)
Specimen 1	64	53
Specimen 2	113	70
Specimen 3	79	55
Specimen 4	81	67
Mean efficiency	84	61

Whereas the reference beams lose more than 50% of their stiffness, this does not happen for the self-healing beams. The table above shows that there is a higher regain in strength than without vascular healing system. For droplet 2, the values are exceptional, but as already said, this phenomenon cannot be stated.

5.7.3 Rugby ball form tubes

The beams containing a vascular system with tubes in rugby ball form are tested upon four-point bending. Again, three load cycles are applied and in between these, healing will take place. For one of the four beams, something went wrong with the acoustic emission data. The most representative beam for the set is taken as beam rugby 3. Its strain field at the beginning of the test, under a small load, is shown below.

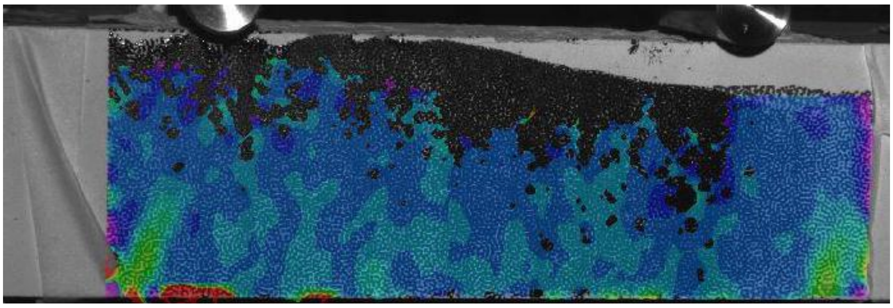

Figure 5.64: Global strain field before first event

Figure 5.64 shows two small strain concentrations at the side. Since the same thing was seen for the beams with clay droplet forms, it is likely that cracks will occur in these places.

First load cycle

In the load curve of figure 5.65, two load drops are seen with coincident high energy events. Two other events are chosen too, one before and one after these load drops.
The first moment contains a lower energy event. This event is chosen because, on the DIC data, a sudden increase in strain field is seen on the left and right side. Following acoustic emission, the event comes from the right side. Some seconds after, a crack initiates. The strain field is illustrated in figure 5.67a

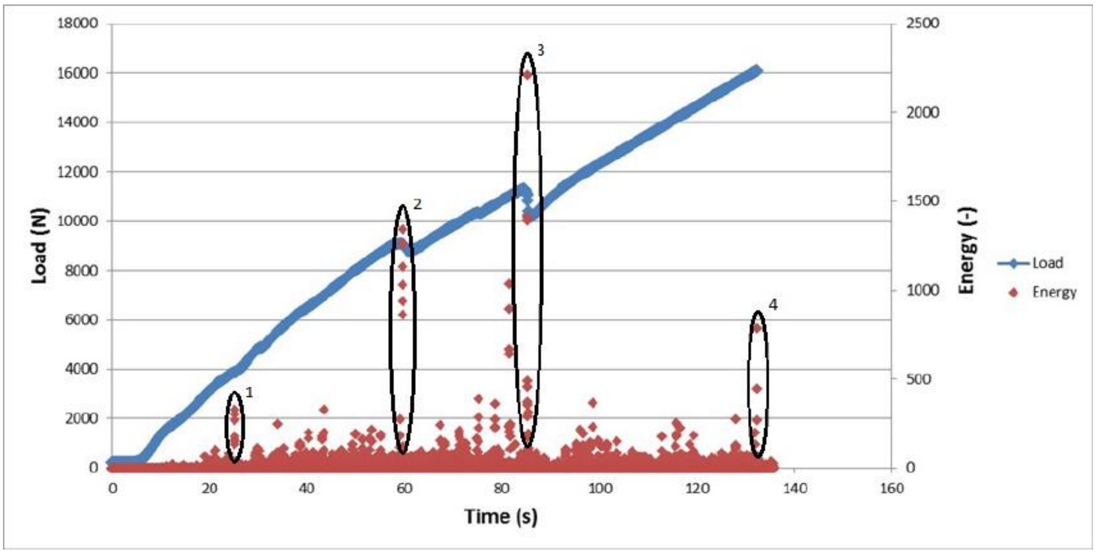

Figure 5.65: Load vs. time and energy vs. time before healing

At the first load drop, an acoustic event of higher energy is seen. The event is linked to a strain field, positioned third from the left, as encircled in figure 5.66. This is not the same crack as shown in figure 5.68. It is only an increased strain field that disappears afterwards. On the DIC pictures, two increased strain fields are seen in the middle of the beam, as shown in figure 5.67b. The right one of these is the second crack on the left in figure 5.68.

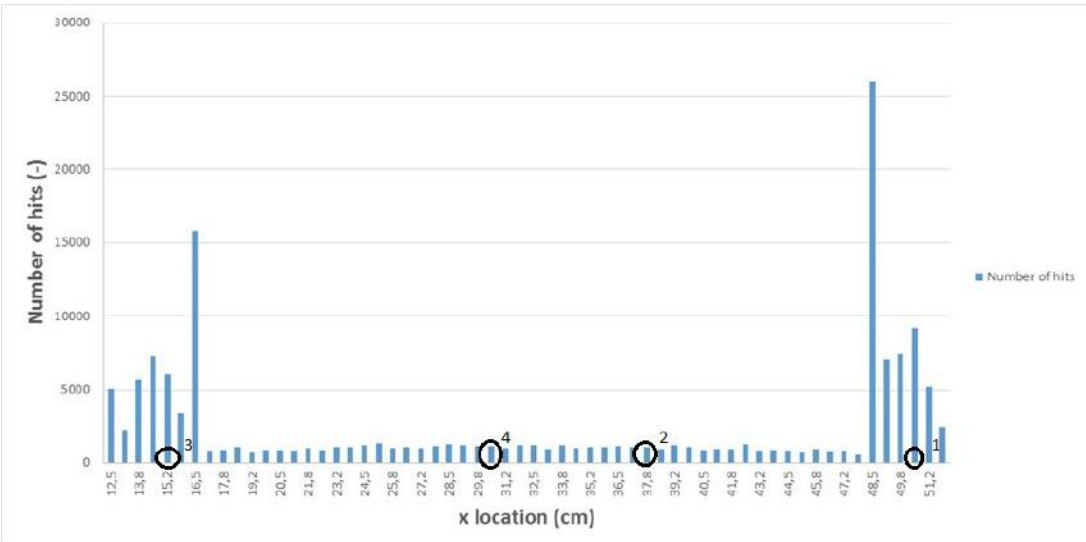

Figure 5.66: Location of events in the x-direction before healing

The second load drop comes together with the highest energy event seen during this load cycle. Acoustic emission links this event to a location totally left on the speckle pattern. A crack was already available in this area and probably opened at this moment in time. The strain field can be seen in figure 5.67c.

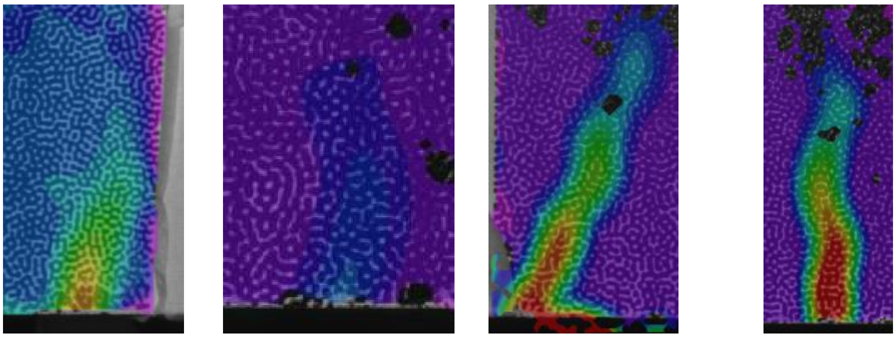

(a) Moment 1 (b) Moment 2 (c) Moment 3 (d) Moment 4

Figure 5.67: Pictures of the DIC data for the different events before healing

At the end of loading, a last increased energy event is captured by the sensors. On figure 5.66, the location is found to be second from the left. DIC data reveal no particularity. The crack in this strain field was already present, but a small opening can be seen on figure 5.67d. The final strain is depicted in the figure below (5.68) and shows four strain concentrations with crack inside.

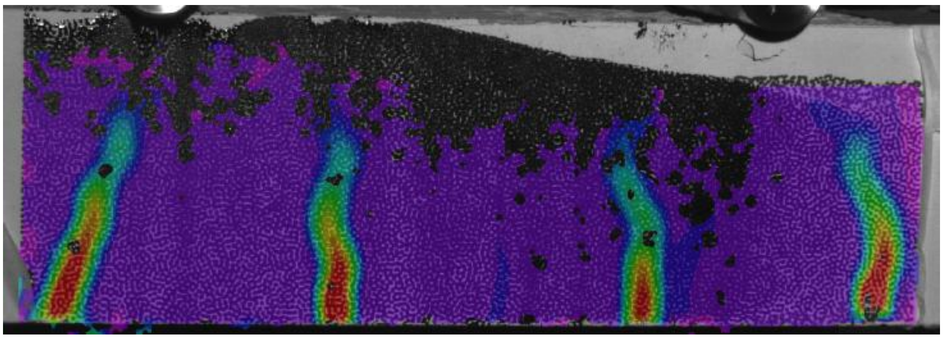

Figure 5.68: Ultimate strain field before healing

The crack widths of beams with rugby shaped tubes are tabulated in table 5.22. Since their values are rather big, they do not prove the healing at crack widths of 200μm to 300μm. However, all cracks that pass the clay tubes, are healed. Note again that visually, the cracks seemed smaller in reality than the values determined on the DIC images.

Table 5.22: Crack widths of droplet beams at ultimate loading, as seen on DIC (accuracy $\pm 70\mu m$)

Crack widths (μm)	Left	Second from left (or middle)	Third from left	Right
Rugby 1	440	426	/	578
Rugby 2	495	481	/	468
Rugby 3	316	426	316	371
Rugby 4	468	412	426	454

Second load cycle

After healing of 24 hours, the beams are reloaded. On the load curve in figure 5.69, two load drops are seen close to each other. These will be discussed together with two events just before. A first increased energy event is seen at the beginning of figure 5.69. The location is found to be left on the beam, illustrated in figure 5.70, concluded by the acoustic emission data. On the DIC picture, the opening of the crack on the left is seen. Some seconds before, this crack was still closed. Since this part of the beam lies outside the healing zone, the crack probably only closed, and not healed, due to the lack of loading upon the beam. The strain field containing the crack is shown in figure 5.71a.

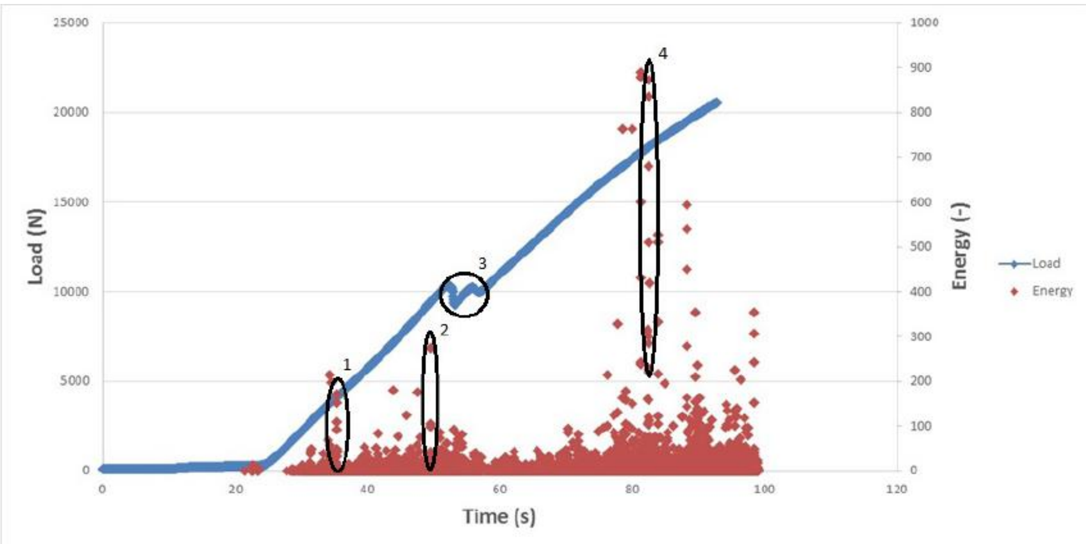

Figure 5.69: Load vs. time and energy vs. time after first healing

Secondly, two events occur almost simultaneously at moment 2 in figure 5.69. These occur just before the load drops (moment 3) and are assumed to be linked with them. The events can be splitted in one that comes from the left side of the speckle pattern, and the other from the right side. Reopening of cracks is found on the DIC pictures. A particular change in view on the left side cannot be seen and therefore only the right crack is shown in figure 5.71b. Most likely, the load drops following these events can be linked to the opening of cracks. When their width becomes larger, the concrete cannot take the load anymore. Steel has to take over, but not instantaneously. At the end of the load drops, three strain field occur in the middle of the beam. The concrete is cracked on the sides and strain is redistributed were sound concrete is available. This moment is depicted in figure 5.71c. The middle strain concentration vanishes afterwards and is thus just an elastic stretch. Both the other show a crack afterwards.

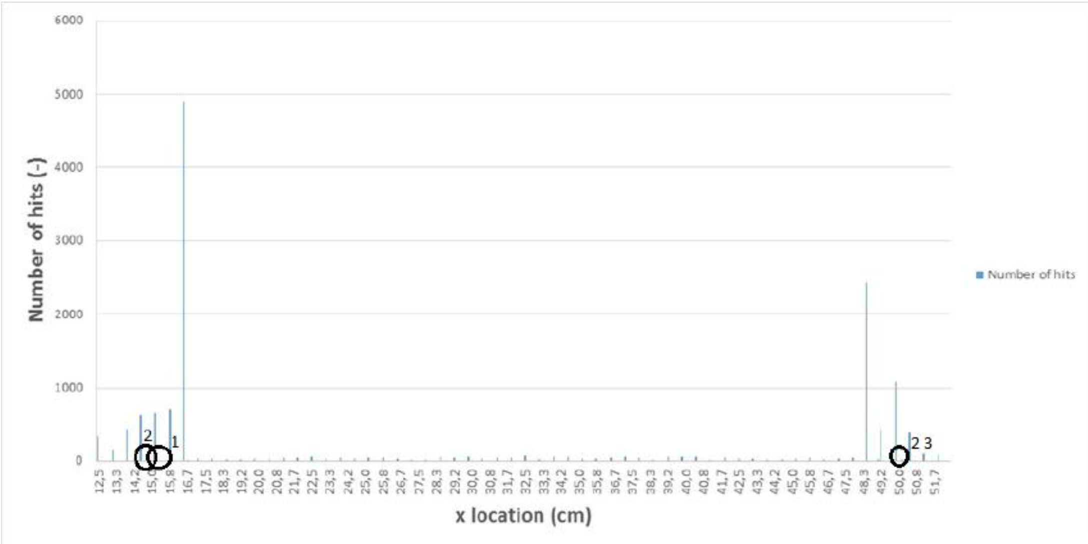

Figure 5.70: Location of events in the x-direction after first healing

In figure 5.70 it can be seen that only a very small number of hits come from the middle of the beam. However, increased strain field and cracks do occur here. It is thought that, because the cracks are filled with healing agent, this hardened liquid damps the sound of cracking.

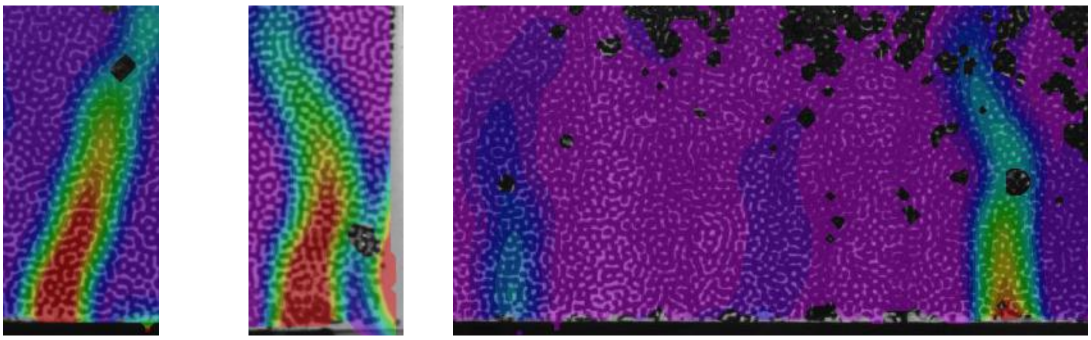

(a) Moment 1 (b) Moment 2 (c) Moment 3

Figure 5.71: Pictures of the DIC data for the different events after first healing

The fourth moment covers the highest energy in this load cycle. The event comes from the right extremity of the speckle pattern, according to AE, but on the DIC pictures nothing special is seen. The ultimate strain field after the second load cycle is shown in figure 5.72. It can be seen that the same four strain fields are present as in the previous load cycle on figure 5.68.

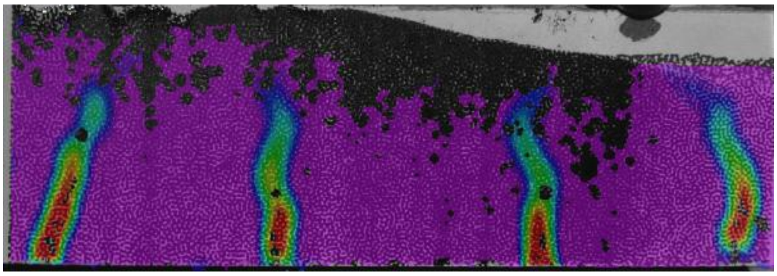

Figure 5.72: Ultimate strain field after first healing

Third load cycle

In the third load cycle, no load drops are present. At the start of loading, the four strain concentrations occur immediately at the same time. This means that these positions are weak and that probably no healing has happened.

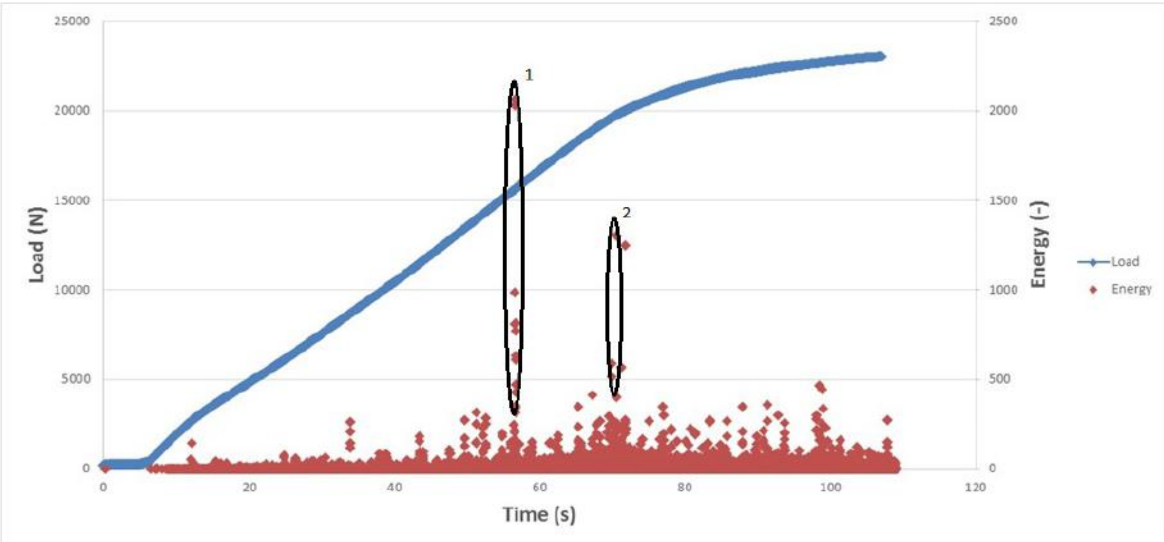

Figure 5.73: Load vs. time and energy vs. time after second healing

Two moments are chosen from graph 5.73. The first one contains the highest energy captured in this last loading cycle. The event is located at the second crack from the left. DIC data does not show any novelties.

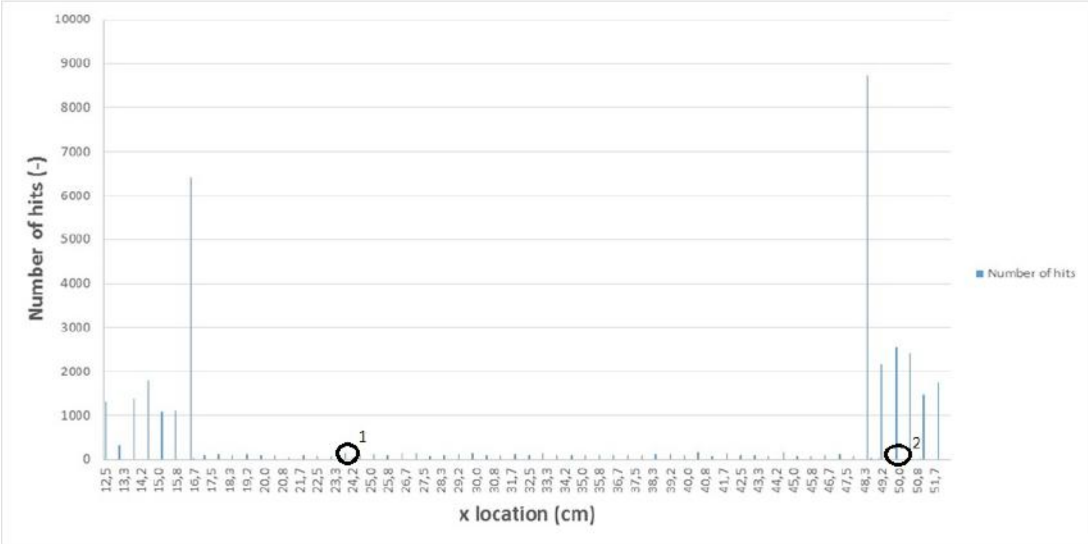

Figure 5.74: Location of events in the x-direction after second healing

At the second high energy event, nothing particular happens in the load curve too. This event should be, according to AE, on the right extremity of the speckle pattern. However, nothing is seen on the DIC pictures. Only the final strain is therefore illustrated in figure 5.75.

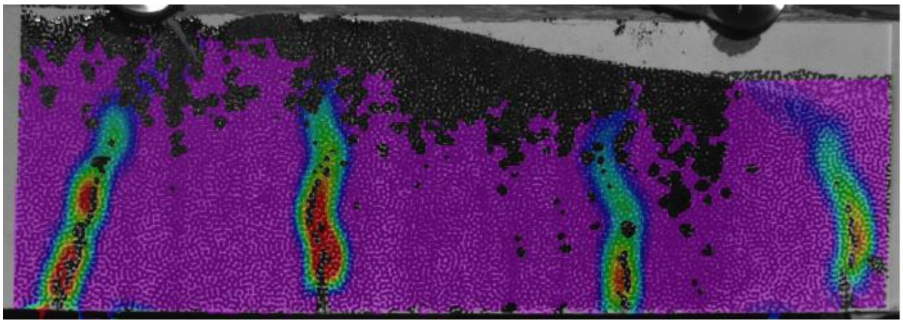

Figure 5.75: Ultimate strain field after second healing

Discussion

The three load cycles of specimen 3 are plotted in figure 5.76. From this graph, the stiffness of the beam in the different stages will be obtained.

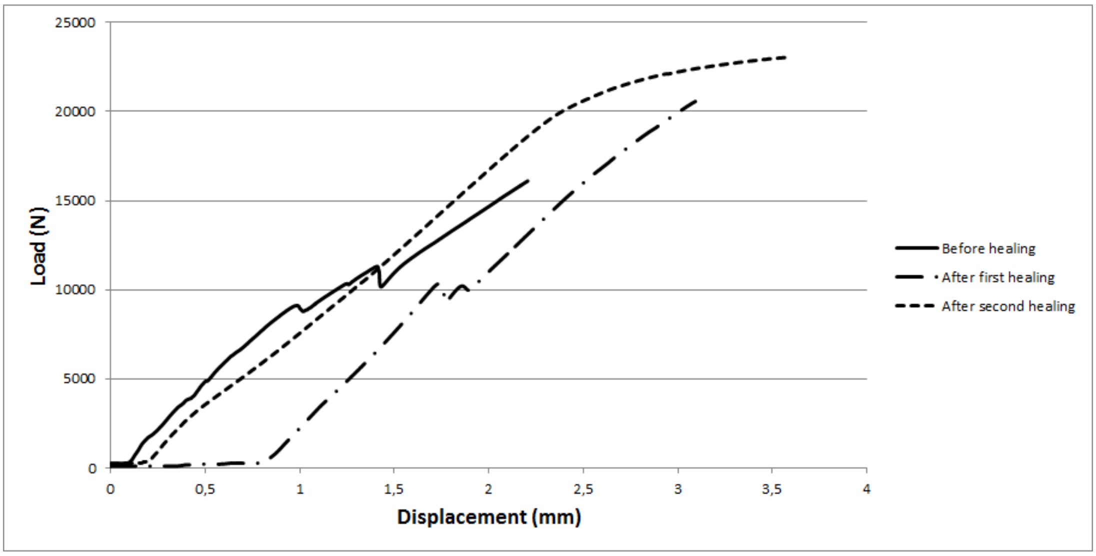

Figure 5.76: Load vs. displacement of the three load cycles

On the graph above, it is hard to make a fundamental distinction between the stiffnesses: all three the slopes look similar. The values found by plotting a trendline are listed below.

Table 5.23: Stiffness of beam rugby 3 in different load cycles

	Stiffness (N/mm)
Before healing	9751
After first healing	10117
After second healing	8840

As already seen in the plot above, the values of stiffness lie close to each other. Moreover, the stiffness of the beam before healing is lower than after the first healing, which would mean that healing made the beam more stiff. This is not as expected and therefore a suitable explanation is not found. Another particularity is that, when looking at the stiffness after the second healing, the beam only lost some 10% of its stiffness. In order to check the representativeness of these values, the stiffnesses of the other beams using rugby shaped tubes are tabulated in table 5.24. Notable is the big variance among this set of beams, especially for the stiffnesses before healing. Heterogeneities due to the complex structure can be a main reason for this, but no decisive answer can be given.

Table 5.24: Stiffness of the beams with rugby tubes in different load cycles

	Stiffness before healing	Stiffness after first healing	Stiffness after second healing
Specimen 1	21629N/mm	14662N/mm	8667N/mm
Specimen 2	14508N/mm	12677N/mm	10540N/mm
Specimen 3	9751N/mm	10117N/mm	8840N/mm
Specimen 4	12381N/mm	17456N/mm	10740N/mm
Mean stiffness	14567N/mm	13728N/mm	9797N/mm
Standard deviation	5094N/mm	3104N/mm	1095N/mm

Table 5.25 lists the healing efficiencies for all beams with rugby clay tubes. No valuable similarities are seen, because the values are too diverse. The third and fourth beam even have an efficiency higher than 100%. Also the difference in regain after first and second healing varies from 13% to 54%. The only consistency is the decrease in regain between second and third loading cycle, which proves that regain of stiffness due to self-healing has at least occured once, after the first loading cycle.

Table 5.25: Self-healing efficiency of beams with rugby clay tubes

	Regain after first healing (%)	Regain after second healing (%)
Specimen 1	68	40
Specimen 2	87	73
Specimen 3	104	91
Specimen 4	141	87
Mean efficiency	100	73

5.7.4 Summary

The main conclusion that can be drawn from these results is similar to the one from the experiments with IPC tubes. The stiffness at first loading of the references are on average higher than all other stiffnesses, establishing the softening that is caused by the vascular system. On the other hand, the stiffness at reloading of the reference beams is lower than all other stiffnesses. Self-healing therefore took place, but no clear distinction between the different shapes can be seen in the results.

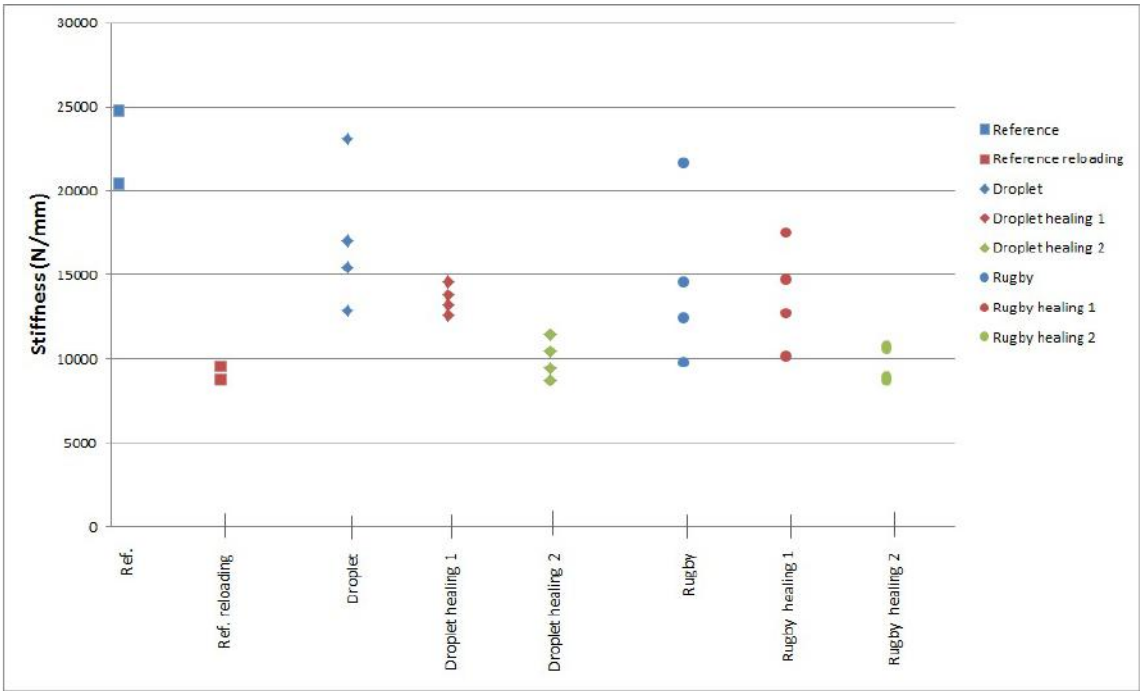

Figure 5.77: Summarizing chart representing stiffnesses of all beams during their load cycles

All cracks that occur between the two reservoirs were filled with healing agent. It is however not quantified at which crack width healing can occur.

The healing efficiency demonstrates that healing, and more precisely the regain of stiffness, occurs. The mean values are similar to the efficiencies of the beams with IPC system. Though, the variance here is bigger. Both clay and IPC seem to be valuable materials concerning the production of vascular system in concrete. Be aware that aside a different material in sections 5.6 and 5.7, also another amount of reinforcement and placing are used.

The first reference beam has a higher stiffness than all others. If one compares the cross sections of both reference beams (figure 5.78), it can be seen that the reinforcement bars are placed further from the neutral axis in the first reference beam. This probably explains the big difference in stiffness between the two reference beams.

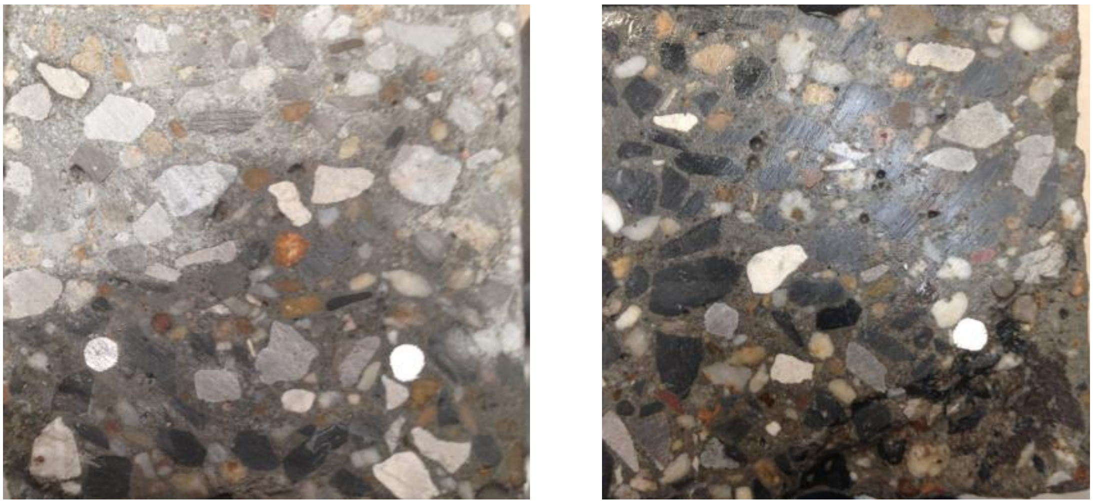

(a) (b)

Figure 5.78: Cross sections of the beams with clay tubes: droplet (a) and rugby (b)

Also with this set of beams, the vascular systems are positioned as it should be, and no debonding is noticed. On figure 5.79, a cut through the reservoir and another in the middle of the beam are displayed.

(a) (b)

Figure 5.79: Cross sections of the beams with clay tubes: droplet (a) and rugby (b)

The cut through the reservoir learns that there is even concrete between reinforcement bar and conncetion piece, and no air bubbles. The pumping of healing agent out of the reservoir turned out not to be efficient after all. At last, it is confirmed that clay is not porous to healing agent.

Conclusion

This master thesis investigates the upscaling of vascular self-healing in terms of survivability, healing efficiency and cost of material and production.
We have been looking for the optimal shape of tubes to minimize the impact load during the casting process. Comparison is made between round, diamond-, droplet- and rugby-shaped tubes. It turned out, either way theoretically and practically, that a rugby form is the ideal shape since it minimizes the drag and maximizes the penetration.
Further on, the production process of tubes is optimized. Clay is chosen over Inorganic Phosphate Cement, since it is the cheaper material and has in addition an easier manufacturing process by extrusion. Also, the permeability of the material is proven not to give a significant change on concrete strength. Hydration water was not absorbed to a large extent and the absorption of healing agent, in the slightly porous clay, is only small. This feature justifies the choice to abandon an expensive sealing powder or glaze, which lowers the cost.
Four-point bending tests are performed on beams containing tubes of either IPC or clay and a different type of vascular healing system. Self-healing was observed at least once in all cases. Multiple healing seems not yet possible: the stiffnesses of the beams are still slightly higher in comparison with the reloading of a reference beam, but it is unsure if this is due to new healing or still a result of first healing. Comparing the healing efficiencies between IPC and clay tubes, no significant differences are seen. Clay can thus without doubt be used as a conductor of healing agent.

Future work

However the results are promising, research should be continued before self-healing by vascular system can be used in real-life structures.
A first suggestion is to implement vascular systems in larger beam elements to investigate healing efficiency and applicability on more realistic dimensions. Therefore, the vascular system should either be enlarged so that reservoirs can be placed outside the cracking zone, or the current vascular systems can be placed along the short direction of the beams. In the first case, tubes should be increased in length or a coupling between multiple tubes must be provided, whether the latter option provides the advantage that the current system can be used.
Secondly, testing on repeated healing is of great interest. Without the possibility to heal multiple times, this concept is poorly efficient and not cost-effective. Continued damage then needs to be repaired manually.
A last suggestion is to keep the idea of placing vascular tubes under reinforcement, as they reduce the casting forces. Research should be performed whether placing the vascular system in proximity of the reinforcement, negatively influences the bound between concrete and reinforcement. As for now, placing tubes under reinforcement and respecting the concrete cover resulted in reinforcement bars close to the neutral axis. Larger specimens solve this issue.

Bibliography

[1] Kim Van Tittelboom and Nele De Belie. Self-healing in cementitious materials - a review. *Materials*, 6(6):2182–2217, 2013.

[2] Victor C Li and Emily Herbert. Robust self-healing concrete for sustainable infrastructure. *Journal of Advanced Concrete Technology*, 10(6):207–218, 2012.

[3] K Van Breugel. Is there a market for self-healing cement-based materials. In *Proceedings of the first international conference on self-healing materials. Noordwijk aan Zee, The Netherlands*, 2007.

[4] Waiching Tang, Omid Kardani, and Hongzhi Cui. Robust evaluation of self-healing efficiency in cementitious materials–a review. *Construction and Building Materials*, 81:233–247, 2015.

[5] Didier Snoeck, Stijn Steuperaert, Kim Van Tittelboom, Peter Dubruel, and Nele De Belie. Visualization of water penetration in cementitious materials with superabsorbent polymers by means of neutron radiography. *Cement and Concrete Research*, 42(8):1113–1121, 2012.

[6] HXD Lee, HS Wong, and NR Buenfeld. Potential of superabsorbent polymer for self-sealing cracks in concrete. *Advances in Applied Ceramics*, 109(5):296–302, 2010.

[7] MJ Lopez-tendero, P Diaz, JM Lloris, and C Gamon. Optimized hydrogel for application as repairing agents in cement based products. *In Proceedings of 3rd International Conference on Self Healing Materials*, 2011.

[8] Mustafa Sahmaran, Mo Li, and Victor C Li. Transport properties of engineered cementitious composites under chloride exposure. *ACI Materials Journal*, 104(6), 2007.

[9] Daisuke Homma, Hirozo Mihashi, and Tomoya Nishiwaki. Self-healing capability of fibre reinforced cementitious composites. *Journal of Advanced Concrete Technology*, 7(2):217–228, 2009.

[10] Tomoya Nishiwaki, Marina Koda, Makoto Yamada, Hirozo Mihashi, and Takatsune Kikuta. Experimental study on self-healing capability of frcc using different types of synthetic fibers. *Journal of Advanced Concrete Technology*, 10(6):195–206, 2012.

[11] Henk M Jonkers, Arjan Thijssen, Gerard Muyzer, Oguzhan Copuroglu, and Erik Schlangen. Application of bacteria as self-healing agent for the development of sustainable concrete. *Ecological engineering*, 36(2):230–235, 2010.

[12] HM Jonkers. Bacteria-based self-healing concrete. *Heron, 56 (1/2)*, 2011.

[13] Filipe Bravo Silva, Nico Boon, Nele De Belie, and Willy Verstraete. Industrial application of biological self-healing concrete: challenges and economical feasibility. *Journal of Commercial Biotechnology*, 21(1), 2015.

[14] Emily Adelsohn and John Hartsock. Bacteria-infused self-healing concrete. 2015.

[15] Haoliang Huang, Guang Ye, and Zhonghe Shui. Feasibility of self-healing in cementitious materials–by using capsules or a vascular system? *Construction and Building Materials*, 63:108–118, 2014.

[16] E Cailleux and V Pollet. Investigations on the development of self-healing properties in protective coatings for concrete and repair mortars. in proceedings of 2nd international conference on self healing materials. *In Proceedings of 2nd International Conference on Self Healing Materials*, 2009.

[17] Zhengxian Yang, John Hollar, Xiaodong He, and Xianming Shi. Laboratory assessment of a self-healing cementitious composite. *Transportation Research Record: Journal of the Transportation Research Board*, 2142(1):9–17, 2010.

[18] Zhengxian Yang, John Hollar, Xiaodong He, and Xianming Shi. A self-healing cementitious composite using oil core/silica gel shell microcapsules. *Cement and Concrete Composites*, 33(4):506–512, 2011.

[19] Eleni Tsangouri, Kim Van Tittelboom, Nele De Belie, DG Aggelis, and Danny Van Hemelrijck. Monitoring of autonomous healing process of concrete by acoustic emission and digital image correlation. In *12th International Conference of the Slovenian Society for Non-Destructive Testing 'Application of Contemporary non-destructive Testing in Engineering', Proceedings*, pages 581–587, 2013.

[20] P Minnebo, K Van Tittelboom, and D Van Hemelrijck. Ideal material properties for capsules or vascular system used in cementitious self-healing materials. 2015.

[21] Benoit Hilloulin, Kim Van Tittelboom, Elke Gruyaert, Nele De Belie, and Ahmed Loukili. Design of polymeric capsules for self-healing concrete. *Cement and Concrete Composites*, 55:298–307, 2015.

[22] C Joseph, AD Jefferson, B Isaacs, R Lark, and D Gardner. Experimental investigation of adhesive-based self-healing of cementitious materials. *Magazine of Concrete Research*, 62(11):831–843, 2010.

[23] Senot Sangadji and HEJG Schlangen. Porous network concrete: A new approach to make concrete structures self-healing using prefabricated porous layer. In *ICSHM 2011: Proceedings of the 3rd International Conference on Self-Healing Materials, Bath, UK, 27-29 June 2011*, 2011.

[24] Senot Sangadji and Erik Schlangen. Novel approach to make concrete structures self-healing using porous network concrete. In *Proceedings pro083: 2nd International Conference on Microstructural-related Durability of Cementitious Composites, Amsterdam, The Netherlands, 11-13 April 2012*. RILEM Publications SARL, 2012.

[25] Kim Van Tittelboom, Nele De Belie, Frank Lehmann, and Christian U Grosse. Acoustic emission analysis for the quantification of autonomous crack healing in concrete. *Construction and Building Materials*, 28(1):333–341, 2012.

[26] D Van Hemelrijck. Measurement of displacement and strain fields by digital image correlation (dic), 2014. Course notes.

[27] D Lecompte, S Bossuyt, S Cooreman, H Sol, and J Vantomme. Study and generation of optimal speckle patterns for dic. In *Proceedings of the annual conference and exposition on experimental and applied mechanics*, volume 3, pages 1643–9, 2007.

[28] Dr Nick McCormick and Dr Jerry Lord. Digital image correlation. *Materials today*, 13(12), 2010.

[29] P Minnebo, DG Aggelis, and D Van Hemelrijck. Monitoring of self-healing activation by means of acoustic emission and digital image correlation. 2015.

[30] TECH PLAS. The tech plas way: Plastic extrusion process. [Online; accessed 27-December-2015].

[31] Wikipedia. Extrusion — wikipedia, the free encyclopedia, 2015. [Online; accessed 27-December-2015].

[32] Nele De Belie, Kim Van Tittelboom, E Tsangouri, G Karaiskos, Didier Snoeck, Jianyun Wang, Maria Adelaide Pereira Gomes De Araujo, and D Van Hemelrijck. Autonomous regeneration of concrete structures by incorporation of self-healing mechanisms. In *International Conference on the Regeneration and Conservation of Concrete Structures (RCCS)*, pages 1–10, 2015.

[33] Kim Van Tittelboom, Jianyun Wang, Maria Araújo, Didier Snoeck, Elke Gruyaert, Brenda Debbaut, Hannelore Derluyn, Veerle Cnudde, Eleni Tsangouri, Danny Van Hemelrijck, et al. Comparison of different approaches for self-healing concrete in a large-scale lab test. *Construction and Building Materials*, 107:125–137, 2016.

[34] M Alshaaer, H Cuypers, G Mosselmans, H Rahier, and J Wastiels. Evaluation of a low temperature hardening inorganic phosphate cement for high-temperature applications. *Cement and Concrete Research*, 41(1):38–45, 2011.

[35] S Verbruggen, T Tysmans, and J Wastiels. Trc or cfrp strengthening for reinforced concrete beams: An experimental study of the cracking behaviour. *Engineering Structures*, 77:49–56, 2014.

[36] E Verwimp, T Tysmans, M Mollaert, and S Berg. Experimental and numerical buckling analysis of a thin trc dome. *Thin-Walled Structures*, 94:89–97, 2015.

[37] J Blom, M El Kadi, J Wastiels, and DG Aggelis. Bending fracture of textile reinforced cement laminates monitored by acoustic emission: Influence of aspect ratio. *Construction and Building Materials*, 70:370–378, 2014.

[38] S De Sutter, O Remy, and T Tysmans. Design and structural feasibility study of a lightweight floor system for renovation. In *19th Int Conf Compos Mater*, 2013.

[39] Harald Budelmann, Karim Hariri, Hans-Werner Krauss, and Tim Malonn. Effects of a clay additive on the properties of no-slump concrete. In *Advances in Construction Materials 2007*, pages 731–739. Springer, 2007.

[40] F Van Duin. Duurzaam keramiek. [Online; accessed 16-February-2016].

[41] i.materialize. 3d printing service. [Online; accessed 8-February-2016].

[42] Joong Kyu Jeon, WooSeok Kim, Chan Ki Jeon, and Jin Cheol Kim. Processing and mechanical properties of macro polyamide fiber reinforced concrete. *Materials*, 7(12):7634, 2014.

[43] De Neef Conchem. Construction chemicals. [Online; accessed 23-May-2016].

[44] Michael Zabarankin. Minimum-resistance shapes in linear continuum mechanics. In *Proceedings of the Royal Society of London A: Mathematical, Physical and Engineering Sciences*, volume 469, page 20130206. The Royal Society, 2013.

[45] O Pironneau. On optimum design in fluid mechanics. *Journal of Fluid Mechanics*, 64:97–110, 6 1974.

[46] Thomas D Montenegro-Johnson and Eric Lauga. The other optimal stokes drag profile. *Journal of Fluid Mechanics*, 762, 1 2015.

[47] NK Gupta, MA Iqbal, and GS Sekhon. Effect of projectile nose shape, impact velocity and target thickness on deformation behavior of aluminum plates. *International Journal of Solids and Structures*, 44(10):3411–3439, 2007.

[48] W Shiu, F Victor Donzé, and L Daudeville. Penetration prediction of missiles with different nose shapes by the discrete element numerical approach. *Computers and Structures*, 86(21 and 22):2079–2086, 2008.

[49] DG Aggelis. Dynamics of structures, elastic wave propagation, 2014. Course notes.

Appendices

Technical sheets

technical data sheet

HA Flex/Flex LV/Flex SLV AF

Next generation, phthalate free, closed cell, 1-component high performance hydrophobic, Hydro-Active, flexible polyurethane injection grouts for waterproofing leaking joints and cracks.

REPLACES HA FLEX/LV/SLV AND TACSS FLEX 44/LV/SLV

• field of application

HA Flex AF/Flex LV AF/Flex SLV AF

- Designed for grouting joints or stopping water leaks in concrete structures, which are subject to settlement and movement.
- Used for protective waterproofing and gap filling around the brush tails of the TBM and for repairing the waterproof gasket.
- For stopping water leaks through joints between tunnel segments.
- For injection of the LDPE or HDPE membrane in tunnel constructions.
- For curtain injections behind tunnel segments.

HA Flex SLV AF (Specific fields of application)

- Specifically developed for injection of fine and ultra fine crack and joints.

Joint and crack dimensions.

Always select a resin based on the crack or joint size to be injected.

Small cracks will require low or ultra-low viscosity resins to ensure good crack penetration.

As a general recommendation, the following crack dimensions can be used:

HA Flex AF : cracks > 4 mm.
HA Flex LV AF : 0.5 mm < Cracks < 4 mm.
HA Flex SLV AF : cracks < 0.5 mm.

• advantages

- ADR free transport.
- Next generation resin with improved waterproofing performance.
- Improved cell structure of the cured compound resulting in better mechanical properties and durability.
- Phthalate free resins, REACH compliant.
- Improved performance at temperatures below 5°C, no crystallisation of HA Flex Cat AF.
- HA Flex AF/Flex LV AF/Flex SLV AF form a flexible gasket or flexible plug in the joint or crack.
- Non-flammable, solvent free.
- Choice of different expansion rates.
- User friendly: 1-component product.
- Controllable reaction times: by using catalyst curing times can be reduced.
- Cured compound is resistant to most organic solvents, mild acids, alkalis and micro organisms.(*)

• description

In its uncured form, HA Flex AF/Flex LV AF/Flex SLV AF are white or yellow, non-flammable liquids without phthalate plasticisers. HA Flex AF/Flex LV AF/Flex SLV AF are next generation 1-component injection resins with improved waterproofing performance. When they come in contact with water, the grout expands and quickly (depending on temperature and the amount of accelerator HA Flex Cat AF used) cures to a tough, flexible, closed-cell polyurethane foam that is essentially unaffected by corrosive environments.

• application

Before commencing the injection, consult the Technical Data Sheets and MSDS in order to be familiar with the materials at hand.

Always shake the HA Flex Cat AF well before use.

<u>1. Surface preparation</u>

- Remove surface contaminants and debris to establish the pattern of the crack or joint. Active leaking cracks larger than 3 mm need to be sealed with an approved method.
- Drill holes of the correct diameter for the selected packer. Drill at an angle of 45°. Preferably the holes should be drilled staggered around the crack to insure good coverage of the crack in case it is not perpendicular to the concrete surface.
- The depth of the bore should be approximately half of the thickness of the concrete. As a rule of thumb the distance of the drill point from the crack is 1/2 the wall thickness.
- Distance between holes can vary by 15 to 90 cm, depending on the actual situation.
- Insert the correctly sized packer into the hole up to 2/3 of its length. Tighten with a wrench or spanner by turning clockwise until sufficient tension has been reached to keep the packer in place during injection.
- Flush the crack with water before injecting with resin. This will flush out dust, debris and prime the crack for the injection resin and improve penetration of the product into the crack. Water in the crack will activate the resin.

<u>2. Resin and equipment preparation</u>

- Prepare the resin with the predetermined amount of catalyst. Shake HA Flex Cat AF well before use. No reaction with the resin will occur until the resin comes into contact with water.
- Do not prepare more resin than can be injected within 4 hours after mixing HA Flex Cat AF in the resin. Avoid mixing full drums, it is recommended to batch mix smaller quantities in a separate pail or in the pump reservoir.
- Protect the resin from water, since this will trigger a reaction in the container used and might cause the resin to harden or foam prematurely within the injection equipment.
- It is highly recommended to use separate pumps for the water and the resin injection to prevent cross contamination and blockages.
- The pumps should be thoroughly primed with Washing Agent Eco to lubricate and dry the system before injection. We recommend the use of pneumatic or electric 1-component pumps.

<u>3. Injection</u>

- Start the injection at the first packer.
- Start injecting at the lowest pressure setting of the pump. Slowly increase the pressure until the resin begins to flow. Pressures may vary from 14 bars to 200 bars depending on the size of the crack, the thickness of the concrete and the general condition of the concrete.
- A little leakage of resin through the concrete or crack is useful in showing the extent of resin travel. Large leaks should be plugged with rags, wait for the resin to set, then inject again.
- During the injection water will first flow from the crack, followed by foaming resin. After this, pure resin will flow from the crack.
- Stop pumping when the pure resin reaches the next packer.
- Move to the next packer and repeat the procedure.

- After injecting through a few of the packers, go back to the first one and re-inject with resin.
- After the resin injection, water can be re-injected into the ports to cure resin left behind.
- Let the resin cure thoroughly before removing packers. The resulting holes can be filled with hydraulic cement.
- When the injection is finished, clean all tools and equipment which have been in contact with the resin with Washing Agent Eco. This should be done within 30 minutes. Never leave the pump filled with resin overnight or for periods beyond 1 shift. Do not use solvents or other cleaning products since they give less positive results and can create hazardous situations. Products should be disposed off according to local legislation.
- Refer to Material Safety Data Sheet for general recommendations. In case of spills and accidents, refer to the Material Safety Data Sheet of the products or when in doubt contact the De Neef Division responsible for your territory. Always wear appropriate protective gear for the job at hand according to local guidelines and regulations. We recommend that gloves and protective goggles are worn when handling chemical products. See MSDS for further recommendations..

4. Reactivity

Reactivity	HA Flex Cat AF	Start reaction			End reaction			Expansion
		HA Flex AF	HA Flex LV AF	HA Flex SLV AF	HA Flex AF	HA Flex LV AF	HA Flex SLV AF	
At 5°C	1%		Approx. 3'30"			Approx.17'00"		Approx.12V
	2%		Approx. 2'15"	Approx. 1'30"		Approx. 8'30"	Approx. 6'30"	Approx. 14V
	5%		Approx. 55"	Approx. 50"		Approx. 4'00"	Approx. 3'25''	Approx. 16V
At 15°C	1%	Approx. 1'40"	Approx. 2'10"		Approx. 8'00"	Approx. 10'50"		Approx. 14V
	2%	Approx. 1'00"	Approx. 1'25"	Approx. 1'10"	Approx. 5'00"	Approx. 7'00"	Approx. 5'10"	Approx. 16V
	5%	Approx. 30"	Approx. 40"	Approx. 35"	Approx. 2'10"	Approx. 3'05"	Approx. 2'35"	Approx. 16V
At 25°C	1%	Approx. 1'00"	Approx. 1'30"		Approx. 7'15"	Approx. 9'00"		Approx. 14V
	2%	Approx. 40"	Approx. 1'05"	Approx. 1'00"	Approx. 4'20"	Approx. 5'35"	Approx. 4'30"	Approx. 16V
	5%	Approx. 25"	Approx. 35"	Approx. 35"	Approx. 1'55"	Approx. 2'10''	Approx. 2'20"	Approx. 17V
At 30°C	1%	Approx. 45"	Approx. 1'05"		Approx. 6'40"	Approx. 7'30"		Approx. 14V
	2%	Approx. 35"	Approx. 45"	Approx. 50"	Approx. 3'45"	Approx. 4'40"	Approx. 4'20"	Approx. 16V
	5%	Approx. 20"	Approx. 25"	Approx. 30"	Approx. 1'35"	Approx. 1'45"	Approx. 2'00"	Approx. 17V
At 35°C	1%	Approx. 45"	Approx. 55"		Approx. 4'15"	Approx. 6'45"		Approx. 15V
	2%	Approx. 35"	Approx. 40"	Approx. 50"	Approx. 3'00"	Approx. 4'00"	Approx. 3'35"	Approx. 17V
	5%	Approx. 20"	Approx. 20"	Approx. 25"	Approx. 1'25"	Approx. 1'35"	Approx. 1'45"	Approx. 18V

HA Flex AF is not suitable for applications below 15 °C.
HA Flex SLV AF should always be used with a minimum of 2 % HA Flex Cat AF.

• technical data/properties

Property	Value			Norm
	HA Flex AF	HA Flex LV AF	HA Flex SLV AF	
Uncured				
Solids	100%	100%	100%	EN ISO 3251
Viscosity at 25°C (mPas)	Approx. 1000	Approx. 550	Approx. 200	EN ISO 3219
Density (kg/dm^3)	Approx. 1,075	Approx. 1,020	Approx. 1,075	EN ISO 2811
Flash Point (°C)	> 132	> 132	> 132	EN ISO 2719
HA Flex Cat AF				
Viscosity at 25 °C (mPas)	Approx. 15			EN ISO 3219
Density (kg/dm^3)	Approx. 0,950			EN ISO 2811
Flash Point (°C)	105			EN ISO 2719
Cured				
Density (kg/dm^3)	Approx. 1,000			EN ISO 1183
Tensile strength (N/mm^2)	Approx. 1,2			EN ISO 527
Elongation (%)	Approx. 250	Approx. 100	Approx. 100	EN ISO 527

• appearance

HA Flex AF : white liquid.
HA Flex LV AF : yellow liquid.
HA Flex SLV AF : yellow liquid.
HA Flex Cat AF : grey transparent liquid.

• consumption

Has to be estimated by the engineer or operator and depends on width and depth of the cracks and voids, which need to be injected and on the expansion rate of the chosen resin.

• packaging

HA Flex AF/Flex LV AF/Flex SLV AF
5 kg, 25 kg or 200 kg metal drums
1 Pallet
180 x 5 kg drum.
24 x 25 kg drum.
4 x 200 kg drum.
HA Flex Cat AF
0,25 or 1 l plastic bottle or 20 kg metal drum.
1 box = 15 x 0,25 l
1 box = 16 x 1 l
1 Pallet
84 boxes with 0,25 l bottles.
24 boxes with 1 l bottles.
24 x 20 kg metal drums.

• storage

HA Flex AF/Flex LV AF/Flex SLV AF are sensitive to moisture and should be stored in original containers in a dry area. Storage temperature must be between 5°C and 30°C. Once the packaging has been opened, the useful life of the material is greatly reduced and should be used as soon as possible.
Shelf life: 2 years.

• accessories

To be ordered separately
- IP 1C-Manual hand pump.
- IP 1C-Compact electric airless diaphragm pump.
- IP 1C-Pro electric airless diaphragm pump.
- Packers and connectors.

(Please consult the relevant data sheet).

• health & safety

HA Flex AF resins are classified as harmful.
HA Flex Cat AF is classified as irritant.
In case of spills and accidents, refer to the Material Safety Data Sheet of the products or when in doubt contact the De Neef responsible for your territory. Always wear protective clothing, gloves and protective goggles when handling chemical products.
For full information, consult the relevant Material Health and Safety Data Sheet.
(*) For chemical resistances please contact your De Neef representative.

de neef® conchem
Industriepark 8 • 2220 Heist-op-den-Berg
BELGIE
Tel.: +32 (0)15 24 93 60
Fax: +32 (0)15 24 80 72
E-mail: conchem@deneef.com
www.deneef.com

TML STRAIN GAUGE TEST DATA

GAUGE TYPE	: FLK-6-11	TESTED ON	: SS 400
LOT NO.	: A514711	COEFFICIENT OF THERMAL EXPANSION	: 11.8 $\times 10^{-6}/℃$
GAUGE FACTOR	: 2.12 ±1%	TEMPERATURE COEFFICIENT OF G.F.	: +0.1±0.05 %/10℃
ADHESIVE	: P-2	DATA NO.	: A0953

THERMAL OUTPUT (εapp : APPARENT STRAIN)

$\varepsilon app = -2.68\times10^{1}+2.42\times T^{1}-6.16\times10^{-2}\times T^{2}+3.93\times10^{-4}\times T^{3}-8.68\times10^{-7}\times T^{4}$ (μm/m)

TOLERANCE : ±0.85 [(μm/m)/℃] , T : TEMPERATURE

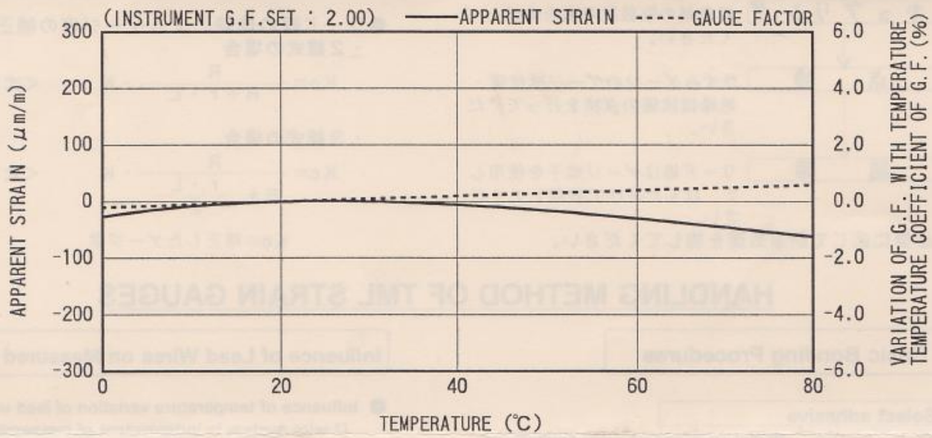

ひずみゲージ取扱いの注意事項

- 上記の特性データは、リード線の取付けによる影響を含んでおりません。裏面記載のリード線の測定値への影響に従って補正してください。
- ゲージの使用温度は、接着剤の耐熱温度などにより変わります。
- 絶縁抵抗などの点検は、印加電圧を５０Ｖ以下にしてください。
- ゲージリード線に無理な力を加えないでください。
- ゲージ裏面に接着剤を塗布して接着してください。
- ひずみゲージの裏面は脱脂洗浄してありますので、汚さないように取扱いしてください。
- ゲージの包装を開封後は、乾燥した場所で保管してください。
- ご使用に際してご不明な点などがございましたら、当社までお問い合わせください。

CAUTIONS ON HANDLING STRAIN GAUGES

- The above characteristic data do not include influence due to lead wires. Correct the data in accordance with the influence of lead wires on measured values described overleaf.
- The service temperature of strain gauge depends on the operating temperature of adhesive, etc.
- Check of insulation resistance, etc. should be made at a voltage of less than 50V.
- Do not apply an excessive force to the gauge leads.
- Apply an adhesive to the back of a strain gauge and stick the gauge to a specimen.
- As the back of strain gauge has been degreased and washed, do not contaminate it.
- After unpacking, store strain gauges in a dry place.
- If you have any questions on strain gauges or installation, contact TML or your local agent.

Made in Japan

TML 株式會社 東京測器研究所

〒140-8560 東京都品川区南大井 6 - 8 - 2
TEL 03 - 3763 - 5611
FAX 03 - 3763 - 6128

Tokyo Sokki Kenkyujo Co., Ltd.

8 - 2, Minami - Ohi 6 - Chome
Shinagawa - ku, Tokyo 140-8560

TMLひずみゲージの取扱い方法

基本的な接着手順

1. **接着剤の選択** 使用する条件に合った、ひずみゲージ用の接着剤を選びます。
2. **表面処理** 被接着面のさび・塗料などを除去し、120〜180番（アルミニウム:240〜320番）のサンドペーパで軽く磨きアセトンなどで清浄して、ゲージ接着位置をけがいてください。
3. **ゲージ接着** 接着剤の取扱説明書を参照してください。
4. **キュアリング** 接着剤の取扱説明書を参照してください。
5. **点検** ひずみゲージのゲージ抵抗値・絶縁抵抗値の点検を行ってください。
6. **結線** リード線はゲージ端子を使用して、はんだ付けで接続してください。

・必要に応じて防湿処理を施してください。

リード線の測定値への影響

●リード線の温度変化による影響。
（3線式結線法では、温度影響はありません。）

$$\varepsilon l = \frac{r \cdot L \cdot \alpha \cdot \Delta T}{K\,(R + r \cdot L)} \quad \text{<式1>}$$

εl ＝リード線の熱出力
r ＝リード線1m当たりの往復の抵抗値（Ω／m）
L ＝リード線の長さ（m）
α ＝リード線の抵抗温度係数（銅線＝3.9×10^{-3}／℃）
ΔT ＝温度変化量
K ＝ゲージ率
R ＝ゲージ抵抗

●リード線の結線によるゲージ率の補正。

・2線式の場合

$$K_o = \frac{R}{R + r \cdot L} \cdot K \quad \text{<式2>}$$

・3線式の場合

$$K_o = \frac{R}{R + \frac{r \cdot L}{2}} \cdot K \quad \text{<式3>}$$

K_o＝補正したゲージ率

HANDLING METHOD OF TML STRAIN GAUGES

Basic Bonding Procedures

1. **Select adhesive** Select an adhesive most suitable for test conditions.
2. **Surface treatment** Remove grease, rust, paint, etc. from the bonding surface of a specimen, lightly polish with an abrasive paper of #120 〜 180 (#240 〜 320 for aluminium), wipe with acetone, etc. and mark gauge installation position.
3. **Gauge installation** Refer to the operation manual of adhesive.
4. **Adhesive curing** Refer to the operation manual of adhesive.
5. **Gauge installation check** Check gauge resistance and insulation resistance.
6. **Lead wire attachment** Solder lead wires to the strain gauges through connecting terminals.

· If necessary, apply waterproof coating.

Influence of Lead Wires on Measured Values

● Influence of temperature variation of lead wires
(3-wire system is independent of temperature.)

$$\varepsilon l = \frac{r \cdot L \cdot \alpha \cdot \Delta T}{K\,(R + r \cdot L)} \quad \text{<Equation 1>}$$

where εl = *thermal output of lead wires*
r = *total resistance per meter of lead wires (Ω /m)*
L = *length of lead wires (m)*
α = *temperature coefficient of resistance of lead wires (copper wire = 3.9×10^{-3} /℃)*
ΔT = *temperature variation*
K = *gauge factor*
R = *gauge resistance*

● Gauge Factor Correction due to Lead Wire Attachment

· In case of 2-wire system

$$K_o = \frac{R}{R + r \cdot L} \cdot K \quad \text{<Equation2>}$$

· In case of 3-wire system

$$K_o = \frac{R}{R + \frac{r \cdot L}{2}} \cdot K \quad \text{<Equation3>}$$

where K_o = *corrected gauge factor*

リード線1m当たりの往復の抵抗値
Total Resistance per Meter of Lead Wires

構成（心数／直径） Lead wires(number of cores / diameter)	ポリイミド線 polyimide	ポリイミド線 polyimide	7/0.12	10/0.12	12/0.18	20/0.18
リード線の直径または断面積 Diameter or cross sectional area of lead wires	φ 0.14mm	φ 0.18mm	0.08 mm²	0.11 mm²	0.3 mm²	0.5 mm²
1m 当たりの往復の抵抗値 Total resistance per meter	2.5 Ω/m	1.5 Ω/m	0.44 Ω/m	0.32 Ω/m	0.12 Ω/m	0.07 Ω/m

Graphs

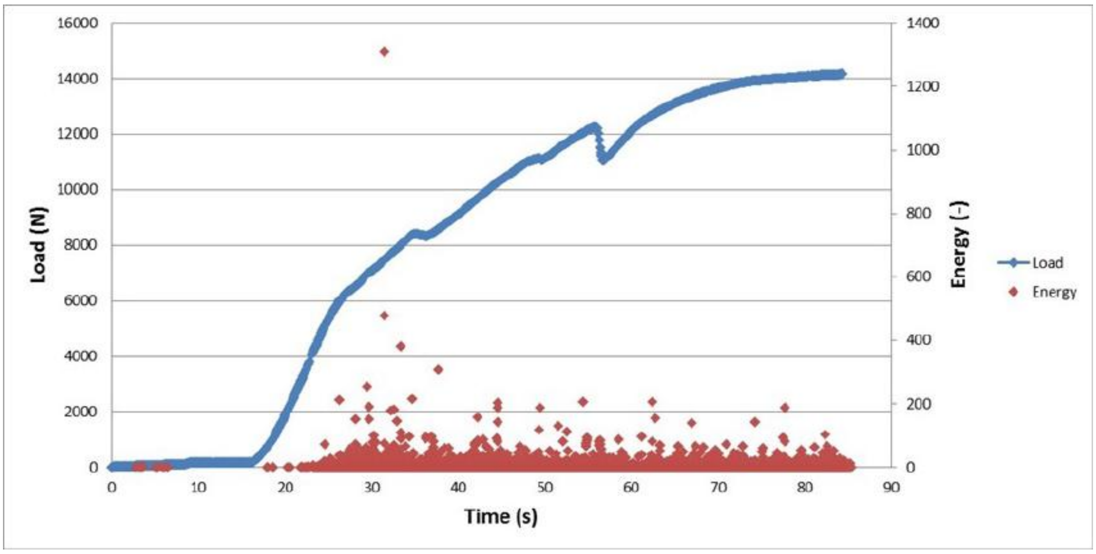

Figure B.1: Load vs. time and energy vs. time of reference 2 IPC before healing

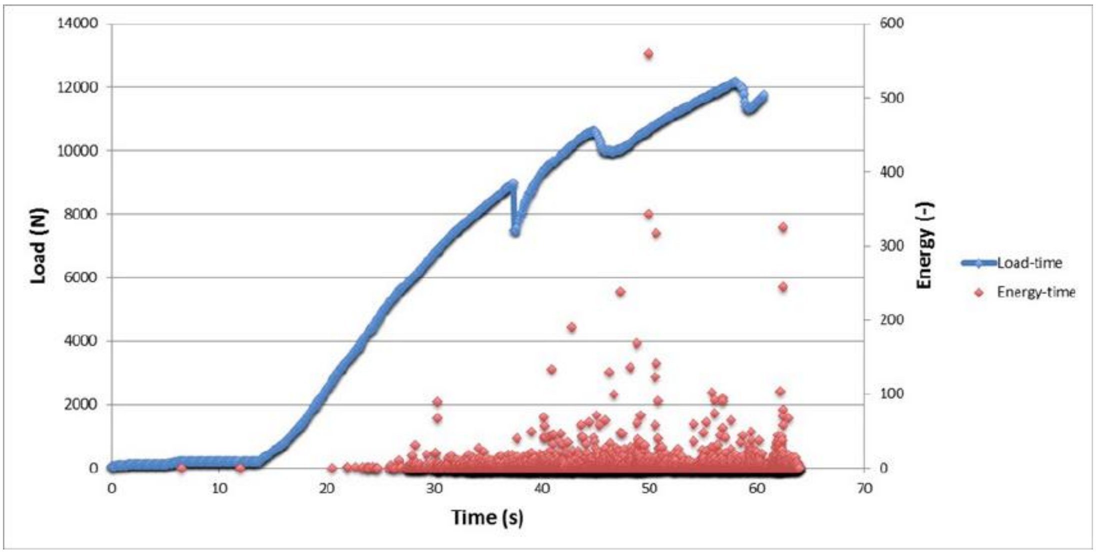

Figure B.2: Load vs. time and energy vs. time of specimen 1 round IPC before healing

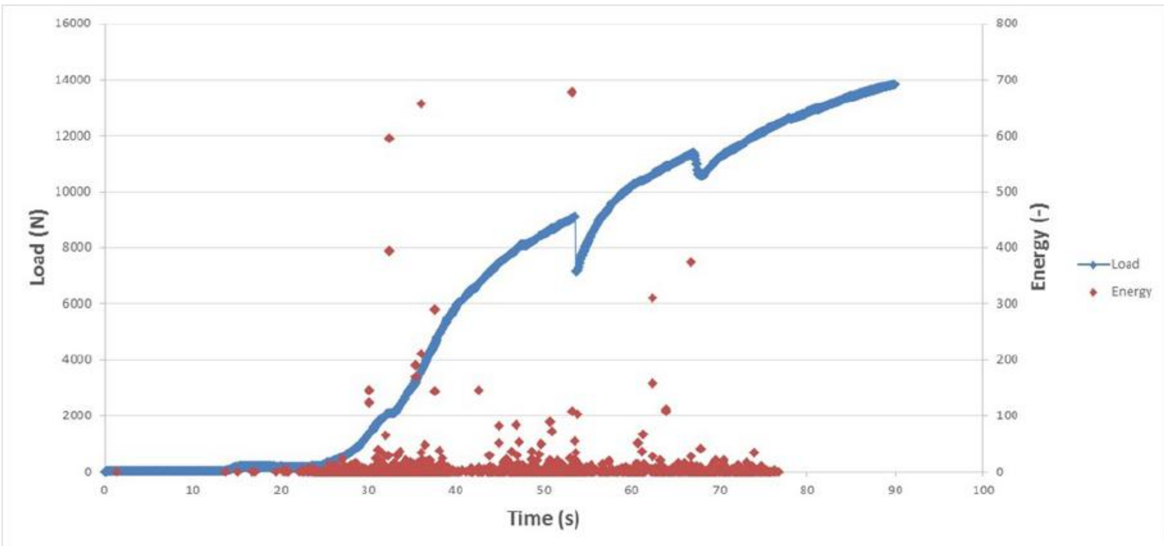

Figure B.3: Load vs. time and energy vs. time of specimen 2 round IPC before healing

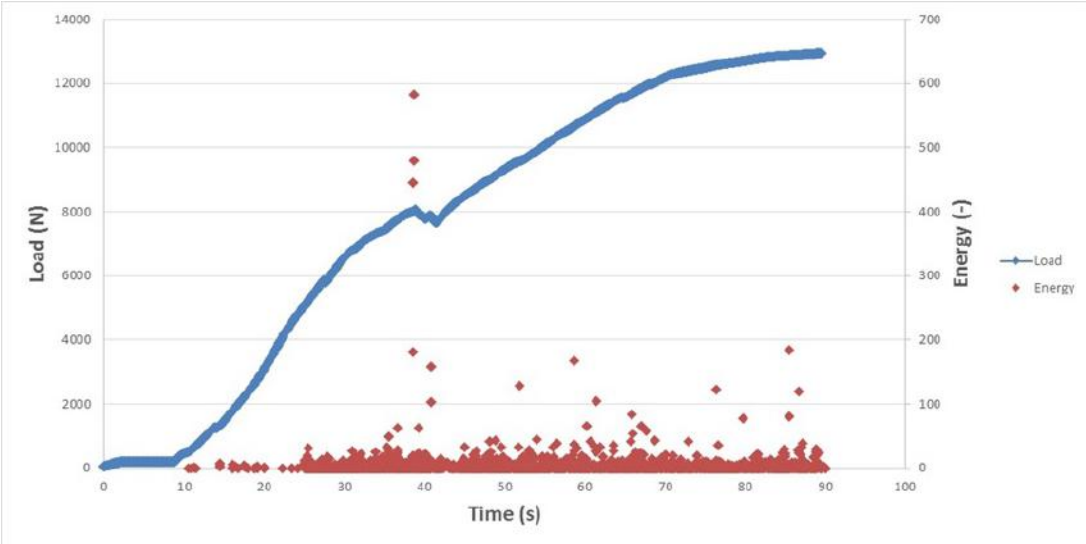

Figure B.4: Load vs. time and energy vs. time of specimen 4 round IPC before healing

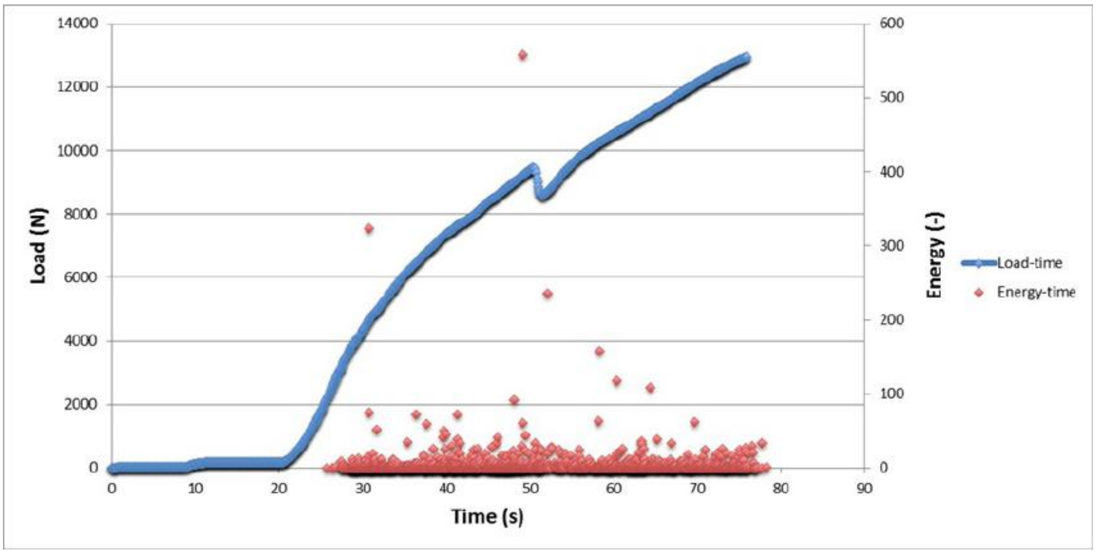

Figure B.5: Load vs. time and energy vs. time of specimen 2 droplet IPC before healing

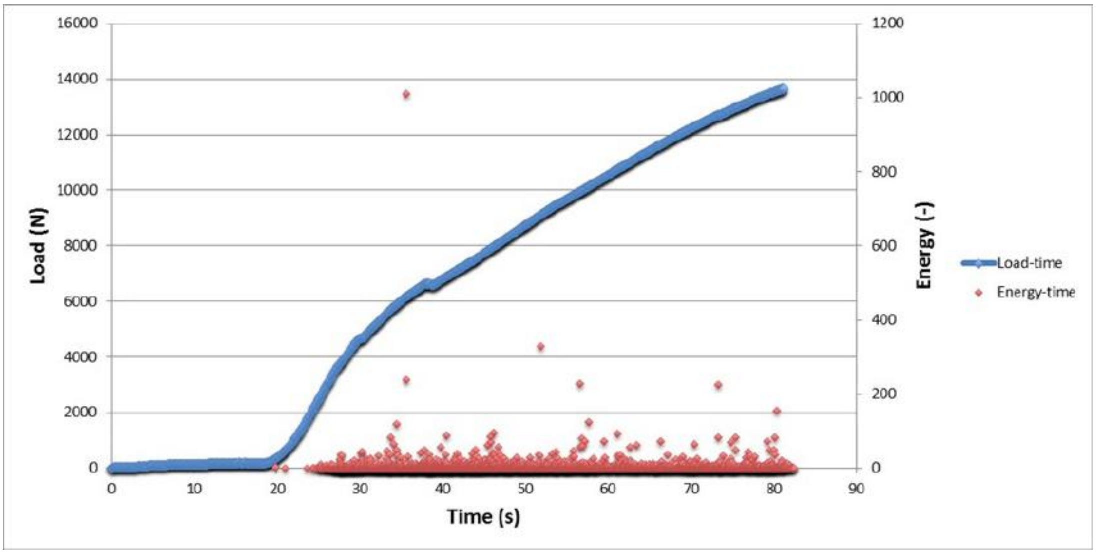

Figure B.6: Load vs. time and energy vs. time of specimen 3 droplet IPC before healing

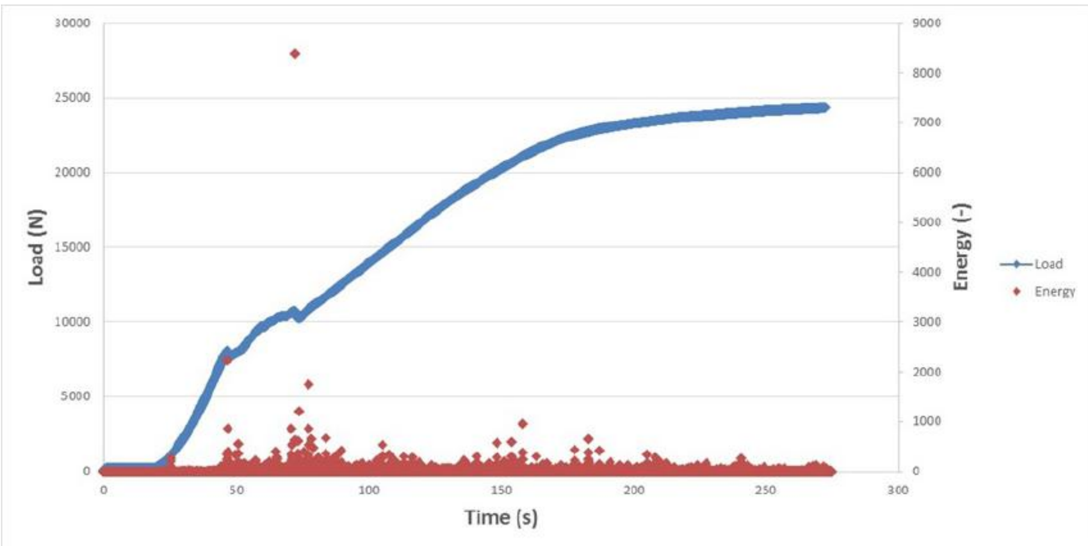

Figure B.7: Load vs. time and energy vs. time of reference 2 clay before healing

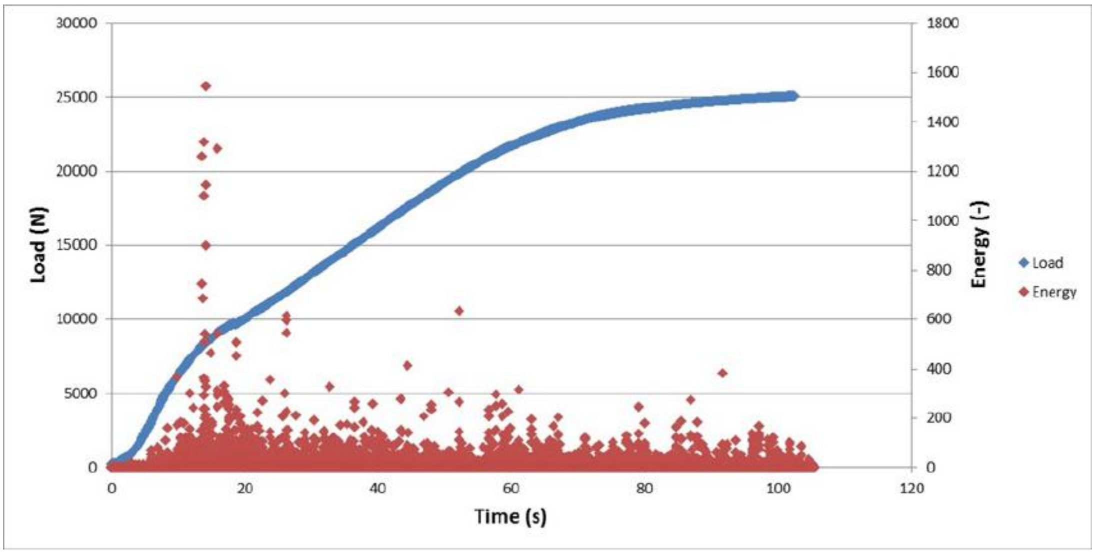

Figure B.8: Load vs. time and energy vs. time of specimen 1 droplet clay before healing

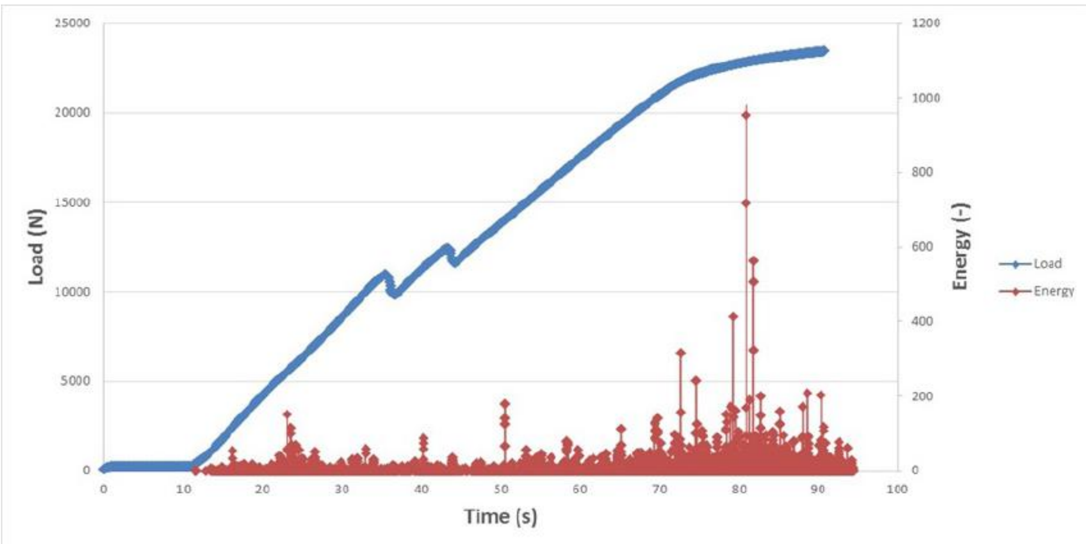

Figure B.9: Load vs. time and energy vs. time of specimen 2 droplet clay before healing

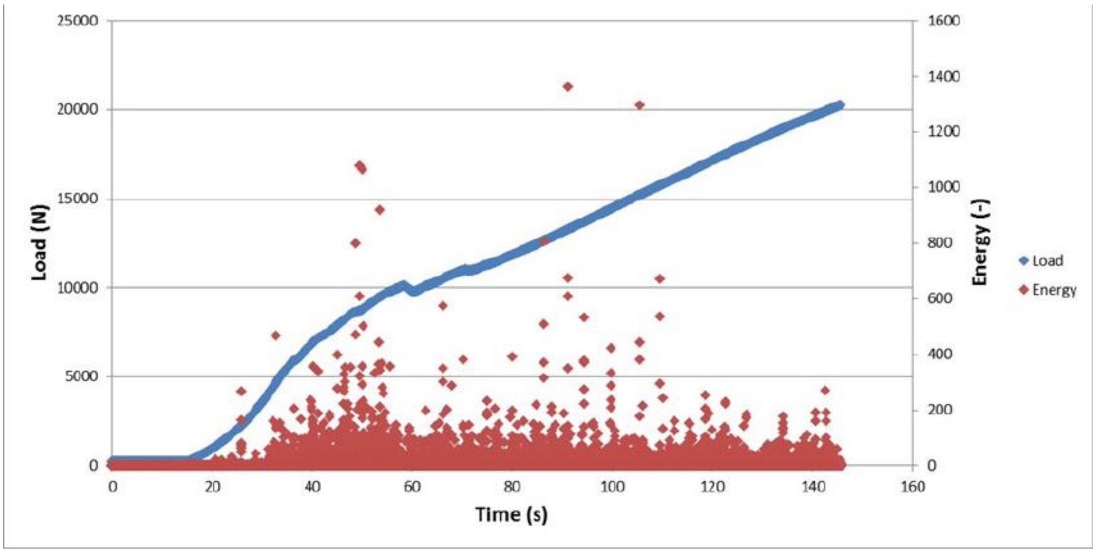

Figure B.10: Load vs. time and energy vs. time of specimen 4 droplet clay before healing

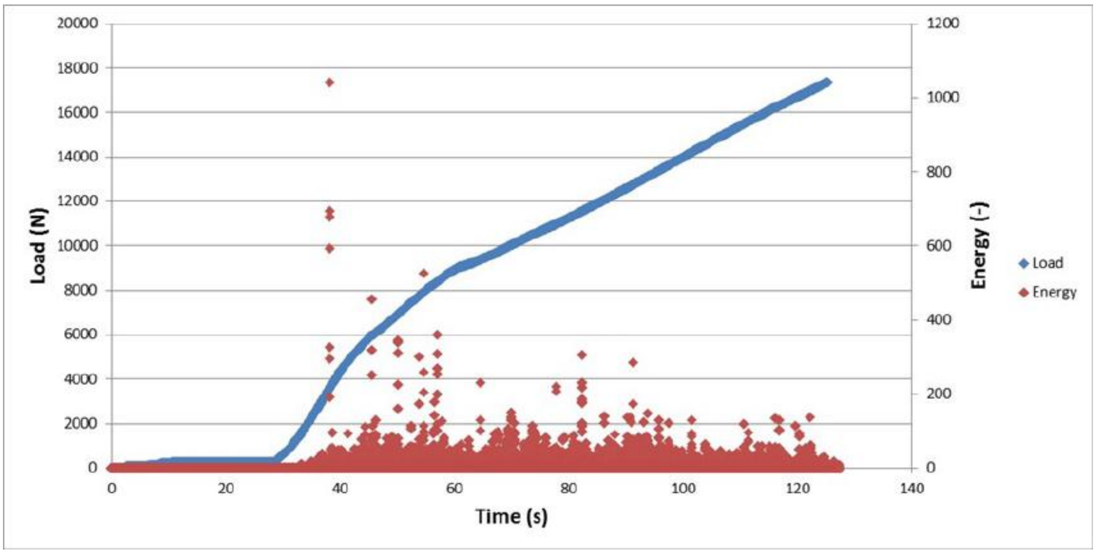

Figure B.11: Load vs. time and energy vs. time of specimen 1 rugby clay before healing

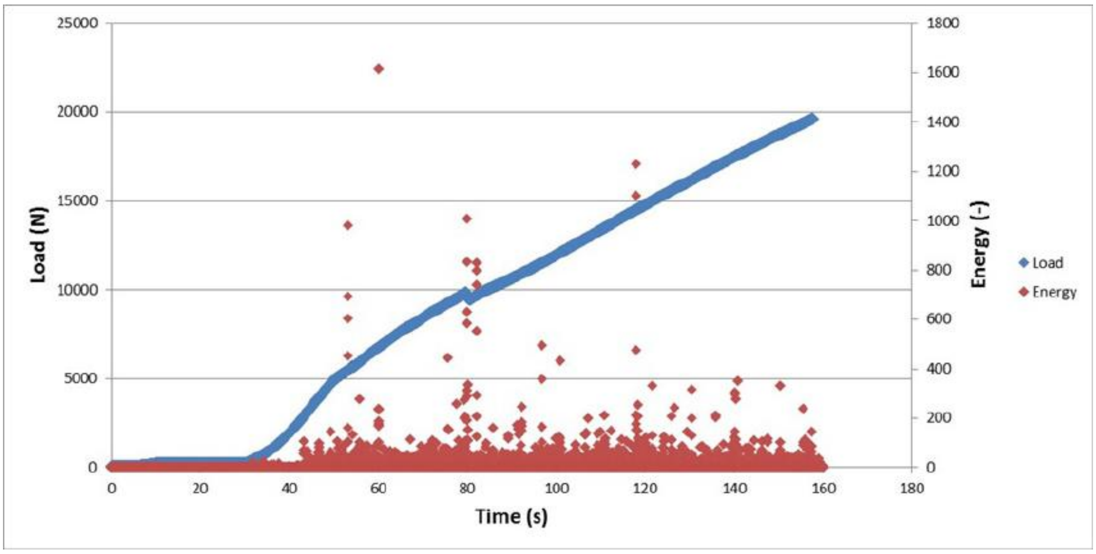

Figure B.12: Load vs. time and energy vs. time of specimen 2 rugby clay before healing

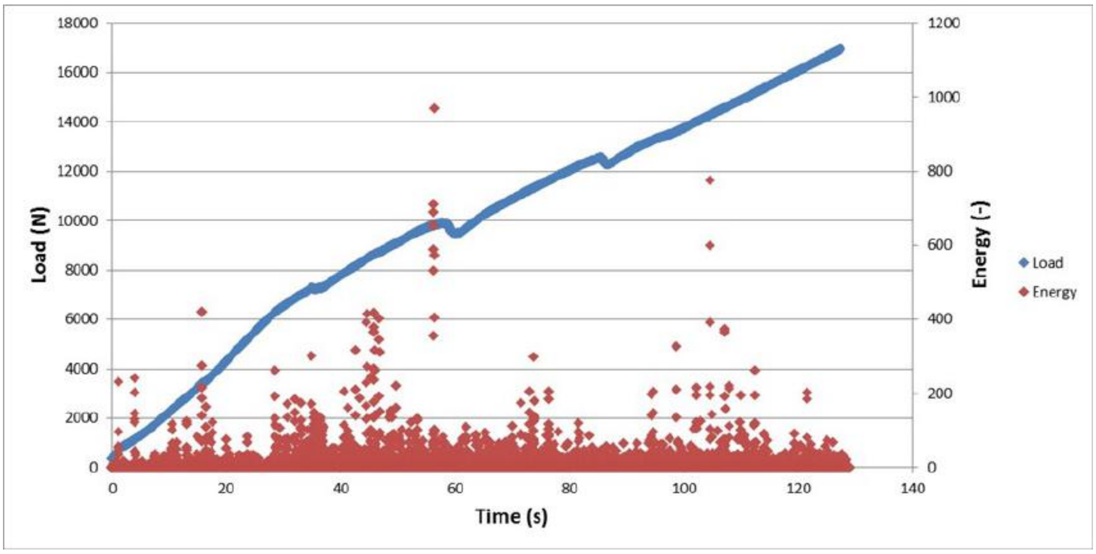

Figure B.13: Load vs. time and energy vs. time of specimen 4 rugby clay before healing